UNIVERSITY OF SOUTHERN CALIFORNIA

Department of Civil Engineering

Liquefaction-induced Ground Deformation and Failure

by

Jean-Pierre Bardet, Nicholas Mace and Tetsuo Tobita

A Report to PEER/PG&E

Task 4A - Phase 1

May 4, 1999

Table of contents

ABSTRACT

Liquefaction-induced ground deformation is a potential source of major damage to gas distribution networks during earthquakes. This type of permanent ground displacement, which has amplitudes ranging from a few centimeters to 10 meters and more, caused substantial damage to lifelines and pile-foundations of buildings and bridge piers along the Kobe shoreline during the 1995 Hyogoken Nanbu, Japan, earthquake. The overall research objective is to develop probabilistic models of liquefaction-induced ground displacement useful for estimating the cost of damage and repair to gas distribution networks during future earthquakes. This report summarizes the findings of the first phase of a long-term research program. It provides some preliminary results and recommendations for estimating (1) the amplitude of liquefaction-induced ground displacement and (2) the probability for these displacements to exceed some threshold amplitude. The amplitude and probabilistic models of liquefaction-induced ground deformation are based on measured displacement data, topographical data, soil borehole information, and earthquake data prior to the 1994 Northridge earthquake and 1995 Hyogoken Nanbu earthquake. In this report, the present state of understanding of the mechanisms of liquefaction-induced ground deformation has been reviewed based on past work in the field, laboratory, shaking table tests, centrifuge experiments, and empirical and analytical modeling. Among all these various approaches, the empirical multi-regression modeling of case histories emerge as the most relevant, practical and feasible approach for predicting liquefaction-induced deformation over the large areas covered by gas distribution networks. Twelve Multiple Linear Regression (MLR) models have been calibrated for modeling liquefaction-induced ground deformations. These MLR models have six and four parameters, respectively, and cover ground-slope and free-face conditions. They were calibrated from two data sets: one for displacements of all magnitudes, and the other for displacements smaller than 2 meters. In parallel to these MLR models, twelve statistical models have been proposed for assessing the confidence interval for predicting liquefaction-induced ground deformation and the probability of exceeding some ground deformation levels. The four-parameter models are more approximate than the six-parameter models and are recommended when there is limited borehole data. Both MLR and probabilistic models are preliminary because they are only based on data from earthquakes prior to 1994. The next phase of the research is presently focusing on the data collection of high-quality case histories of liquefaction-induced ground deformation in the 1994 Northridge and 1995 Hyogoken Nanbu earthquakes. Following the completion of the new database on liquefaction-induced ground deformation, new generations of probabilistic models will be proposed.

ACKNOWLEDGEMENTS

The financial support of the Pacific Earthquake Engineering Research center (PEER)-and the Pacific Gas and Electric Company (PG&E) is acknowledged. The authors thank Norm Abrahamson of PG&E for his help and advice during the conduct of the research project. The authors thank Prof. L. Youd of Brigham Young University, and Dr. S. Bartlett of the Utah Department of Transportation, for sharing their databases.

1. INTRODUCTION

Liquefaction-induced ground deformations have been identified as a potential source of major damage to pipeline networks during earthquakes. These permanent displacements have amplitude ranging from few centimeters to 10 meters and more. They were numerous during the 1995 Hyogoken-Nanbu earthquake (Hamada et al., 1996a and 1996b) and caused substantial damage to lifelines and pile-foundations of building and bridge piers along the Kobe shoreline (Hamada et al, 1996a; Karube and Kimura, 1996; Matsui and Oda, 1996; and Tokimatsu et al., 1996).

The overall research objective is to develop and improve methods for assessing and quantifying the liquefaction potential of ground deformation utilizing regional geologic data and detailed borehole data. Ultimately, this research is to produce probabilistic models of liquefaction-induced ground displacement useful for estimating the cost of damage and repair to gas distribution network during future earthquakes.

The specific objectives of the first research phase are:

(1) Review the present state of understanding of the mechanisms of liquefaction-induced deformation,

(2) Review and examine the case histories of liquefaction occurrences and liquefaction-induced ground deformation, and the models for liquefaction-induced lateral deformation, and

(3) Develop empirical and probabilistic models for liquefaction-induced lateral deformation applicable to deformations smaller than 2 meters.

This report summarizes the research results obtained during the first research phase, and gives some preliminary results and recommendations for estimating the amplitude and probability of liquefaction-induced ground displacement.

This report has six sections. The first section describes the phenomenon of liquefaction-induced deformation observed during earthquakes. The second section reviews the explanations for the mechanisms of liquefaction-induced ground displacement based on laboratory observations, shaking table tests, and centrifuge experiments, and surveys the analytical models for describing liquefaction-induced deformation. The third section examines the existing databases on liquefaction-induced deformation. The fourth section describes the empirical models calibrated from these databases. The fifth section presents the newly developed multiple-linear-regression models for assessing liquefaction-induced deformation. The last section presents the probabilistic models generated from the MLR models for assessing the confidence intervals for liquefaction-induced ground deformation and the probability for liquefaction-induced deformation to exceed some amplitude level.

1.1 Liquefaction-induced lateral spreads

During past earthquakes, large areas of ground were observed to shift laterally due to soil liquefaction. These liquefaction-induced lateral ground deformation have amplitudes ranging from

small (1 cm) to very large (>10 m) in the case of flow slides. They can take place for gently sloping ground conditions (0.1% to 6%). Examples of liquefaction-induced ground deformation during the 1994 Northridge earthquake were observed at the Power Plant Tailrace (>1 m) in the Van Norman Complex, and the Lower San Fernando Dam (0.3 m) (Bardet and Davis, 1996). As illustrated in Fig.1, liquefaction-induced ground deformations are generally observed close to open faces, or in gently sloping ground. These deformations are usually driven by a combination of transient and static shear stresses and attributed to the loss of shear strength of underlying saturated soils. As illustrated in Fig. 2, the permanent ground deformations, which have complicated patterns, may extend beyond liquefied areas.

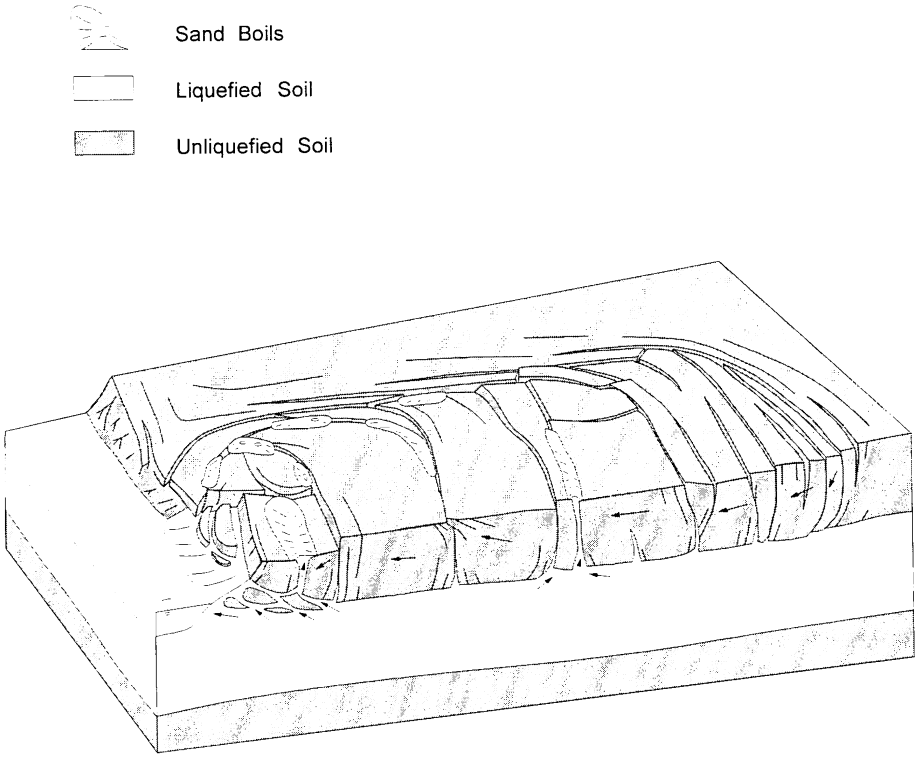

Figure 1-1. Schematic description of a lateral spread resulting from soil liquefaction during an earthquake (Rauch, 1997).

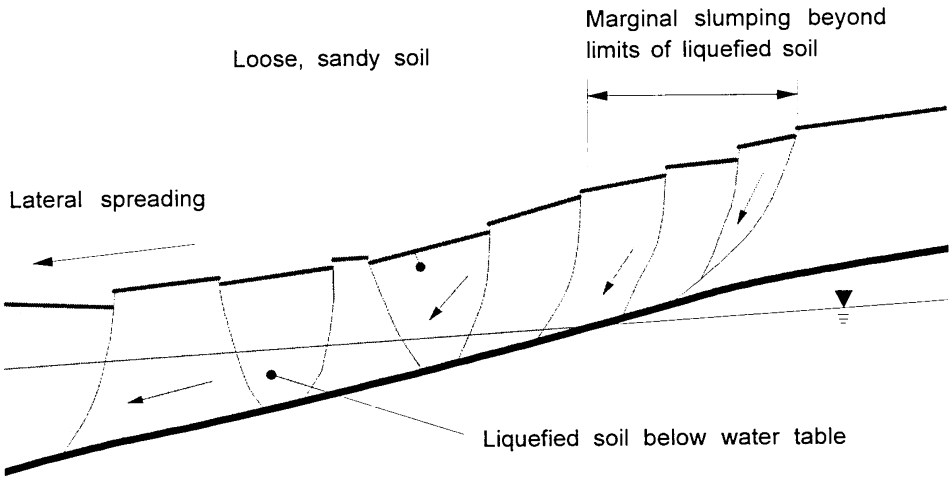

Figure 1-2. Extent of lateral spread beyond liquefaction areas (Rauch, 1997).

During the 1995 Hyogoken-Nanbu earthquake, liquefaction induced lateral ground deformation was one of the major causes of damage to lifelines and pile-foundations of building and bridge piers along the Kobe shoreline (Hamada et al, 1996; Karube and Kimura, 1996; Matsui and Oda, 1996; and Tokimatsu et al., 1996). As shown in Figs. 3 and 4, lateral ground deformations can cause bending and axial compression in buried pipes, which may damage pipes during earthquakes.

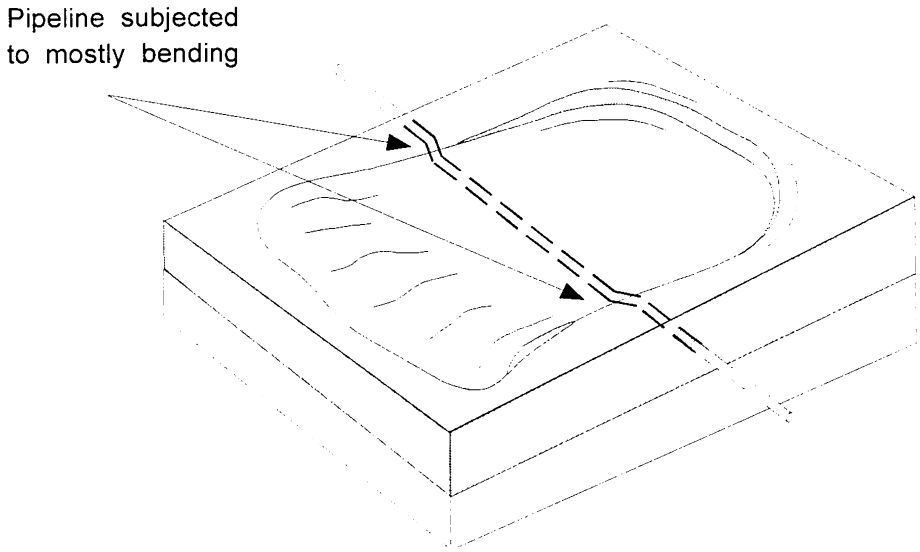

Figure 1-3. Illustration of damage to pipeline subjected to liquefaction-induced lateral spread after an earthquake (Rauch, 1997).

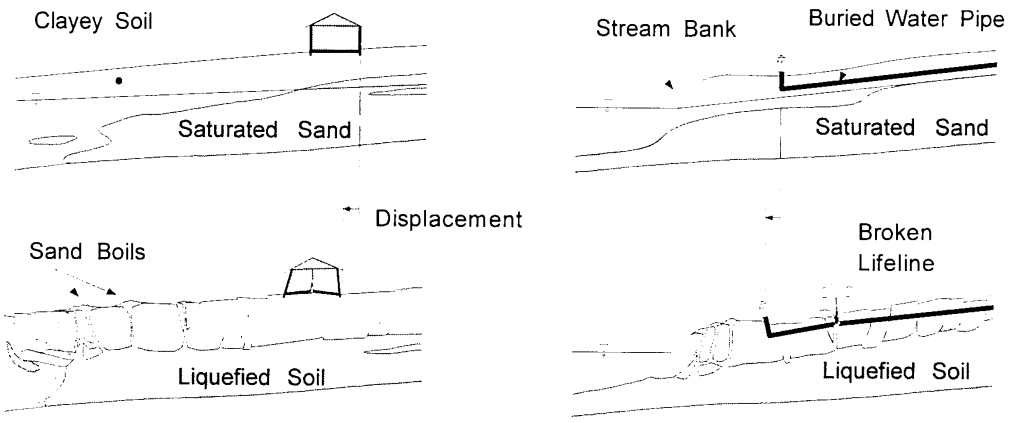

Figure 1-4. Illustration of liquefaction-induced ground deformation and associated damage to buried pipelines for ground-slope and free-face cases (Rauch, 1997).

1.2 Field measurement of lateral ground deformation

A large number of case histories of liquefaction-induced lateral spreads have been compiled in the two volumes edited by Hamada and O'Rourke (1992). Some examples of case histories are:

- 1964 Niigata earthquake (Youd and Kiehl, 1996)
- 1971 San Fernando earthquake, Van Norman Complex areas
- 1983 Ninhonkai-Chubu
- 1983 Borah peak, Idaho, earthquake (Youd et al., 1985)
- 1987 Superstition Hills, California, Earthquake (Wildlife Site, Youd and Holtzer, 1994; and Scott and Hushmand, 1995)
- 1989 Loma Prieta earthquake, Watsonville (Holtzer et al., 1994)
- 1993 Hokkaido Nansei-oki Earthquake (Isoyama, 1994)
- 1994 Northridge earthquake, Balboa Blvd (Holzer et al., 1996) and Van Norman Complex (Bardet and Davis, 1996; Davis and Bardet, 1996)
- 1995 Hyogoken-Nanbu earthquake (Hamada et al., 1996, Ishihara et al., 1996)

There are two main techniques for measuring permanent lateral ground deformation: ground surveying and processing of aerial photographs.

Ground surveys are commonly used in assessing the damage to constructed facilities. They are based on well-established optical measurements, and are sometimes tied up with satellite global positioning system (GPS) techniques. Ground surveying is extremely accurate (<5 mm) but unfortunately limited to areas that have been equipped with survey monuments prior to earthquakes. Examples of accurate ground surveying can be found in Bardet and Davis (1996). In

the studies of permanent ground deformation, the main drawback of ground survey is that their results are confined to areas of limited extent, and may be missing the global modes of deformation of larger areas.

Aerial photographs have been used to display comprehensive fields of permanent displacement after earthquakes (e.g., Hamada et al., 1996). Figure 5 shows an example of such field of ground displacement obtained using aerial photographs in Kawagachi-cho, Niigata, Japan, after the 1964 Niigata, Japan, earthquake (Hamada et al., 1993).

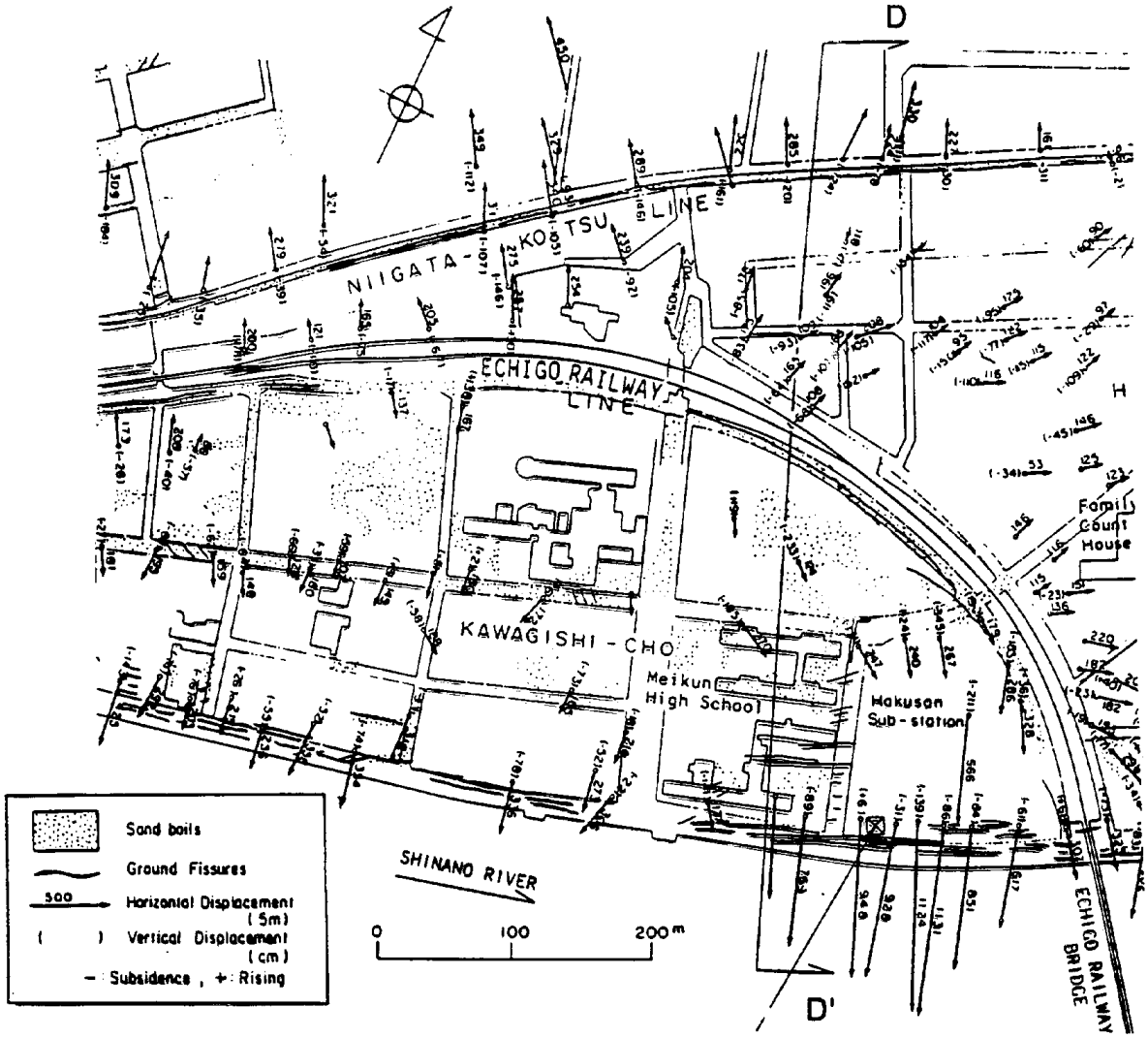

Figure 1-5. Examples of ground displacement vectors obtained in Kawagachi-cho, Niigata, Japan, after the 1964 Niigata, Japan, earthquake using aerial photographs (Hamada et al., 1993).

The determination of ground displacement requires aerial photographs taken before and after the earthquake. The accuracy of the measured amplitude of ground displacements depends on the scale and timing of the aerial photographs. The best measurements correspond to low-altitude

photographs taken just before and after the earthquake. In general, low-altitude photographs are much more difficult to find before rather than after the earthquake, which mostly limits the accuracy of past analyses. In the 1994 Northridge earthquake, the aerial photographs faced a new problem posed by the tectonic deformation, which had amplitudes comparable to that of permanent surficial ground deformation (Bardet and Davis, 1996).

2. MECHANISMS OF LATERAL GROUND DEFORMATION

The physical mechanisms causing liquefaction-induced ground deformation have been investigated by the means of laboratory tests, shaking table tests, and centrifuge experiments.

2.1 Laboratory approach

Laboratory experiments are useful to investigate under controlled conditions the aspects of soil behavior related to liquefaction-induced deformation. Laboratory experiments attempt to simulate the field conditions of the saturated soils during and after the cyclic loads applied by earthquakes.

2.1.1 Pre-liquefaction behavior

The behavior of saturated sands leading to liquefaction has been extensively studied in the laboratory under undrained conditions (e.g., Ishihara, 1993 and 1996). Figure 1 illustrates the typical response of saturated sand observed in cyclic undrained triaxial tests. During the axial loading cycles, the porepressure gradually increases (Fig. 1c) and the effective mean pressure decreases until it reaches a zero value (Fig. 1f). As the mean effective pressure approaches zero, large shear strains are developed in the soil sample. The magnitudes of these shear strains are limited by the effects of stress-dilatancy, which increases the mean effective pressure and therefore the shear strength of sands. Based on the typical results shown in Fig. 1, it is concluded that shear deformations in the field may accumulate due to shear stress cycles during the earthquake shakings. This cyclic accumulation of permanent shear strain (or rachetting) is certainly a plausible interpretation of the physical mechanisms of liquefaction-induced deformation in the field.

2.1.2 Post-liquefaction volumetric deformation

There is another aspect of soil behavior in the laboratory, besides the undrained response shown in Fig. 1, which is relevant to liquefaction-induced ground deformation. This particular behavior, which follows the reduction of mean effective pressure caused by cyclic loadings, is referred to as post-liquefaction behavior. As shown in Fig. 2, the amount of post-liquefaction volumetric deformation depends on not only the initial relative density D_r, but also the maximum amplitude of cyclic strain applied to soils. Ishihara (1993 and 1996) defines the onset of initial liquefaction when the soil sample undergoes cyclic shear strain in excess of 3.5%. As shown in Fig. 3, this maximum shear strain applied to the liquefied soil can also be expressed in terms of the factor of safety against liquefaction, F_l:

$$F_l = (\tau_{av,l}/\sigma'_v)/(\tau_{av}/\sigma'_v)$$

where $\tau_{av,l}/\sigma'_v$ is the ratio of shear stress amplitude $\tau_{av,l}$ to effective vertical stress σ'_v required for liquefaction, and the applied ratio of shear stress amplitude τ_{av} to effective vertical stress. As shown in Fig. 4, the amount of volumetric strain can therefore be related to F_l. The post-liquefaction volumetric strain of soils therefore depends on their initial density and the safety factor against liquefaction. Figure 4 also shows some approximate correlations between relative density, normalized standard penetration test (SPT) blow count, and normalized cone penetration test (CPT) resistance.

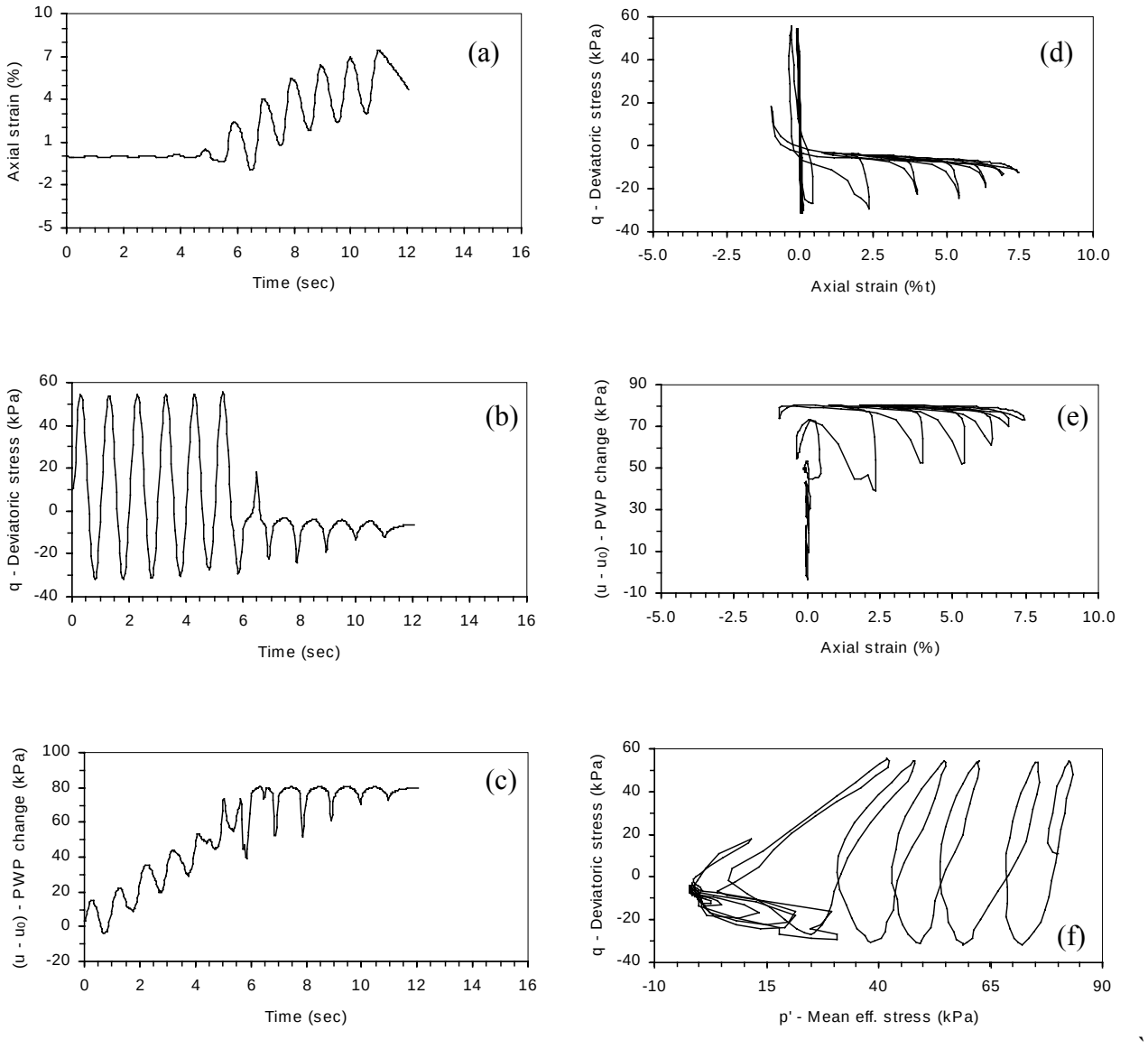

Figure 2-1. Cyclic triaxial undrained test at 80 kPa confining pressure on 60% relative density Nevada Sand. Time histories of (a) axial strain; (b) deviator stress; and (c) porepressure change; (d) stress-strain response, (e) porepressure-strain response, and (f) effective stress path (Arulmoli et al., 1992).

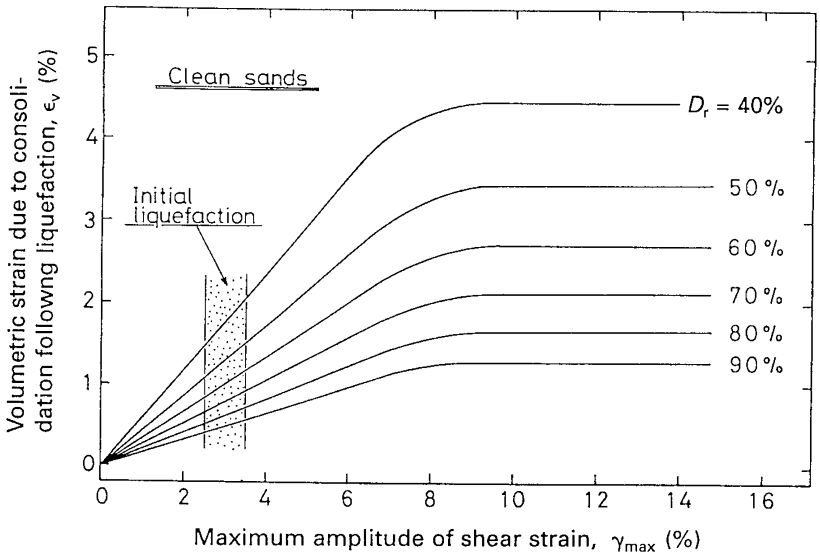

Figure 2-2. Post-liquefaction volumetric strain of clean sands plotted against maximum shear strain (Ishihara, 1996).

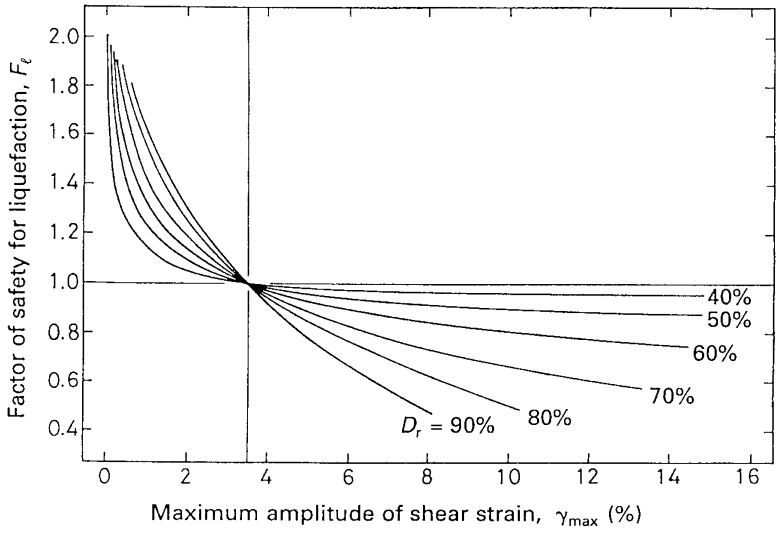

Figure 2-3. Relation between factor of safety F_l and maximum shear strain for clean sands (Ishihara, 1996).

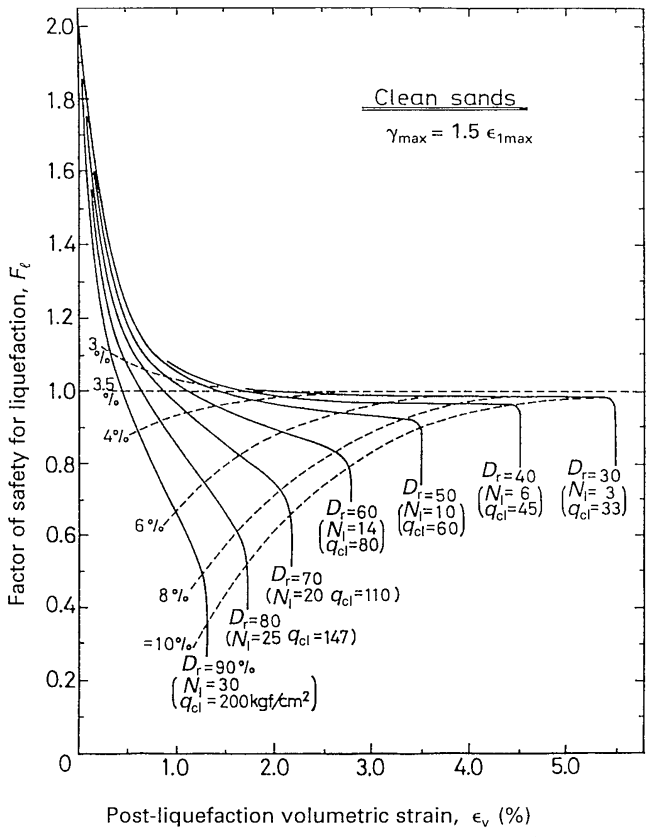

Figure 2-4. Chart for determination of post-liquefaction volumetric strain of clean sands as a function of factor of safety (Ishihara, 1996).

2.1.3 Post-liquefaction shear deformation

The mechanism of post-liquefaction shear deformation in saturated sands were experimentally investigated by using torsional test (e.g., Yasuda et al., 1994; and Shamoto et al., 1997) and triaxial tests (e.g., Nakase et al., 1997). Both undrained torsional tests (Yasuda et al., 1994; and Shamoto et al., 1997) and undrained triaxial tests (Nakase et al., 1997) indicate that liquefied soils regain shear-strength beyond some shear strain threshold γ_L. Figure 5 shows an example of such a re-hardening during a monotonic undrained torsional shear test following cyclic liquefaction (Peiris and Yoshida, 1996). As shown in Fig. 5, the liquefied sand gradually regains shear strength when it is sheared beyond some threshold shear strain γ_L. The value of γ_L depends on the relative density D_r and the amount cyclic shear strain prior to liquefaction, or the factor of safety against liquefaction. As shown in Figs. 5 and 6, Yoshida (1996) proposed a stress-dilatancy model, which describes well the stress-strain curves in the post-liquefaction range. This strain-dependent type of stress-dilatancy is a new in constitutive modeling, and deserves further investigation. The strain threshold γ_L is related to the maximum displacement of lateral spreads, and is useful for predicting the upper-bound of liquefaction-induced lateral displacements.

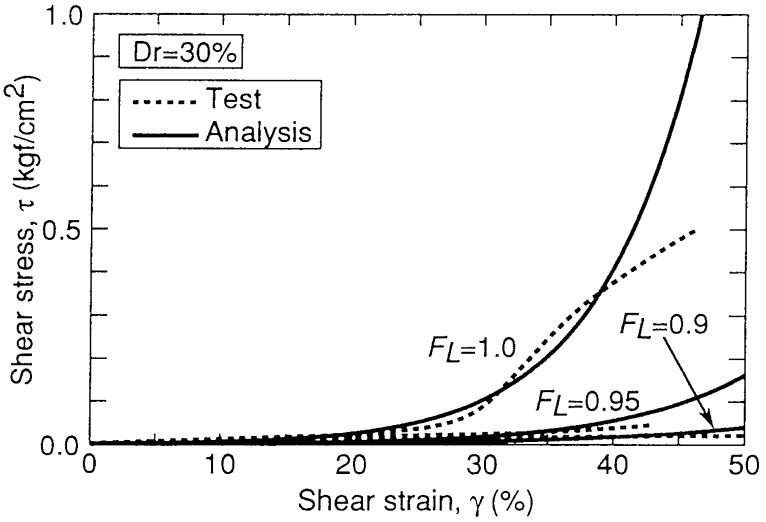

Figure 2-5. Stress-strain response of Toyoura sand at 30% relative density in the post-liquefaction range during undrained torsional tests (data after Yasuda et al., 1994; model after Yoshida, 1996).

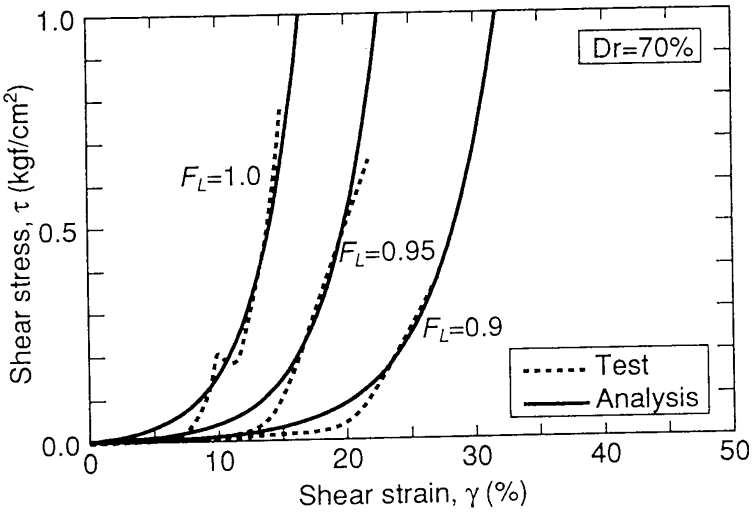

Figure 2-6. Stress-strain response of Toyoura sand at 70% relative density in the post-liquefaction range during undrained torsional tests data after Yasuda et al., 1994; model after Yoshida, 1996).

2.1.4 Example of calculation of lateral spread displacement based on laboratory tests

The results of laboratory tests on post-liquefaction shear deformation can be used to estimate the maximum amount of lateral displacement in a saturated soil layer. An example of calculation is shown in Table 1 and Figure 7. The 10-m thick layer is gently sloping. It is made of clean sand

with a 30% relative density and a saturated unit weight of 18.62 kN/m^3. The water table is assumed to be at the ground surface. The sand is assumed to have liquefied during the earthquake, and the liquefaction severity is estimated by using F_L, the factor of safety against liquefaction. In this example, $F_L = 0.95$. As shown in Table 1, the laboratory test results give the limiting strain γ_L for three different values of initial effective stress σ'_v. The experimental results indicate that γ_L increases with σ'_v, e.g., γ_L increases from 28% to 47 % when σ'_v varies from 24.5 kPa to 98 kPa. Based on these laboratory results, the limiting strain is calculated from the vertical effective stress at three different depths in the layer, and the resulting displacement is calculated in each layer. The maximum total displacement, which is the sum of the displacements of each layer, is found to be 3.5 m. This displacement corresponds to an average shear strain in the complete layer equal to 35%. The displacement calculated above corresponds to very large strain. It is an upper bound of the possible strain that may develop in this particular slope. According to these calculations, the upper bound does not depend on the slope angle and inertial effects.

Table 2-1. Calculation of the maximum amplitude of lateral spread based on laboratory test results.

γ_{sat} =	18.62 kN/m^3		σ'_v (kPa)	γ_L (%)
D_r =	30%		24.5	28
F_l =	0.95		49.0	42
			98.0	47
Depth (m)	σ'_v (kPa)	Thickness (m)	γ_L (%)	Displacement (m)
1.7	14.7	3.3	22.4	0.7
5.0	44.1	3.3	39.2	1.3
8.3	73.5	3.3	44.5	1.5
		Total displacement =		3.5 m

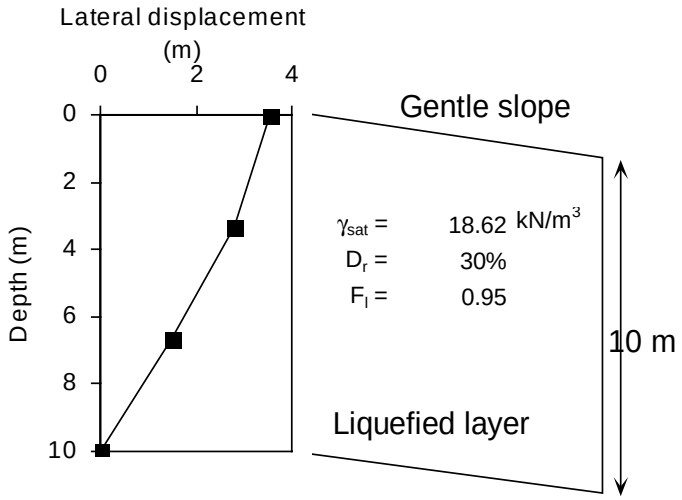

Figure 2-7. Example of calculation of maximum lateral displacement based on laboratory tests (after Yasuda et al., 1994).

2.2 Centrifuge modeling of liquefaction induced ground displacement

The principles of centrifuge modeling are well described in several technical papers (e.g., Ko, 1988). In centrifuge modeling, reduced-scale models are constructed to represent larger prototypes and subjected to a centrifugal acceleration *n* generated by the rotation of the centrifuge arm. In the case of centrifuge modeling of soil deposits shaken by earthquakes, the model is enclosed in a laminar box, and is shaken in flight by an hydraulic shaker through its base (Figs. 8, 9, and 10).

As shown in Table 2, all physical quantities in the centrifuge models are scaled to determine the prototype responses. In these scaling relations, the stresses and strains have identical scaling in the model and prototype, which preserve the nonlinear stress-strain relationships of soils. Lengths are scaled with *n*. Time in dynamic processes is scaled with *1/n*, whereas time in diffusion processes is scaled with $1/n^2$. Consequently, the prototypes involving simultaneously dynamic and diffusion processes cannot be modeled exactly in the centrifuge by simply reducing the model size. This is the case of liquefaction-induced lateral displacements, which involve nonlinear transient soil behaviors coupled to the diffusion of interstitial water (i.e., consolidation). The modeling of such phenomena requires the introduction of viscous additives into the interstitial water to scale the consolidation time (e.g., Ko, 1988).

The interpretation of lateral spread with centrifuge experiments is described Dobry et al. (1995). In a particular experiment, Dobry simulated lateral spreads in inclined laminar boxes (Fig. 11) using a 10-m thick clean Nevada sand deposit, which has a gentle slope inclination of 2%. Three different relative densities were used: 40%, 65% and 80%. The sand was saturated by using interstitial water without viscous additives. The laminar box was shaken by a sine-like input ground motion at its base. The pore pressure, acceleration, and lateral displacement were recorded at various depths. As shown in Figs. 12 to 15, the centrifuge results indicate that (1) the lateral ground deformation is associated with unsymmetric spikes of ground acceleration in the downhill direction, (2) there are negative pore pressure spikes which increase the effective stress and stop the downhill ground deformation, (3) the lateral ground deformation does not continue after the shaking, and (4) the lateral displacement and the thickness of the liquefied layer decreases with relative density.

The centrifuge test results indicate that permanent lateral ground deformation is a rachetting phenomenon, the amplitude of which is controlled by stress-dilatancy. They also show that the magnitude of permanent ground displacement is related to relative density and thickness of liquefied layer. However, the timing of lateral spreading observed in centrifuge experiments does not agree with the delayed ground deformations and failures observed after the 1964 Niigata earthquake. In future work, there is a need for increasing the interstitial fluid viscosity and for examining the effects of properly-scaled diffusion on lateral spreading. In spite of some limitations, the centrifuge remains a useful tool for comprehending the mechanism of lateral ground deformation.

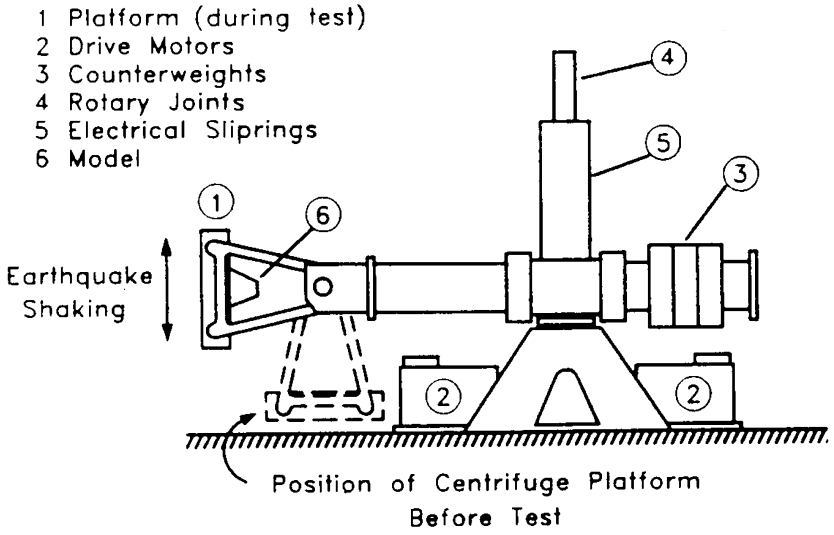

Figure 2-8. Sketch of RPI geotechnical centrifuge (Dobry et al., 1995).

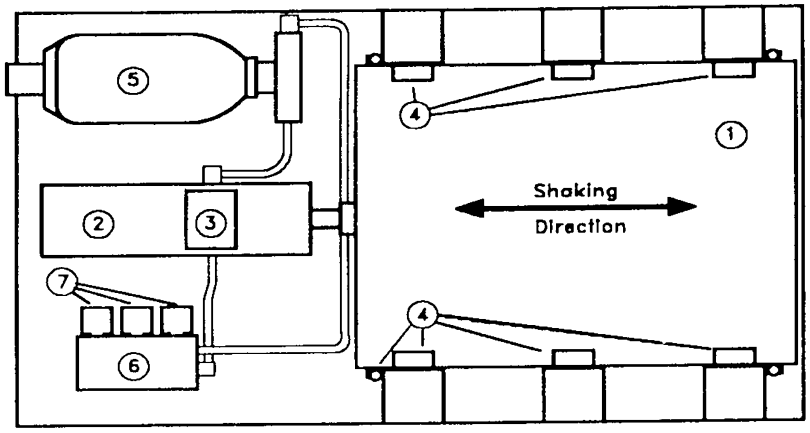

Figure 2-9. Schematic view of in-flight shaker at RPI (Dobry et al., 1995).

Table 2-2. Scaling relations used for centrifuge modeling (Dobry et al., 1995).

Parameter	Model units	Prototype units
Length	1/n	1
Velocity	1	1
Acceleration	n	1
Stress	1	1
Strain	1	1
Time:		
Dynamic	1/n	1
Diffusion	$1/n^2$	1
Frequency	n	1

(n = centrifuge acceleration in g)

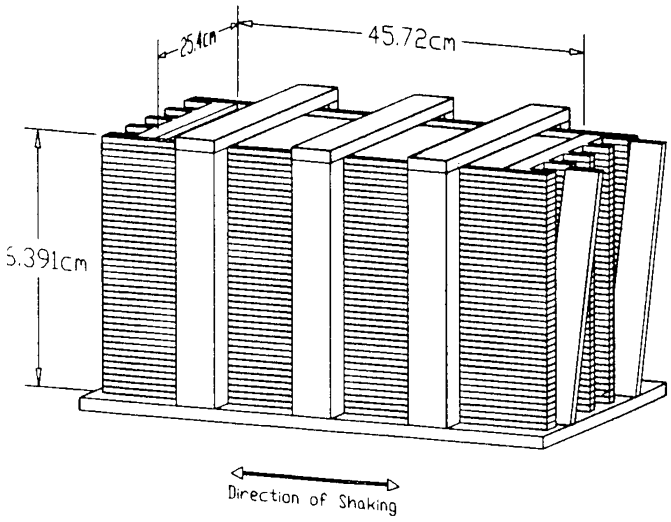

Figure 2-10. Schematic view of the RPI laminar box (Dobry et al., 1995).

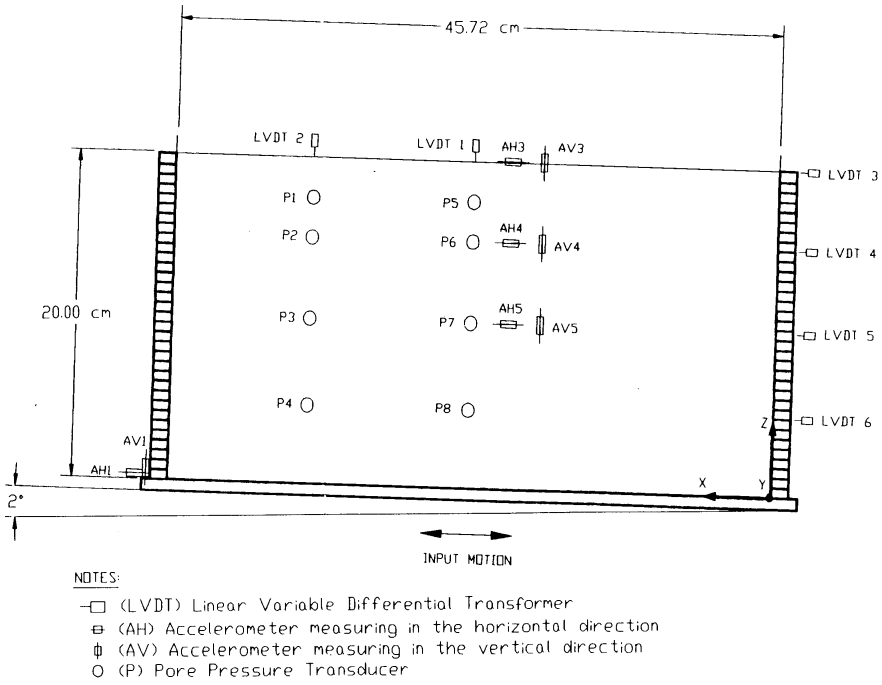

Figure 2-11. RPI laminar box and Model No.2 (Dobry et al., 1995).

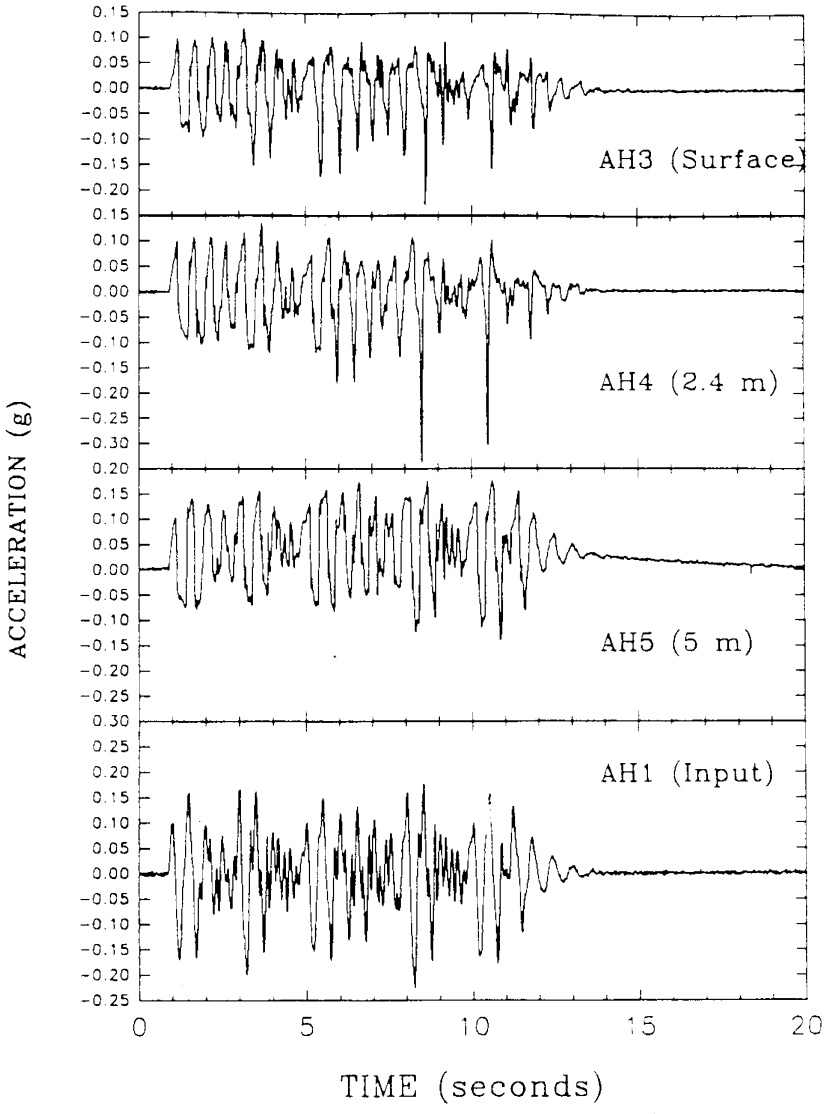

Figure 2-12. Lateral acceleration time histories for Model No. 2 (Dobry et al., 1995).

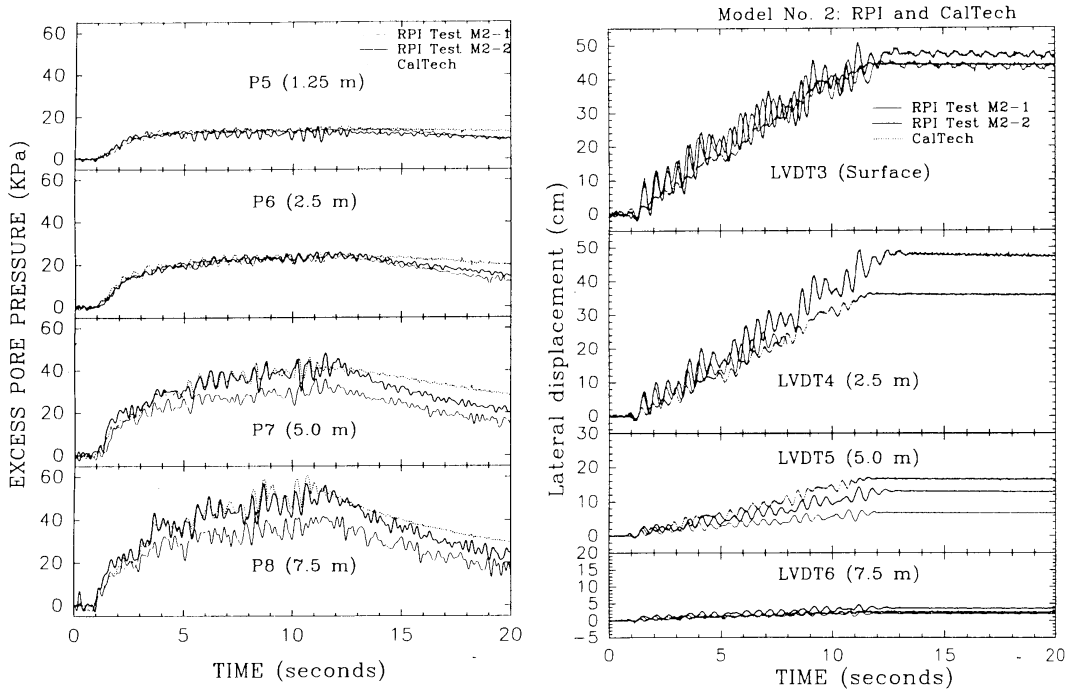

Figure 2-13. Time histories of excess pore pressure and lateral displacement recorded at Caltech and RPI for Model No. 2 (Dobry et al., 1995).

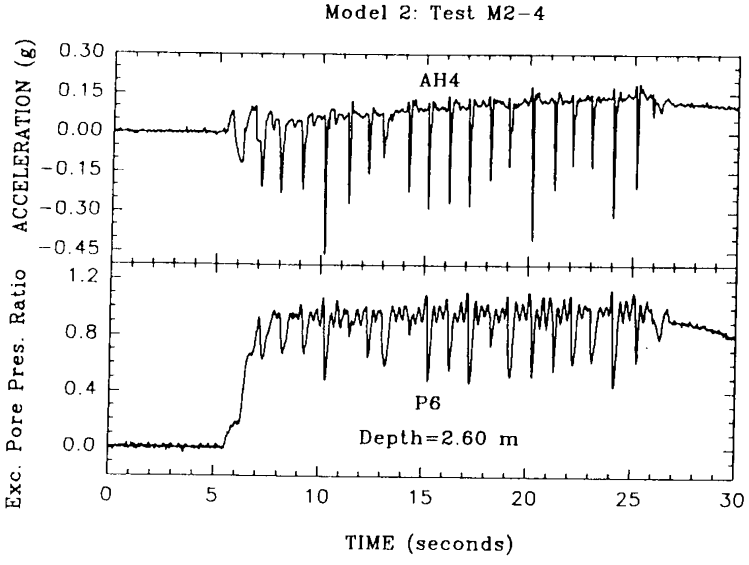

Figure 2-14. Time histories of acceleration and excess pore pressure recorded at RPI for Model No. 2-4 (Dobry et al., 1995).

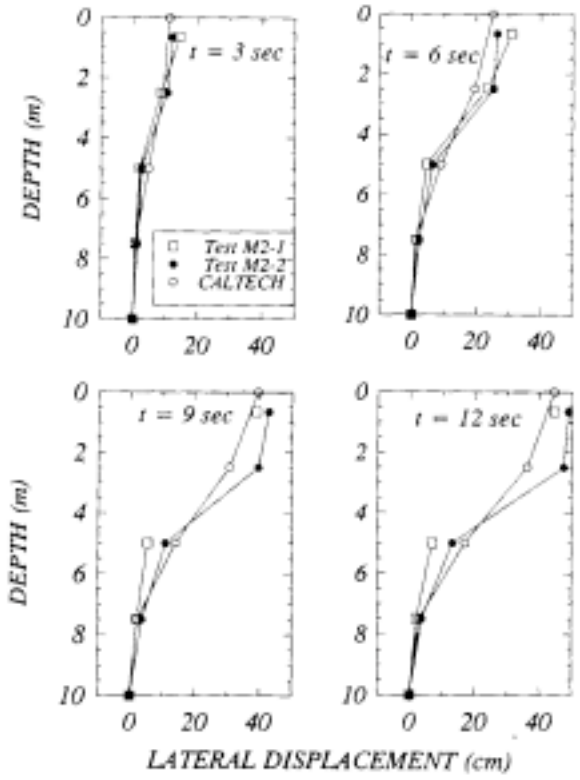

Figure 2-15. Lateral displacement profiles at various times during shaking for tests at Caltech and RPI, Model No. 2 (Dobry et al., 1995).

2.3 Shaking Table Experiments

Liquefaction-induced lateral spreads have extensively been investigated using shaking tables (e.g., Towhata et al., 1996). In these types of experiments, a reduced-scale model of soil deposits is subjected to short pulses or continuous time history of acceleration simulating the earthquake ground motion. Figure 16 shows typical results of ground deformation obtained in shaking table tests. The acceleration, pore pressure, and displacement are measured at various locations in the reduced-scale model, which is 2 m long and 50 cm high. In the impact test (Fig. 16a), the model is subjected to a very short acceleration pulse. The pore pressure rises very quickly, and the deformation takes place over an extended period of time. In the shaking test (Fig. 16b), the model is subjected to a sine-like base acceleration. The porepressure gradually builds up until the soil liquefies. The ground deformations are progressive, and stop with the base acceleration. This observation is in agreement with those of centrifuge experiments without viscous additives. However, the observations for the impact test in shaking table test do not agree with the centrifuge observations.

Figure 17 summarizes possible explanations proposed by Towhata et al. (1996) for ground deformation simultaneous to ground shaking, or delayed after the ground shaking. Due to the

seismic shaking, the pore pressure raises until the soil liquefies. The onset of liquefaction is generally reached during the earthquake shaking. The state of liquefaction is sustained during some time interval, then pore pressure decreases depending on drainage conditions. The timing of the liquefaction-induced deformation depends on the time history of driving stress and shear strength. The deformation starts when the shear strength is smaller than the driving shear stress, and stops when the shear strength is larger than the driving shear stress. In the case of rapid drainage, the shear strength is likely to be regained after the shaking stops, and the deformation will stop with the shaking. In the case of slower drainage, the shear strength may be regained much more slowly, and the deformation may extend after the shaking.

In shaking table tests, Kokusho et al. (1998) reported that a water film formed beneath a thin layer of silt sandwiched between sand layers. They observed that, when such a film appeared, the soil mass above the silt layer glided in the downward direction not only during but after the shaking. When the film did not form, the lateral flow took place mainly during the shaking. This shaking table test experiment clearly demonstrates liquefaction-induced deformations are influenced by drainage conditions.

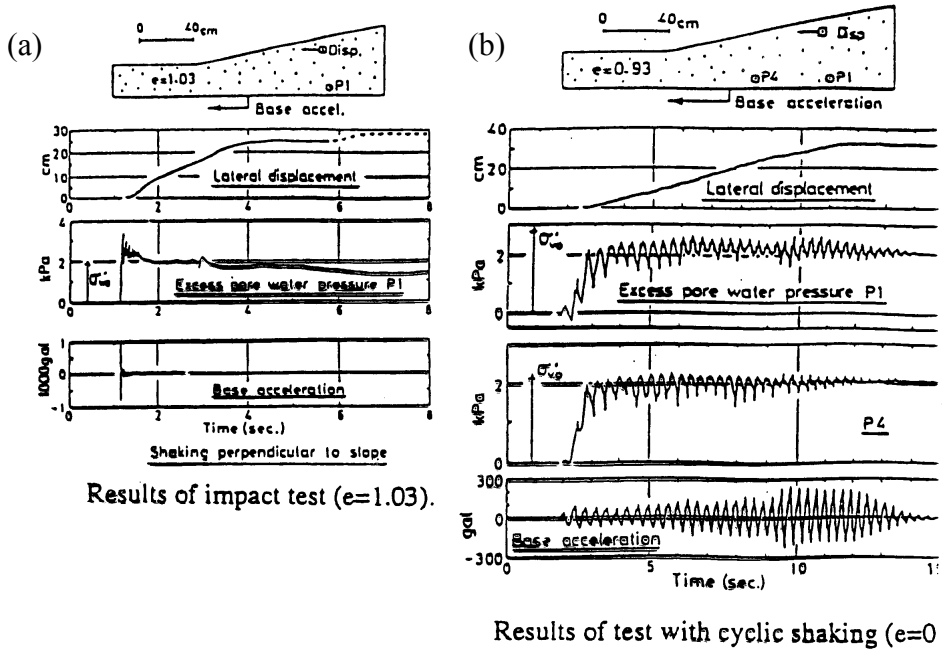

Figure 2-16. Time history of acceleration, porepressure, and lateral displacement observed in shaking table test: (a) impact test; and (b) cyclic shaking (Towhata et al., 1996).

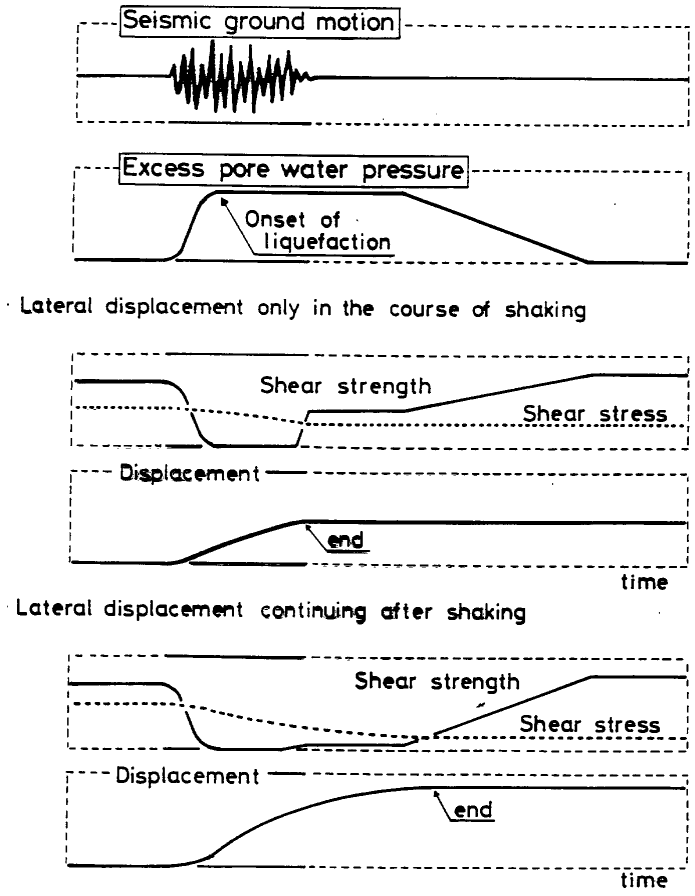

Figure 2-17. Possible explanations for the continuation and cessation of liquefaction-induced ground deformation after the earthquake shaking (after Towhata et al., 1997).

2.4 Summary of observations from laboratory, shaking table, and centrifuge experiments

The results of laboratory, shaking table and centrifuge experiments are useful to understand the physical mechanisms of liquefaction-induced deformation generated by earthquakes. The laboratory tests indicate that liquefied soils may deform during and after transient earthquake loadings. The lower range of liquefaction-induced deformation correspond mainly to cyclic ratchetting during transient earthquake loading, and is controlled by transient shear stress, number of loading cycles, relative density and stress-dilatancy. The upper range of liquefaction-induced deformation corresponds to post-liquefaction behavior with a regain of shear strength, which is also induced by stress-dilatancy. This regain of shear strength is observed for a threshold shear strain γ_L, which depends on the initial relative density and the maximum amplitude of cyclic shear strain. The inclusion of post-liquefaction re-hardening effects into constitutive modeling offers a promising approach for predicting the maximum magnitude of lateral spread. The centrifuge and shaking table experiments indicate that the slope of the ground surface affects significantly the permanent displacement in ground-slope cases. There are still some disagreements about the timing of liquefaction-induced ground deformation between the field observations and the experiments in shaking table, centrifuge and laboratory. There is not yet a rational explanation for the occurrence of lateral ground deformation after the earthquake shaking. Such delayed ground

deformations need to be investigated and understood for modeling accurately lateral ground deformation in simplified engineering analyses and advanced analytical procedures.

2.5 Analytical Modeling of liquefaction-induced deformation

Several analytical models have been proposed to simulate the amplitude of liquefaction-induced ground deformation. These models are based on different types of approaches, and fall in the following categories:

- Newmark sliding block model
- Minimum potential energy model
- Model with shear strength loss and strain rehardening
- Viscous model
- Effective stress model

2.5.1 Newmark sliding block model

Several models have been proposed based on the concept that Newmark (1965) developed for calculating the deformation of earth dams during earthquakes.

Yegian et al. (1991) proposed that the amplitude D of permanent displacement is:

$$D = N_{eq}\, T^2\, a_p\, f(a_y/a_p) \tag{2.1}$$

where N_{eq} is the number of cycles equivalent uniform base motion, T the period (s), a_y the yield acceleration, a_p the peak acceleration (g), and f the dimensionless function depending on base motion.

Baziar et al. (1992) proposed that D depends on peak velocity:

$$D = N_{eq}\, v^2_{max}/a_{max} \,/\, f(a_y/a_{max}) \tag{2.2}$$

where a_{max} is the peak acceleration, and v_{max} the peak velocity.

Jibson (1993) proposed that D (cm) depends on the Aria intensity:

$$Log\ D = 1.46\ log\ I_a - 6.642\ a_y + 1.546 \tag{2.3}$$

where I_a the Aria intensity (m/s), and a_y the yield acceleration (g).

The models based on Newmark sliding blocks assume that the deformation takes place on a well-defined failure surface, the yield acceleration remains constant during shaking, and the soil is perfectly plastic. However, these assumptions do not hold in the case of liquefied soils and lateral spreads, because (1) the shear strain in liquefied soil does not concentrate within a well defined surface, (2) the shear strength (and yield acceleration) of saturated soils varies during cyclic loading as pore pressure varies, and (3) soils are generally not perfectly plastic materials, but commonly harden and/or soften.

Byrne (1991) extended the concepts of Newmark sliding block by introducing a resisting force varying with displacement. As shown in Fig. 18, the mass *M* with an initial velocity *V* is subjected to a driving force *D* due to the gravity and slope inclination α, and a resisting force *R*. The mass stops when the initial kinetic energy (i.e., $MV^2/2$) is dissipated by the resisting force *R*. As shown in Fig. 18, the final displacement can be much greater when the resisting force vary linearly with displacement. Byrne (1991) claimed that the total displacement may well be 2 or 3 times the standard Newmark estimate. Byrne's method requires the selection of a final residual shear strength S_R and limiting strain γ_R. Typical values of S_R and γ_R are listed in Table 4.

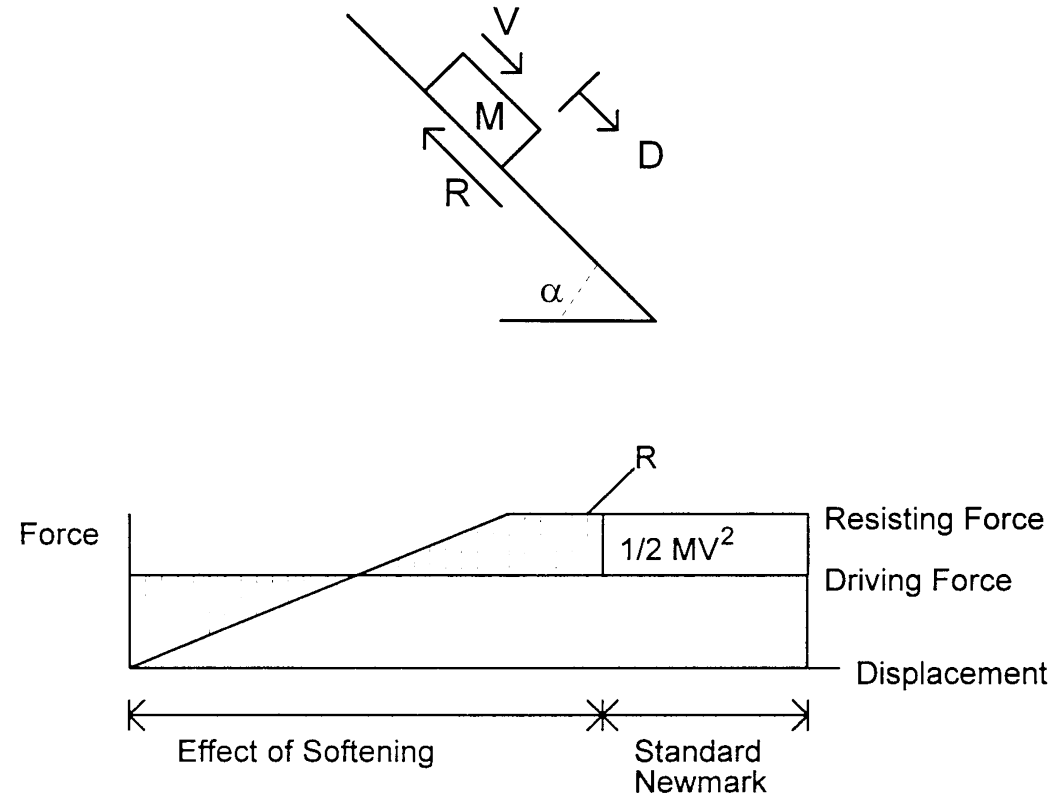

Figure 2-18. Extended Newmark sliding block concept for calculation of liquefaction-induced lateral spread (Byrne, 1991).

Table 2-4. Estimated values of shear strain and residual shear strength for extended Newmark sliding block analysis (Byrne, 1991).

$(N_1)_{60}$	s_u/p	γ_F (%)	
		$F_{TRIG} \approx 1.0$	$F_{TRIG} = 0.5$
0 - 4	0.05 - 0.10	25 - 50	>100
4 - 10	0.10 - 0.20	10 - 25	30 - >100
10 - 15	0.15 - 0.4	8 - 15	20 - 35
15 - 20	0.3 - 0.5	5 - 10	15 - 25
>20	> 0.5	< 5	< 15

2.5.2 Model with shear strength loss and strain rehardening

Byrne (1997) proposed to calculate the final position of a slope that liquefies by using the finite difference program FLAC (1995). In the zone of liquefaction, the liquefied material is assumed to be initially free of shear, and to undergo isotropic pressure. Following this instantaneous melting of the liquefied soil, the shear stress τ is assumed to increase with shear strain until it reaches some residual shear strength τ_{ST} (Fig. 19). While the liquefied soil regains shear strength, the shear modulus is assumed to take a constant value G_{LIQ}. The final position of the slope is calculated by using the dynamic equation of motion.

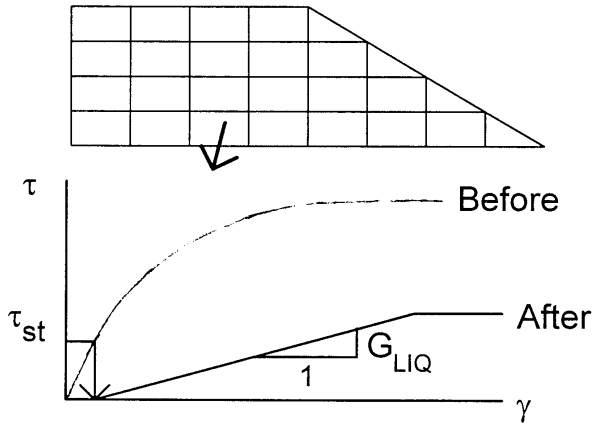

Figure 2-19. Illustration of principle in the dynamic method of Byrne (1997).

2.5.3 Minimum potential energy model

Towhata et al. (1997) developed a minimum potential energy model, the principles of which are schematized in Fig. 20. Soil layers of irregular shape are divided into vertical slices in which the lateral displacement is assumed to vary as a sine function with depth. The model determines the final position of the soil layers that liquefy by invoking the principle of minimum potential energy. The model also predicts the variation of displacement with time by using Lagrangian equations of motion. As shown in Fig. 21, the model was successfully applied to model various shaking table test results. The model was extended to three-dimensions (Orense and Towhata, 1996), and applied to simulate case histories of liquefaction-induced lateral ground deformation during the Niigata, 1964, earthquake.

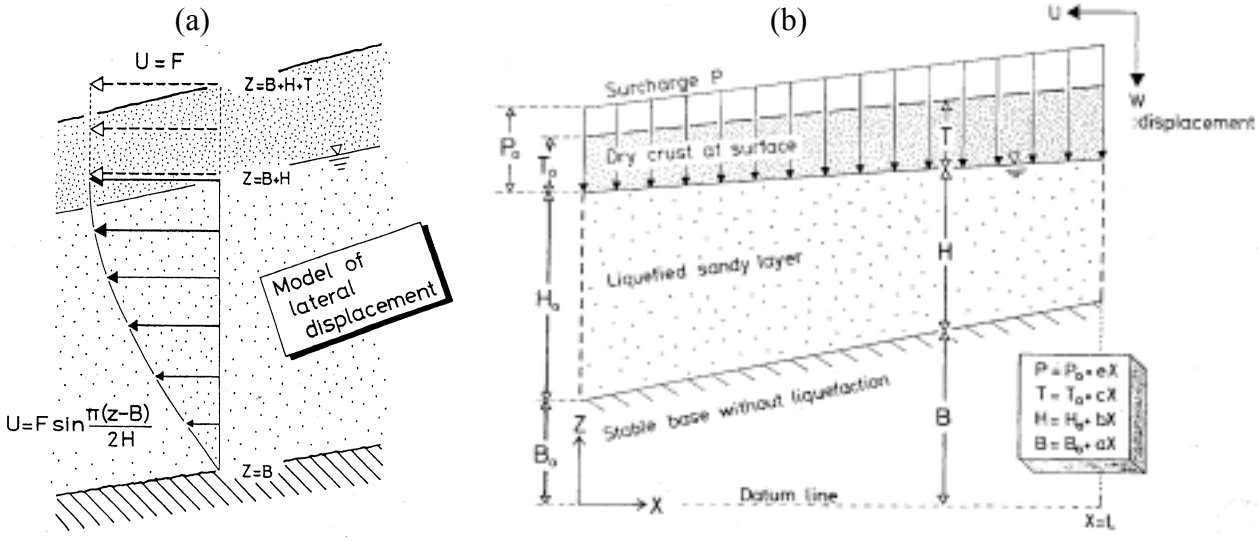

Figure 2-20. Towhata et al. (1997) minimum potential energy model: (a) Sinusoidal variation of lateral displacement along vertical axis; and (b) Simplified model of liquefied slope..

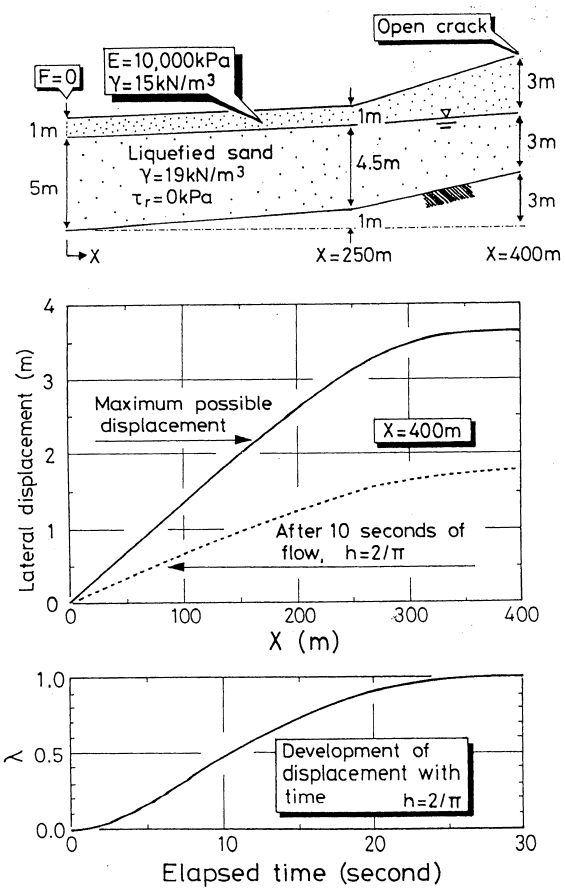

Figure 2-21. Analysis of lateral displacement of gentle slope with the minimum potential energy model of Towhata et al. (1997).

2.5.4 Viscous models

Hamada et al. (1994) proposed the use of viscous models to simulate the liquefaction-induced deformation of soils and the forces applied to buried structures such as piles. The apparent viscosity of liquefied soils was determined in the laboratory by measuring the drag force applied to a sphere immersed in liquefied soils.

Yashima et al. (1997) used a viscous model and the finite difference method for simulating the displacement of a liquefied embankment. As shown in Fig. 22, the liquefied material of the compacted fill is assumed to become instantaneously a viscous fluid, and the displacement of the viscous fluid is calculated at various time intervals. This numerical approach allows the calculation to proceed for very large shear strains.

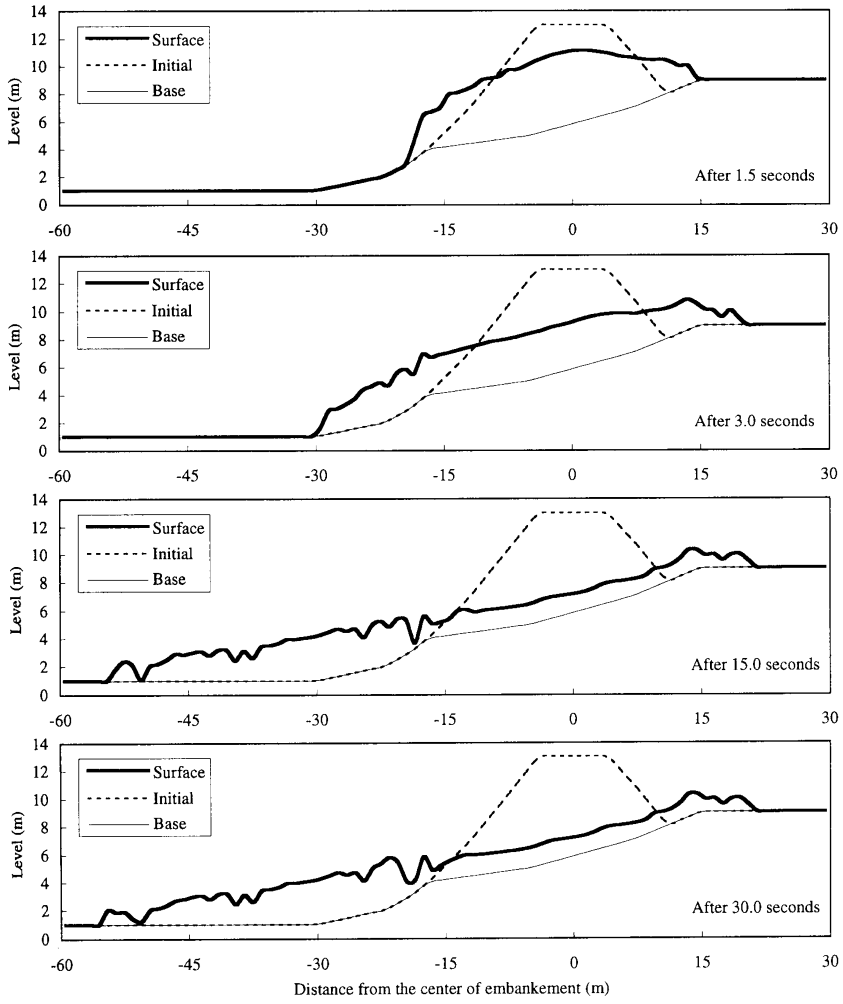

Figure 2-22. Simulated progressive failure configurations of embankment at various times after the initial liquefaction (Yashima et al., 1997).

2.5.5 Constitutive modeling and numerical analysis

Many effective stress models (e.g., Dafalias and Herman, 1982; Pastor et al., 1985; Bardet, 1986, 1990, and 1995; Adachi and Oka, 1982; and Taguchi et al., 1995) have been proposed to calculate liquefaction-induced lateral deformations. There are too many constitutive models applicable to liquefied soils to reference them all. Some models are described in the VELACS project (Arulanandan and Scott, 1993-1994; Bardet et al., 1993; and Smith, 1994). These models are usually based on a constitutive model formulated in terms of effective stress, the Biot dynamic consolidation theory, and a finite element or finite difference computer program with step-by-step time integration (e.g., Zienkiewicz et al., 1984 and 1990). Several of these models were used in the VELACS project (Arulanadan and Scott, 1993, 1994), especially for Model No.3 of VELACS which simulates a gentle slope made of liquefiable Nevada Sand.

However, several important aspects of soil behavior are not yet incorporated into these constitutive models – especially post-liquefaction behavior and low-mean effective pressure behavior of soils.

Most models (e.g., Parra-Colmenares, 1996) are only applicable to model cyclic strain, and cannot describe the post-liquefaction re-hardening, because they were not designed for this purpose. Peiris and Yoshida (1995, 1996) developed new one-dimensional constitutive models, capable of describing the post-liquefied stress-strain response of saturated sands. However, their models remain to be generalized to three-dimensions and used in finite element analysis.

3. DATABASES OF LIQUEFACTION CASE HISTORIES

The past section reviewed several analytical approaches, which have been proposed to model liquefaction-induced ground deformation. These analytical models are capable of explaining successfully a few, but not all, aspects of liquefaction-induced deformations. Most of the analytical models require the calibration of numerous parameters for predicting liquefaction-induced deformation, and are therefore impractical to apply over the large areas covered by gas distribution networks. The empirical methods based on case histories of liquefaction-induced deformation are alternate approaches readily applicable for assessing damage to gas distribution networks after earthquakes. This section reviews the databases of case histories of liquefaction-induced deformation, and the next section the empirical models based on these databases.

The case histories of liquefaction occurrence and liquefaction-induced ground deformation during past earthquakes are essential for understanding and characterizing the effects of liquefaction, and for developing physical and empirical models to predict liquefaction damage. In this project, the following liquefaction databases have been examined:

- Liquefaction occurrence database (Harder, 1991)
- Liquefaction-induced ground deformation databases (Bartlett and Youd, 1992; Rauch, 1997; Bartlett, 1998)

These databases have been organized into Excel workbooks, and are listed in Appendix A.

3.1 Liquefaction occurrence database (Harder, 1991) and liquefaction analysis (Youd and Idriss, 1998)

Harder (1991) reported a database for case histories of liquefaction occurrence. This database includes case histories for which there was either evidence of liquefaction or no evidence for liquefaction. Such a database is the basis of most liquefaction analysis procedures, as recently described by Youd and Idriss (1998). Since 1991, new databases of liquefaction occurrence have been developed based on shear wave velocity (Stokoe et al., 1988) and cone penetration test (CPT) data (Robertson and Campanella, 1985). However, these databases have not been considered in the present study.

As shown in Figs. 1 and 2, the liquefaction occurrence database has 125 entries from 17 earthquakes. The soil properties are characterized by standard penetration tests (SPT) and normalized blow counts $N1_{60}$. The blow count N, which is measured in the field, is normalized by using a procedure accounting for the diversity of SPT equipment and depth of testing (Youd and Idriss, 1998). The earthquake intensity at the site is characterized by the peak ground acceleration and magnitude, and the loading on the soil at a particular depth is defined by the cyclic stress ratio $\Delta\tau/\sigma'_0$ where $\Delta\tau$ is the equivalent cyclic stress amplitude and σ'_0 is the initial vertical effective stress.

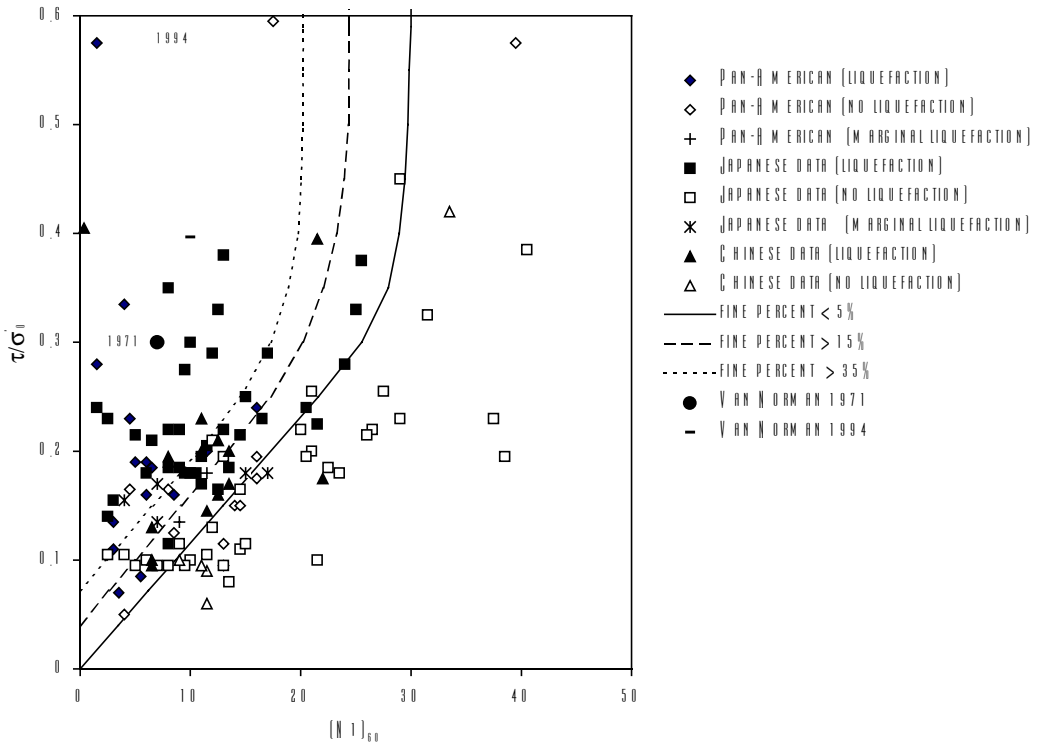

Figure 3-1. Cyclic stress ratio and normalized blow count for case histories in liquefaction occurrence database (Harder, 1991).

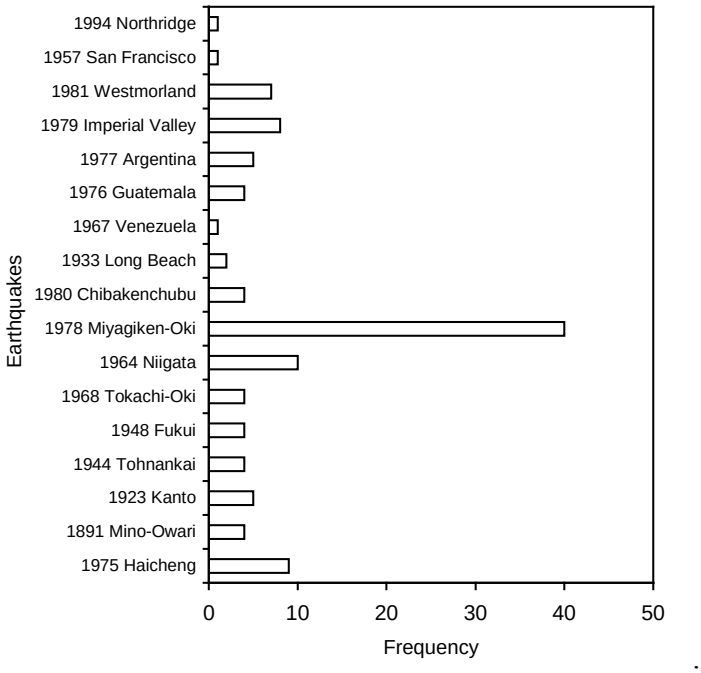

Figure 3-2. Distribution of earthquakes in liquefaction occurrence database (Harder, 1991).

3.2 Liquefaction-Induced ground deformation database (Bartlett and Youd, 1992)

In the database of liquefaction-induced ground deformation compiled by Bartlett and Youd (1992), there are 448 entries from 7 earthquakes:

- 1906 San Francisco, California
- 1964 Anchorage, Alaska
- 1964 Niigata, Japan
- 1971 San Fernando, California
- 1979 Imperial Valley, California
- 1983 Nihonkai-Chubu, Japan
- 1987 Superstition Hills, California

The data in the Bartlett and Youd (1992) database can be divided into four main categories:

- Ground displacement amplitude data
- Borehole data
- Ground-slope and free-face topographical data
- Seismic data

3.2.1 Seismic data

Table 1 summarizes the seismic parameters on the seven earthquakes in the database. There are minor variations in site specific parameters, i.e., epicentral distance (distance between the epicenter and location at which ground displacements are measured), and peak ground acceleration (PGA). During the earthquakes prior to 1979, the transient ground motion was poorly recorded, mainly because there were very few strong motion instruments deployed before 1979.

Table 3-1. Seismic parameters for earthquakes in Bartlett and Youd (1992) database.

Earthquake Name	Magnitude	PGA (g)	Epicentral distance (km)
1906 San Francisco Earthquake	7.9	0.28-0.26	13-27
1964 Alaska Earthquake	9.2	0.21-0.39	35-100
1964 Niigata, Japan Earthquake	7.5	0.19	21
1971 San Fernando Earthquake	6.4	0.55	1
1979 Imperial Valley Earthquake	6.5-6.6	0.21-0.51	2-6
1983 Nihonkai-Chubu, Japan Earthquake	7.7	0.25	27
1987 Superstition Hills Earthquake	6.6	0.21	23

3.2.2 Ground displacement amplitude data

Table 2 summarizes the number of data on ground displacement amplitudes per earthquake and site. For Bartlett and Youd (1992), a site is an area in which the measured displacement vectors can be regrouped to delineate a consistent slide. The vectors inside slide area are included in the database, while the vectors which are isolated or too distant from geotechnical boreholes, are excluded. The delineation of liquefaction-induced slides from aerial maps is not straightforward in

all cases, and requires some engineering judgement. It becomes difficult when there are a few displacement vectors and small displacement amplitudes. Figure 3 shows the distribution of displacement amplitude. In most instances, the amplitude of permanent ground deformation was measured directly from vector maps. The position coordinates and vector coordinates corresponding to each amplitude were however not defined, which make it difficult to verify the amplitude data from the original maps with a large number of vectors (e.g., data from Niigata and Noshiro).

Table 3-2. Distribution of ground deformation data in Bartlett and Youd (1992) database.

Earthquake Name	Number of Site	Number of vector
1906 San Francisco Earthquake	4	4
1964 Alaska Earthquake	5	7
1964 Niigata, Japan Earthquake	14	299
1971 San Fernando Earthquake	2	28
1979 Imperial Valley Earthquake	2	32
1983 Nihonkai-Chubu, Japan Earthquake	1	72
1987 Superstition Hills Earthquake	1	6

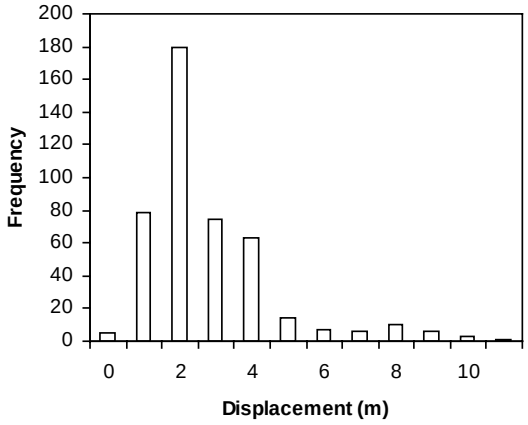

Figure 3-3. Distribution of vectors with amplitude in liquefaction-induced ground deformation database.

3.2.3 Slope and free face data

The ground slope and free-face data characterizes the geometry of ground surface at the location of the displacement vectors. This topographical data is related to the static shear loads that drive liquefaction-induced displacements. As shown in Fig. 4, the ground slope *S* is the inclination of the ground surface at the location of the displacement vector. As shown in Fig. 4, the free-face data is characterized by the free face ratio *H/L*, where *H* is the height of the free face (i.e., difference between crest elevation and toe elevation) and *L* the horizontal distance from the toe of free face to the displacement vector.

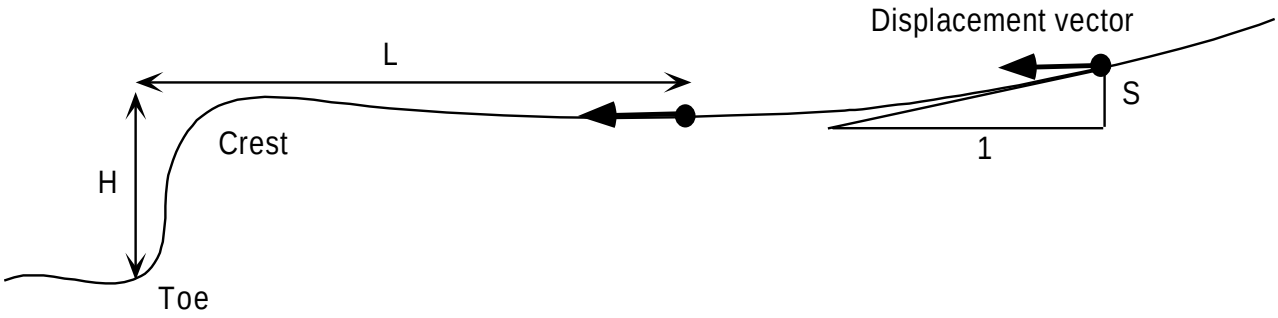

Figure 3-4. Definition of free-face ratio *H/L* and ground slope *S* in Bartlett and Youd (1992) database.

The distributions of ground-slope *S* and free-face ratio *H/L* are shown in Fig. 5. In most instances, this data has been obtained by measuring slopes on topographical maps by hand. The ground slope is measured from the elevation contours, and some control points whenever present. The free-face height and the distance to the free-face is also measured or estimated from topographical maps.

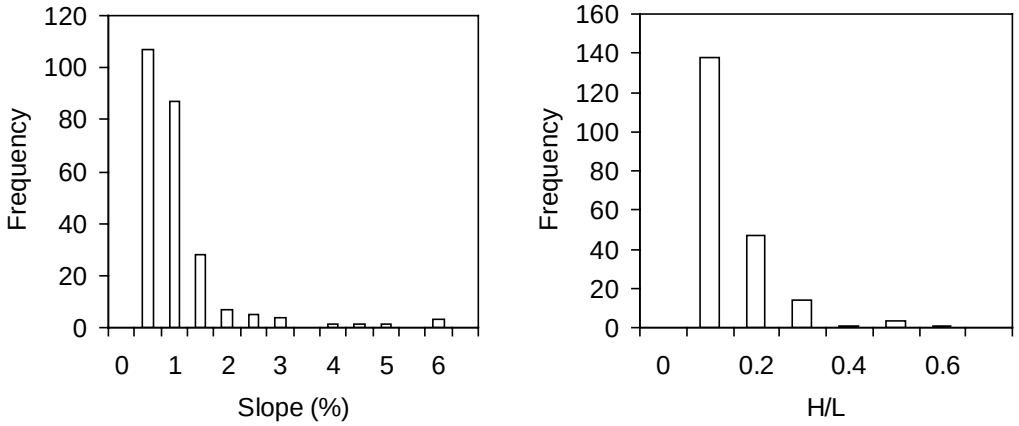

Figure 3-5. Distribution of ground slope *S* and free-face ratio *H/L* in Bartlett and Youd (1992) database.

3.2.4 Borehole data

The borehole data characterizes the geometry of soil profile and soil properties at the borehole location and its immediate vicinity. Table 3 summarizes the various types of borehole data and their number.

Table 3-3. Type and number of borehole data in Bartlett and Youd (1992) database.

Earthquake	Type of Samplar	Penetration	Number used	Reference
1906, San Francisco	2 Inch Sampler Assumed	SPT	1	*Youd and Hoose, 1978*
	Non Standard Sampler	SPT	2	*O'Rourke et al., 1991*
	2 Inch Standard Sampler	SPT	1	*Youd and Bennett, 1981*
1964, Alaska	2 Inch Standard Sampler	SPT	16	*Utermohle, 1963*
	Cpt Data Converted To Spt Data	CPT	2	*Bartlett and Youd, 1992*
	2 1/2 In. Penetrometer	NON STANDARD SPT	3	*Mcculloch and Bonilla, 1970*
	2 Inch Standard Sampler	SPT	6	*Mcculloch and Bonilla, 1970*
	1.4 Inch Sampler	SPT	1	*Mcculloch and Bonilla, 1970*
	2 Inch Sampler Assumed	SPT	3	*Bartlett and Youd, 1992*
1964, Niigata	2 Inch Sampler Assumed	SPT	119	*Unpublished Logs From Hamada*
1971, San Fernando	Ado Sampler	SPT	6	*Bennett, 1989*
	2 Inch Sampler Assumed	SPT	17	*O'Rourke et al., 1990*
1979, Imperial Valley	Cpt Data Converted To Spt	CPT	8	*Bennett et al., 1981*
	2 Inch Standard Sampler	SPT	7	*Bennett et al., 1981*
1983, Borah Peak, Id.	2 Inch Sampler Assumed	SPT	1	*Andrus et. al., 1991*
	2 Inch Standard Sampler	SPT	3	*Andrus and Youd, 1987*
1983, Nihonkai-Chubu	2 Inch Sampler Assumed	SPT	33	*Hamada et al., 1986*
1987, Superstition Hills	2 Inch Standard Sampler	SPT	5	*Bennett et al., 1984*
	Cpt Data Converted To Spt	CPT	5	*Bennett et al., 1984*

The parameters which characterizes borehole data are:

- N, the standard penetration blow count
- D_{50}, the mean grain diameter, and
- F, fines contents (percent by weight smaller than 75 μm)
- Visual soil classification and/or soil classification (e.g., USCS)

In geotechnical engineering, the blow count *N* is measured by counting the number of blows required to push a spilt barrel sampler 30 centimeters in the ground. The vertical resolution of the SPT data is therefore larger than 30 cm. However, Bartlett and Youd (1992) calculated the SPT blow counts at 10 cm interval by using linear interpolation, and introduced additional layers at the interfaces between two different soil layers to account for the sudden jump of blow count at interfaces.

In some instances, the blow counts *N* were not directly measured in the field but calculated from CPT data using correlations (e.g., Seed and DeAlba, 1986). The variations of fine contents and mean grain size with depth were obtained based on grain size distribution analysis, and engineering judgement. Based on our experience, the data on fine contents and grain size distribution is the most difficult data to reconstitute from the original soil reports. In some instances (e.g., samples lost during SPT sampling), this data had to be assumed in order to complete the analysis.

3.2.5 Determination of average soil properties at vector location

Bartlett and Youd (1992) define three average soil properties at the location of the displacement vectors: T_{15}, the cumulated thickness of saturated cohesionless soils having a blow count $N1_{60}$ smaller than or equal to 15; F_{15}, the average fine contents in the layer(s) of thickness T_{15}; and $D50_{15}$, the mean grain size in the layer(s) of thickness T_{15}). The values of T_{15}, F_{15} and $D50_{15}$ are first determined at the borehole location. The values of SPT blow count $N1_{60}$, fine contents *F* and

mean grain size *D50* are calculated for every 10 cm depth increment by interpolating the discrete borehole data. At each depth, a liquefaction analysis is performed to check whether $N1_{60}$ is smaller or equal to 15, and whether liquefaction occurs. When these two conditions are met, the average thickness T_{15} of liquefiable layers is incremented by 10 cm, and the values of *F* and *D50* are included to the average values F_{15} and $D50_{15}$.

Since boreholes and displacement vectors have usually different locations, Bartlett and Youd (1992) had to devise an interpolation scheme to determine the average soil properties at the location of the displacement vectors. As shown in Fig. 6, the average soil properties $\overline{X}$ at the location of the displacement vectors are calculated from the average soil properties X_i surrounding the displacement vector through the following weighted average:

$$\overline{X} = \sum_{i=1}^{n} \frac{X_i}{d_i \sum_{j=1}^{n} \left(\frac{1}{d_j} \right)} \tag{3.1}$$

where *n* is the number of boreholes used for averaging (the maximum value of *n* is 4), and d_i is the distance between the ith borehole and the displacement vector.

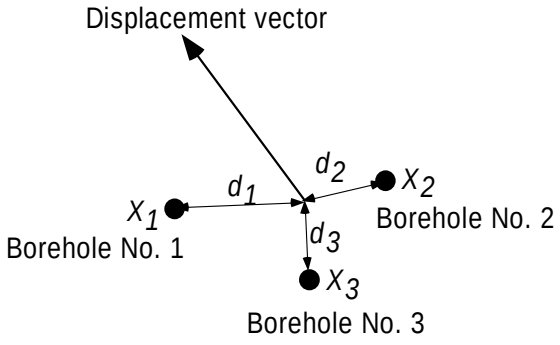

Figure 3-6. Relation of displacement vectors and boreholes (after Bartlett and Youd, 1992).

The displacement vectors obtained from field surveys and/or aerial photographs were selected from existing maps based on their significance and proximity to boreholes. Figure 7 shows the distribution of the minimum distance between the locations of displacement vectors and borehole data. In some cases, the minimum distance exceeds 400 m, which raises legitimate questions on the correlation between geotechnical and displacement data.

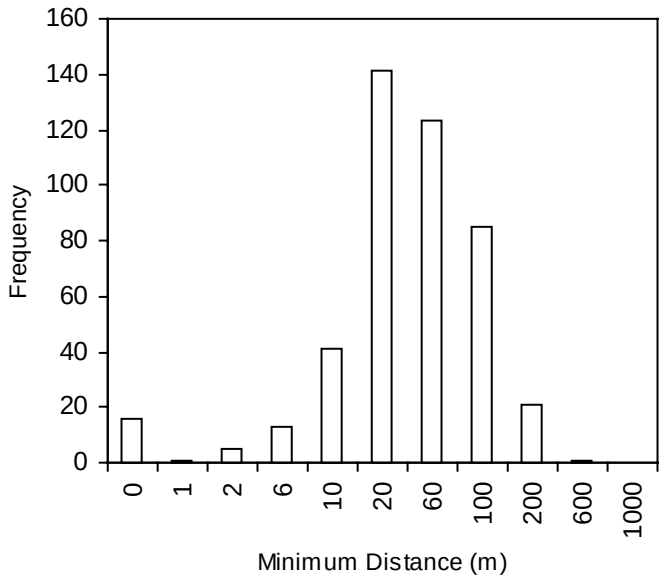

Figure 3-7. Minimum distance between location of boreholes and displacement vectors in Bartlett and Youd (1992).

3.2.6 Comparison of Harder (1991) and Bartlett and Youd (1992) databases

Figure 8 compares the databases of Harder (1991) and Bartlett and Youd (1992). Almost all cases of lateral spreading fall within the boundaries of liquefaction occurrence. The rare cases, for which lateral spreads occurred outside the accepted boundaries of liquefaction occurrence, deserve to be studied in detail. In default of detailed information on these particular cases, it is speculated that these lateral deformations were generated by the deformation of nearby liquefied soils. This explanation is consistent with the mechanism of ground deformation shown in Fig. 1-2.

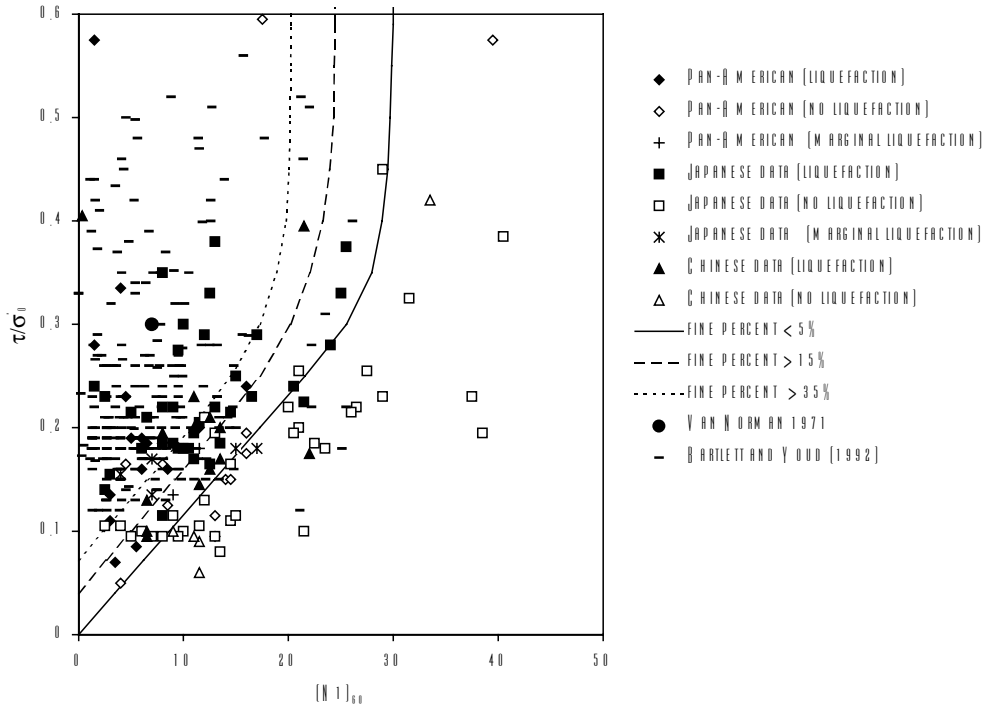

Figure 3-8. Comparison of databases of Harder (1991) and Bartlett and Youd (1998).

3.2.7 Parameters controlling ground deformation

Based on the examination of various parameters through statistical means, Bartlett and Youd (1992) identified the following parameters as controlling parameters of liquefaction induced ground deformation:

D	horizontal displacement (m)
M_w	moment magnitude
R	nearest horizontal distance (km) to seismic energy source or fault rupture
S	slope (%) of ground surface
W	free face ratio (%)
T_{15}	thickness (m) of saturated cohesionless soils (excluding depth >20 and >15% clay content) with $N1_{60}<15$
F_{15}	average fine content (% finer than 75 μm)
$D50_{15}$	average D_{50} grain size (mm) in T_{15}

Figure 9 shows the statistical distribution the parameters listed above in the Bartlett and Youd (1992) database. As shown in Fig. 9, some of these parameters (e.g., M_w, A_{max}, F_{15}, and $D50_{15}$) have a narrow value range, which introduces bias in the database.

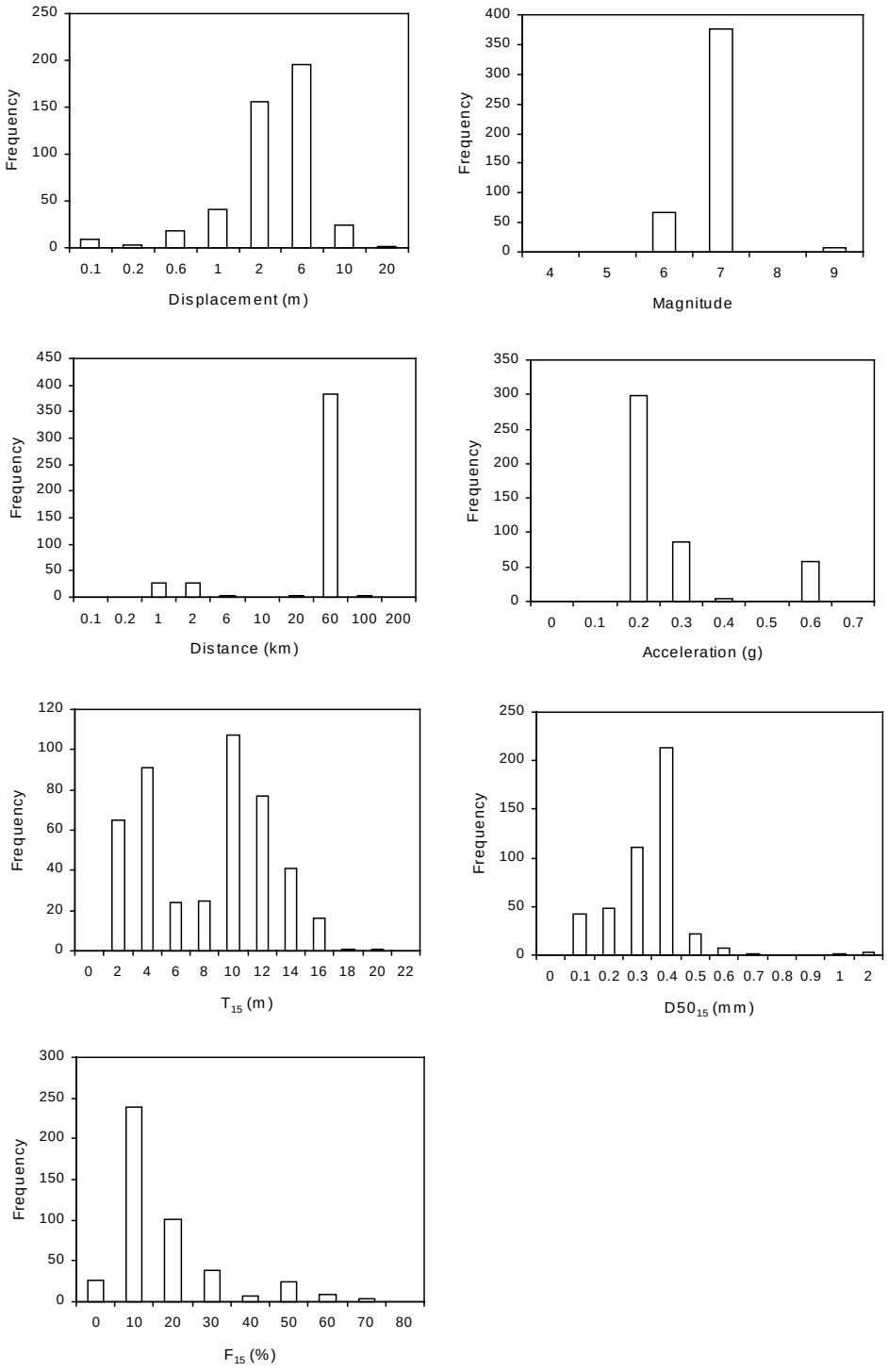

Figure 3-9. Bartlett and Youd (1992) database of liquefaction-induced lateral displacement: Distribution of main parameters including amplitude of displacement, earthquake magnitude, distance, peak ground acceleration, T_{15} thickness of soil zones with $N1_{60}$ <15, $D50_{15}$ average mean grain size in T_{15}, and F_{15} percent of fines in T_{15}.

3.3 Liquefaction-Induced lateral spread database (Rauch, 1997)

Rauch (1997) extended the Bartlett and Youd (1992) database, and added data from the following earthquakes:

- 1923 Kanto, Japan
- 1989 Loma Prieta, California
- 1990 Luzon, Philipipines
- 1991 Telire-limon, Costa Rica
- 1993 Hokkaido Nansei-oki, Japan
- 1994 Northridge, California

Like Bartlett and Youd (1992), Rauch (1997) delineates liquefaction-induced slides from the map of displacement vectors, and annotations on ground cracking. As shown in Fig. 10, the individual displacement vectors are regrouped to delineate slides. As previously mentioned, the delineation of slides from aerial maps becomes difficult and subjective when the displacement vectors are scarce and have small amplitudes. Figure 11 show the histograms of the slide area, slide length, number of vectors per slide, and number of boreholes per slide in Rauch (1997) database. The slide areas vary from 0.08 to 0.864 km^2, while the slide lengths vary from 20 to 1360 m. As shown in Table 4, there is a total of 78 slides, and 1385 vectors.

Whereas Bartlett and Youd (1992) delineate slides only for including or excluding displacement vectors in their database, Rauch (1997) define for each slide the average and standard deviation of displacement vectors, and average borehole properties. In some instances, there are unfortunately not enough vectors and borehole data for a specific slide, and the statistical quantities become meaningless. The databases of Bartlett and Youd (1992) and Rauch (1997) are based on almost the same field measurements, i.e., use the same displacement vectors, borehole data, seismic parameters, and topographic information. However, they use different variables to characterize liquefaction-induced ground deformation. Bartlett and Youd (1992) consider individual displacement vectors and average soil properties at the vector locations, while Rauch (1997) considers average deformation of liquefaction-induced slides and averages soil properties within these slides.

Table 3-4. Number of field measurements and data points in Bartlett and Youd (1992) and Rauch (1997) databases.

Quantity	Bartlettand Youd (1992)	Rauch (1997)
Data points	448	78
Boreholes	267	248
Displacement vectors	448	1385

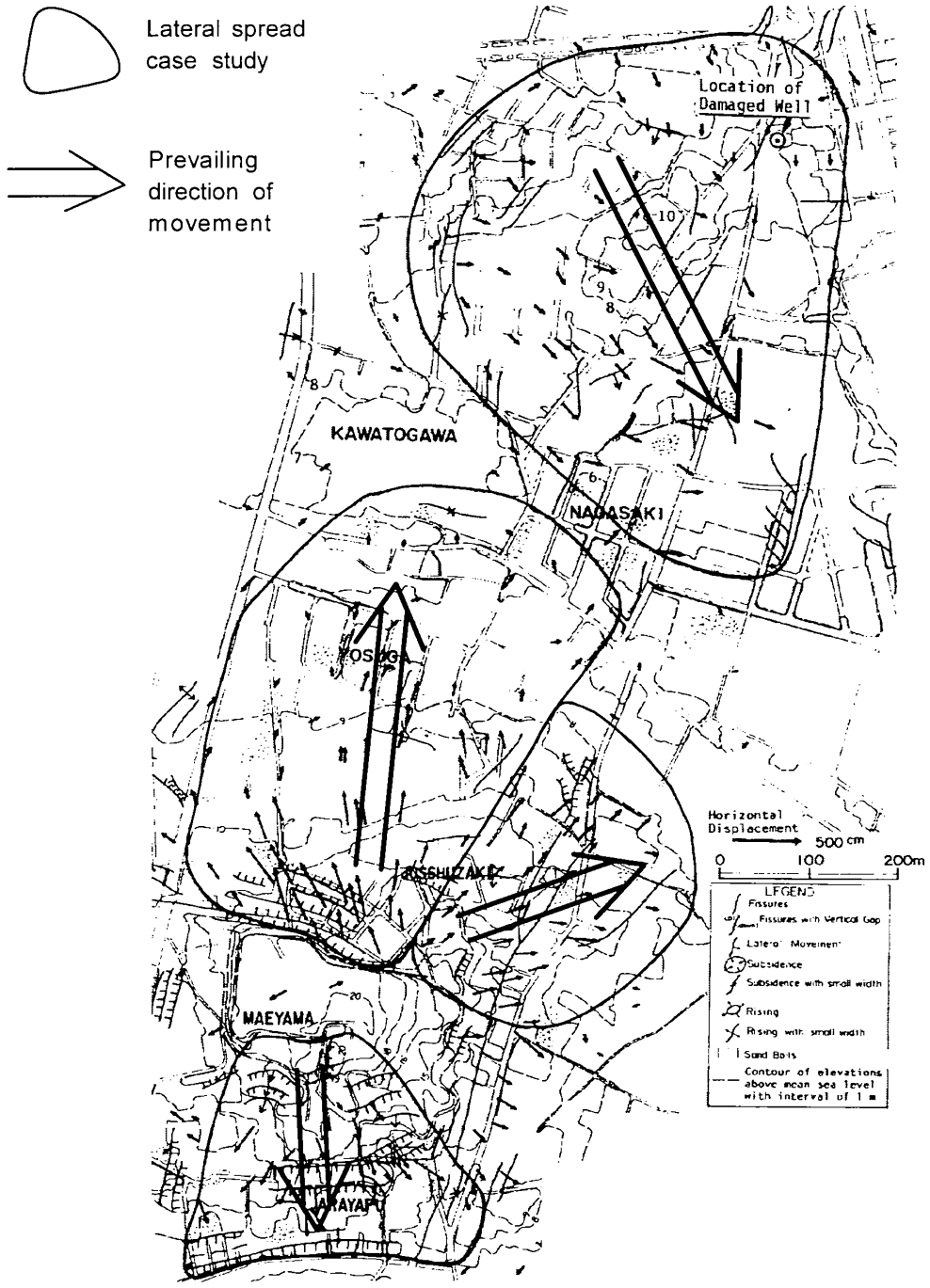

Figure 3-10. Delineation of four lateral spreads in Noshiro, Japan, in Rauch (1997) database.

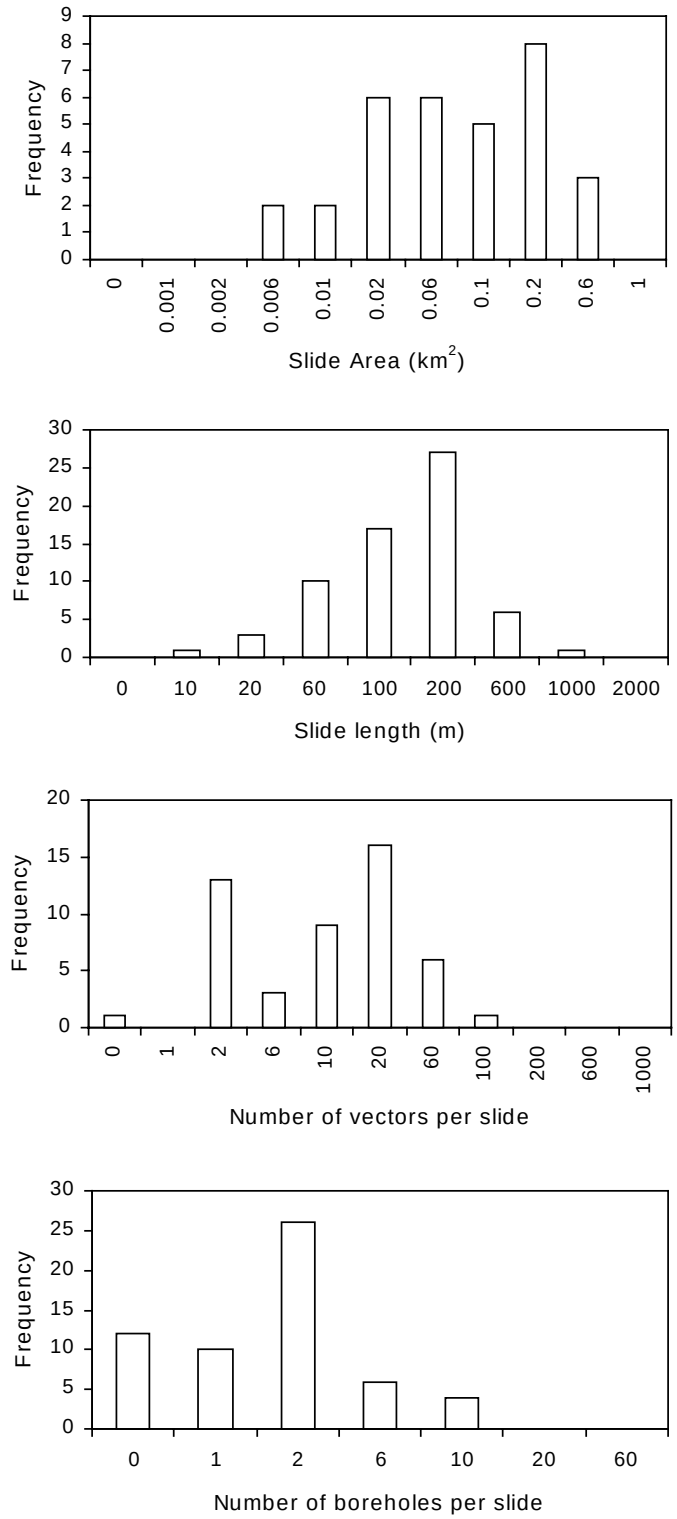

Figure 3-11. Rauch (1997) database of liquefaction-induced lateral displacement: Distributions of slide area, slide length, number of displacement vectors per slide and number of boreholes per slide.

4. REVIEW OF EMPIRICAL MODELS

In geotechnical earthquake engineering practice, liquefaction-induced ground deformations are usually estimated using three different types of empirical models which predict separately (1) the occurrence of liquefaction (e.g., Seed et al., 1985), (2) the ground settlement (e.g., Ishihara, 1996), and (3) the lateral ground deformation (e.g., Hamada et al., 1986; Pease and O'Rourke, 1993; Youd and Perkins, 1987; and Barlett and Youd, 1995). There are four basic models for assessing liquefaction-induced lateral displacements:

- Youd and Perkins (1987) LSI model
- Hamada (1986)
- Bartlett and Youd (1992) model
- Rauch (1997) model

4.1 Youd and Perkins (1987) LSI model

The LSI model has similarities to attenuation curves for peak ground acceleration. It relates the amplitude of horizontal ground deformation to distance from seismic energy source and moment magnitude as follows:

$$\log LSI = -3.49 - 1.86 \log R + 0.98 M_w \qquad (4.1)$$

where LSI is the general maximum amplitude of ground failure displacement (inch), R is the horizontal distance (km) to seismic energy source, and M_w is the earthquake moment magnitude.

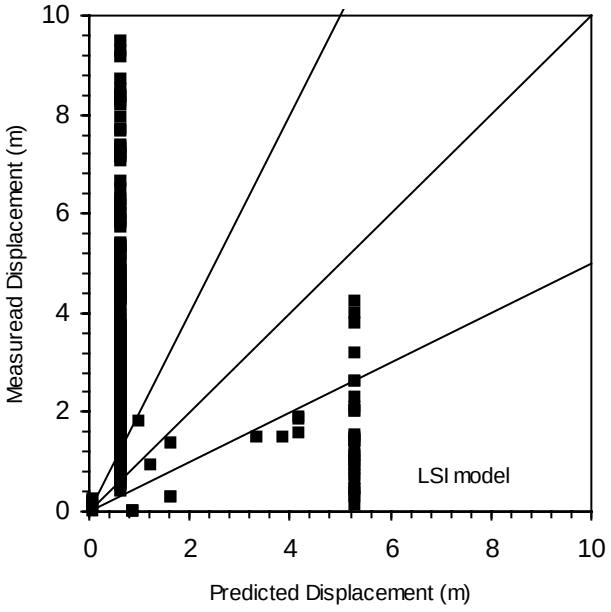

Figure 4-1. LSI model (Youd and Perkins, 1987): measured versus predicted liquefaction-induced lateral displacement (data points from Bartlett and Youd (1992) database).

Figure 1 shows the comparison between the measured displacements and those calculated using Eq. 1 for all the entries in the Bartlett and Youd (1992) database. The points should fall on the line with a 1:1 slope for a perfect prediction, and on the lines with 1:0.5 and 1:2 slope when the prediction is half or twice the measured value, respectively. As shown in Fig. 1, there is a poor agreement between measured and calculated displacements, which implies that distance R and magnitude M_w are not sufficient for predicting liquefaction-induced displacement.

4.2 Hamada et al. (1986)

Hamada et al (1986) predict the amplitude of horizontal ground deformation only in terms of slope and thickness of liquefied layer:

$$D = 0.75\, H^{0.5} \theta^{0.33} \tag{4.2}$$

where D is the horizontal displacement (m), θ is the slope (%) of ground surface or base of liquefied soil, and H is the thickness (m) of liquefied soil

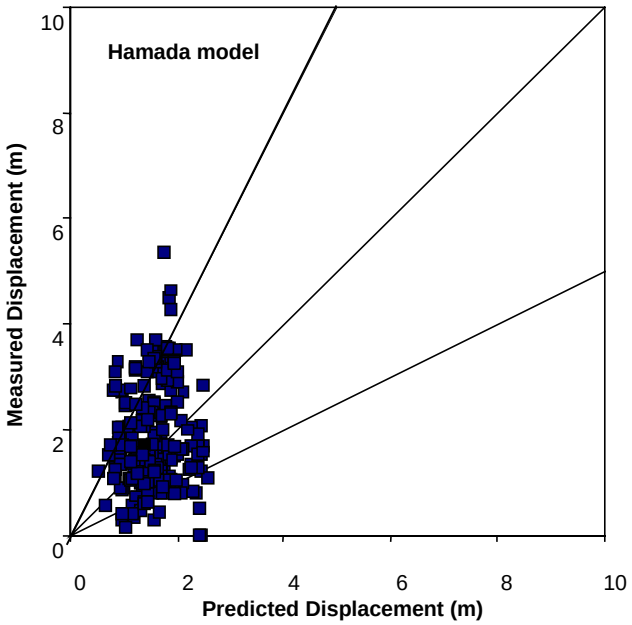

Figure 4-2. Hamada model (Hamada et al., 1986) for ground slope: measured versus predicted liquefaction-induced lateral displacement (data points from Bartlett and Youd (1992) database).

The Hamada model is only based on topographic and geotechnical parameters (i.e., S and H), and no seismic parameters (e.g., R and M_w). Figure 2 shows the comparison of measured displacement with those calculated using Eq. 2 for the ground-slope entries in the Bartlett and Youd (1992) database. In this comparison, the liquefied thickness H was assumed to be equal to T_{15}, the cumulated thickness of zones with $N1_{60}$ smaller than 15.

4.3 Bartlett and Youd (1992) MLR model

Bartlett and Youd devised two separate models: one for ground slope of infinite extent, and the other for free face:
Ground slope

$$\log (D+0.01) = -15.787+1.178\, M_w-0.927\, \log R -0.013\, R + 0.429 \log S + 0.348 \log T_{15} + 4.527 \log(100-F_{15})-0.922\, D50_{15} \quad (4.3)$$

Free face

$$\log (D+0.01) = -16.366+1.178\, M_w-0.927\, \log R -0.013\, R + 0.657 \log W + 0.348 \log T_{15} + 4.527 \log(100-F_{15})-0.922\, D50_{15} \quad (4.4)$$

where

D	horizontal displacement (m)
M_w	moment magnitude
R	nearest horizontal distance (km) to seismic energy source or fault rupture
S	slope (%) of ground surface
W	free face ratio (%)
T_{15}	thickness (m) of saturated cohesionless soils (excluding depth >20 and >15% clay content) with $N1_{60}<15$
F_{15}	average fine content (% finer than 75 μm)
$D50_{15}$	average D_{50} grain size (mm) in T_{15}

As shown in Fig. 3, most of the model predictions are scattered within the lines with 1:0.5 and 1:2 slope, while they should fall close to the line with a 1:1 slope for a perfect prediction.

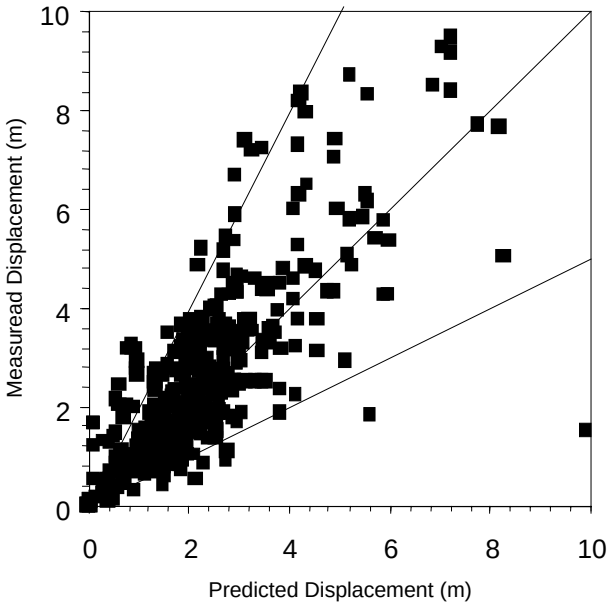

Figure 4-3. Bartlett and Youd (1992) model: measured versus predicted liquefaction-induced lateral displacement (data points from the database of Bartlett and Youd, 1992).

4.4 Rauch (1997) models

Rauch (1997) considered liquefaction-induced ground deformation as slides of finite area, instead of individual displacement vectors. He applied multiple-linear-regression methods to these liquefaction-induced slides. Rauch proposed three different models for the average lateral ground displacement, which are referred to as regional, site and geotechnical:

Regional average

$$D = (D_R - 2.21)^2 + 0.149 \quad (4.5a)$$

$$D_R = (613\ M_w - 13.9\ R_f - 2420\ A_{max} - 11.4\ T_d)/1000 \quad (4.5b)$$

D average horizontal displacement (m)
R_f shortest horizontal distance (km) to fault rupture
M_w moment magnitude
A_{max} peak horizontal acceleration (g) at ground surface
T_d duration (s) of strong earthquake motions (>0.05g)

Site average

$$D = (D_R + D_S - 2.44)^2 + 0.111 \quad (4.6a)$$

$$D_S = (0.523\ L_{slide} + 42.3\ S_{top} + 31.3\ H_{face})/1000 \quad (4.6b)$$

L_{slide} length (m) of slide area from head to toe
S_{top} average slope (%) across the surface of lateral spread
H_{face} height of free face (m) measure vertically from toe to crest

Geotechnical average

$$D = (D_R + D_S + D_G - 2.49)^2 + 0.124 \quad (4.7a)$$

$$D_S = (50.6\ Z_{FSmin} - 86.1\ Z_{liq})/1000 \quad (4.7b)$$

Z_{FSmin} average depth (m) corresponding to minimum factor of safety
Z_{liq} average depth (m) to top of liquefied layer

Figure 4 shows the comparison of measured versus calculated average displacements, using the entries of Rauch (1997) database. As shown in Fig. 4, there are less data points in Rauch's database than in Bartlett and Youd's database, because the data on average slide displacement is less abundant than data on individual displacement vectors. As shown in Fig. 4, there is a poor agreement between measurement and prediction.

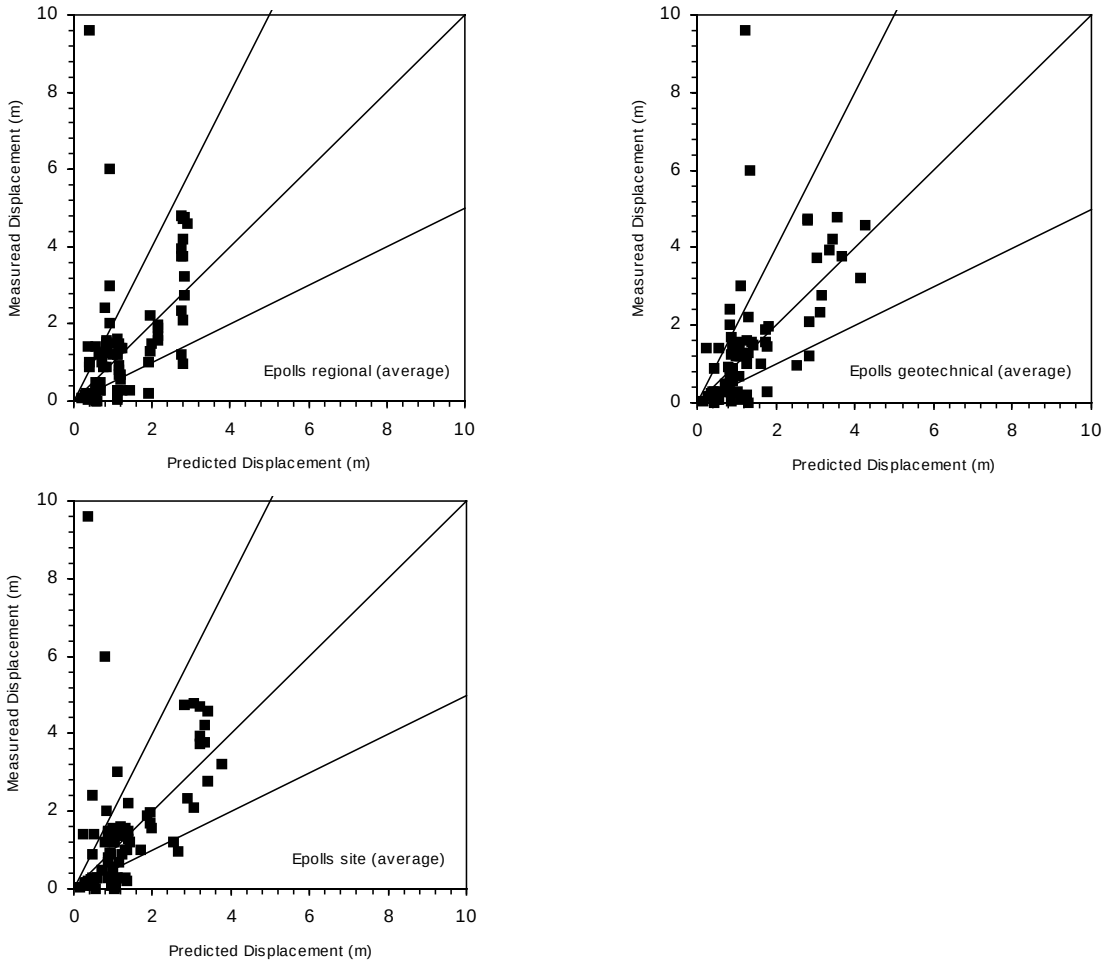

Figure 4-4. Regional, site and geotechnical models (Rauch, 1997): measured versus calculated average displacements (data points form Rauch (1997) database).

Rauch (1997) also proposed the following three models for characterizing the standard deviation from the average predictions of displacement:

$\sigma_D = 0.589\ D$ Regional standard deviation (4.11)

$\sigma_D = 0.560\ D$ Site standard deviation (4.12)

$\sigma_D = 0.542\ D$ Geotechnical standard deviation (4.13)

These standard deviations describe the variation of displacement amplitude about the average displacement of a slide.

4.5 Comparison of existing models

The empirical models of liquefaction-induced lateral spreads relate selected physical parameters by fitting data points with a multiple linear regression. Their parameters are of seismological, topographical or geotechnical origins.

4.5.1 Seismological parameters

Youd and Perkins (1987) and Bartlett and Youd (1992) characterize the ground motion at a given site by using two parameters:

- R horizontal distance (km) to seismic energy source, and
- M_w moment magnitude of earthquake.

whereas Rauch (1997) requires four seismic parameters

- R_f shortest horizontal distance (km) to fault rupture
- M_w moment magnitude
- A_{max} peak horizontal acceleration (g) at ground surface
- T_d duration (s) of strong earthquake motions (>0.05g)

In the models of liquefaction occurrence (e. g., Idriss and Youd, 1998), the ground motion is characterized by only two parameters:

- M_w moment magnitude
- A_{max} peak horizontal acceleration (g) at ground surface

The cyclic stress ratio τ/σ'_0 is proportional to A_{max}, and increases with M_w (Youd and Idriss, 1998). Therefore the potential for occurrence of liquefaction increases with A_{max} and M_w.

In the Rauch regional model (Eq. 5), the amplitude of lateral spread D decreases unrealistically with A_{max}, which may result from the dependence on M_w, A_{max} and T_d. The Rauch model is therefore applicable within a particular range of seismic parameters, and may give unrealistic predictions outside this range. For instance, Table 1 gives examples for which Rauch overestimates D in cases of unlikely liquefaction. In these cases, LSI model gave reasonable predictions.

Table 4.1. Examples of unrealistic predictions by Rauch (1997) model.

				Rauch(1997)	LSI
M_w	A_{max} (g)	R_f (km)	T_d (sec)	D (m)	
4	0.01	1	0.1	0.19	0.07
5	0.01	10	1	0.61	0.01
5	0.05	10	1	0.49	0.01

It would be logical to use the same seismic parameters for models of liquefaction occurrence and liquefaction-induced deformation, i.e., M_w and A_{max}. However, there is a definite bias in the database, which is demonstrated in Fig. 5 by the decrease of displacement D with increasing peak ground acceleration A_{max}. Bartlett and Youd (1992) avoided this problem by using R instead of A_{max} in their model.

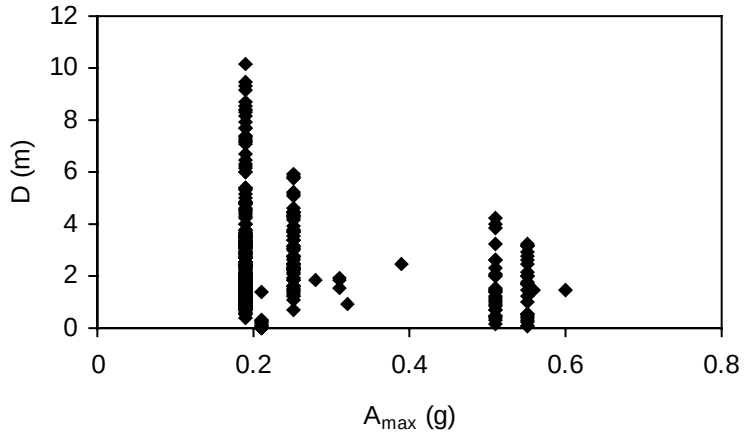

Figure 4-5. Variation of peak ground acceleration with lateral ground deformation in Youd and Bartlett (1992) database.

4.5.2 Topographical parameters

The topographical parameters used by Bartlett and Youd (1992) are:

S	slope (%) of ground surface
W	free face ratio (%)

while those of Rauch (1997) are:

L_{slide}	length (m) of slide area from head to toe,
S_{top}	average slope (%) across the surface of lateral spread, and
H_{face}	height of free face (m) measure vertically from toe to crest

Rauch (1997) use non symmetric distribution for modeling the systematic decrease in displacement amplitude with distance away from free-faces, which has been well-documented after the 1995 Hyogoken-Nanbu earthquake (e.g., Fig. 6).

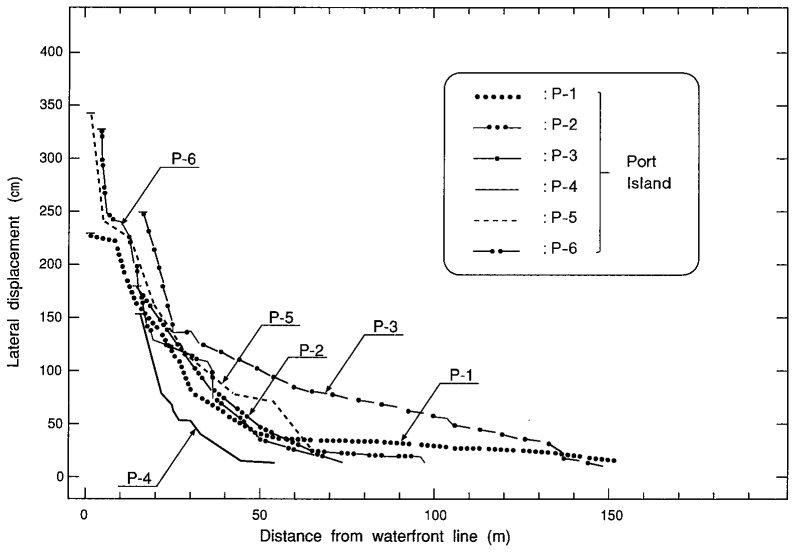

Figure 4-6. Typical variation of liquefaction-induced displacement behind quaywalls in Port Island after the 1995 Hyogoken-Nanbu earthquake (Ishihara et al., 1996, 1997).

4.5.3 Geotechnical parameters

The geotechnical parameters used by Bartlett and Youd (1992) are:

- T_{15} thickness (m) of saturated cohesionless soils (excluding depth > 20 m and clay content >15%) with $N1_{60}<15$
- F_{15} average fine content (% finer than 75 μm)
- $D50_{15}$ average D_{50} grain size (mm) in T_{15}

while those of Rauch (1997) are:

- Z_{FSmin} average depth (m) corresponding to minimum factor of safety
- Z_{liq} average depth (m) to top of liquefied layer

Rauch's parameters are derived from liquefaction analyses, whereas those of Bartlett and Youd are directly obtained from borehole measurements.

5. MLR MODELS FOR LIQUEFACTION-INDUCED GROUND DEFORMATION

Based on the review and comparison of empirical existing models and databases, it was decided to model liquefaction-induced ground displacement using a MLR approach similar to that of Bartlett and Youd (1992), and to use the most recent database of liquefaction-induced ground deformation (Bartlett, 1998).

5.1 Selection of database

The new database (Bartlett, 1998) was corrected for some digitizing errors on displacement vectors in the original database (Bartlett and Youd, 1992). As shown in Fig. 1, the difference between the new and old databases is significant enough to be detectable from the histograms of displacement amplitude. As shown later, the difference in data will lead to MLR models slightly different from that of Bartlett and Youd (1992).

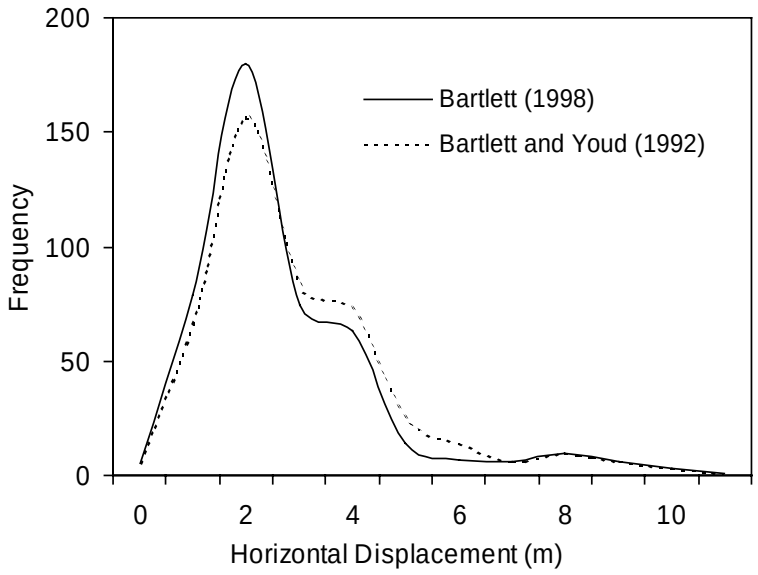

Figure 5-1. Comparison of histograms of displacement amplitude for original database (Bartlett and Youd, 1992) and corrected database (Bartlett, 1998) on liquefaction-induced lateral displacement.

The data in the new database was divided in two data sets: (a) complete data for all ranges of displacement amplitude; and (b) data limited to displacement amplitudes smaller than 2 meters. The former data set will be referred to as A, and the latter as B. The latter data set, in which displacement amplitudes in excess of 2 m were excluded, was intended to be more relevant to engineering design. Amplitudes in excess of 2 m were assumed to be too large for accurate measurement, and to cause excessive ground damage impractical to mitigate. Table 1 gives the number of entries in data sets A and B, with their respective partition in free-face and ground slope cases.

Table 5-1. Data sets used in MLR models

Notation	Definition	Number of data points
A	All data	467
	All free-face (FF) data	213
	All ground slope (GS) data	254
B	All data with displacement smaller than 2 m	283
	Free-face (FF) data with displacement smaller than 2 m	118
	Ground slope (GS) data with displacement smaller than 2 m	165

5.2 Selection of variables and models

The identification of controlling variables is a critical step in MLR analysis. The controlling parameters in the MLR analysis were identified as those of Bartlett and Youd (1992) after careful consideration of other combinations of variables. One of the main criteria for selecting variables was their direct relation to measured data, with as little influence as possible from analysis. For instance, the thickness T_{15} can be directly obtained from SPT profiles. In contrast, the average depth corresponding to minimum factor of safety Z_{Fsmin}, which is used by Rauch (1997), depends on liquefaction analysis. Given the limitations of the seismic and geotechnical data in the existing database, combinations of variables other than those used by Bartlett and Youd (1992) did not seem promising. However, future MLR studies will need to examine other combinations of variables as other types of entries (e.g., CPT data) are made to the database.

Table 2 lists all the variables used in the MLR modeling. There is a total of 6 independent variables. The free-face ratio *W* and ground slope *S* are independent variables, which are not used simultaneously. The present MLR modeling assumes that liquefaction-induced deformation depends on the distance *L* to the free face divided by the free-face height *H* in close proximity of the free face, and not on ground slope. The distinction between free-face and ground slope conditions may not always be obvious in all circumstances. It is still unclear how far the free-face effects can extend from free faces, and how they combine with ground slope effects.

Table 5-2. List of controlling variables for MLR analysis.

Notation	Definition
D_H (m)	Amplitude of ground deformation (Output)
M	Earthquake moment magnitude
R (km)	Closest distance to source
W	Free face ratio $W = 100H/L$ *L*: Distance to the free face from the point of displacement in m *H:* Height of free face in m)
S (%)	Ground slope
T_{15} (m)	Thickness of saturated cohesionless soils with $(N1)_{60}<15$
F_{15} (%)	Average fines content (<75 μm) in layer of thickness T_{15}
$D50_{15}$ (mm)	Average mean grain size D_{50} in layer of thickness T_{15}

Table 3 shows the range of values for the MLR variables in the data sets A and B, and their corresponding free-face and ground-slope data subsets. The data set are referred to as *FF, GS* and *FFGS*, which stands for Free-Face, Ground-Slope, and Free-Face & Ground-Slope, respectively. In data set A, the maximum ground-slope displacement (i.e., 5.35 m) is half the maximum free-face displacement. In data set B, both maxima are set equal to 2 m. The range of variables *M, R, W, S,* T_{15}, F_{15} and $D50_{15}$ are almost identical for data sets A and B, and their free-face and ground-slope subsets. Table 3 is useful to define the domain of applicability of MLR models. It is not recommended to use MLR models for variable values that fall outside the ranges of Table 3.

Table 5-3. Range of values for MLR variables in data sets A and B, and their free-face and ground-slope subsets.

	Data Set A			Data Set B		
Variables	Complete FFGS-A	Free-Field FF-A	Ground-Slope GS-A	Complete FFGS-B	Free-Field FF-B	Ground-Slope GS-B
DH (m)	0 - 10.15	0 - 10.15	0 - 5.35	0-1.99	0-1.98	0-1.99
M	6.4 - 9.2	6.4 - 9.2	6.4 - 9.2	6.4 - 9.2	6.4 - 9.2	6.4 - 9.2
R (km)	0.2 - 100	0.5 - 100	0.2 - 100	0.2 - 100	0.5 - 100	0.2 - 100
W_{ff}	1.64 - 55.68	1.64 - 55.68	-	1.64 - 48.98	1.64 - 48.98	-
S (%)	0.05 - 5.90	-	0.05 - 5.90	0.05 - 2.5	-	0.05 - 2.5
T_{15} *(m)*	0.2 - 19.7	0.2 - 16.7	0.7 - 19.7	0.2 - 19.7	0.2 - 13.6	0.7 - 19.7
F_{15} *(%)*	0 - 70	2 - 70	0 - 68	0 - 70	3 - 70	0 - 68
$D50_{15}$ *(mm)*	0.04 - 1.47	0.04 - 1.47	0.06 - 1.19	0.04 - 1.47	0.04 - 1.47	0.06 - 1.19

Figures 2 to 9 show the distribution of variable values over their respective ranges. As shown in Fig. 2, ground displacements are much larger in the case of free-face than in the case of ground slope.

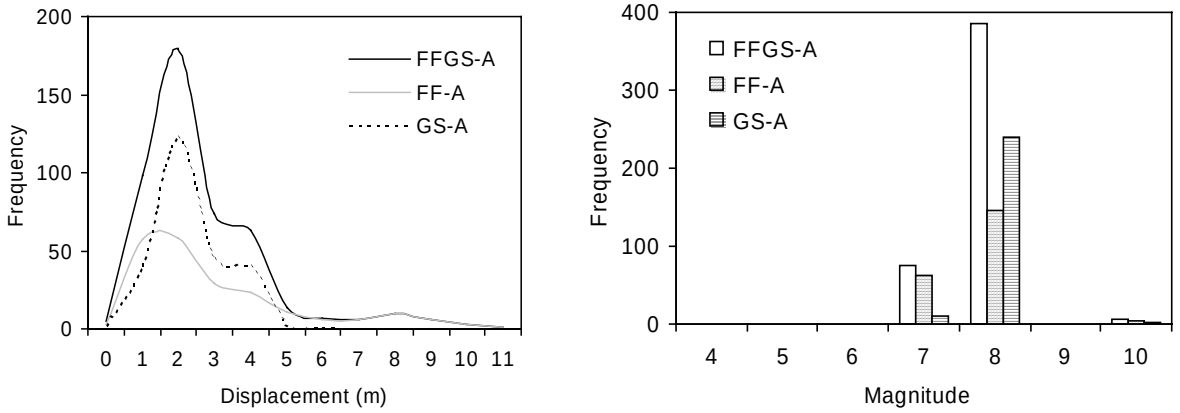

Figure 5-2. Histograms of displacement-amplitudes and earthquake-magnitudes in data sets FFGS-A, FF-A and GS-A.

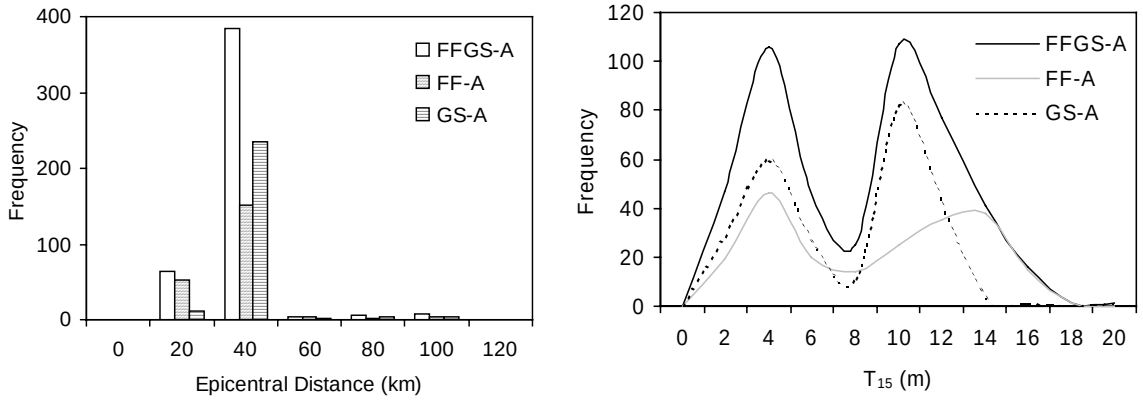

Figure 5-3. Histograms of epicentral distance and thickness T_{15} in data sets FFGS-A, FF-A and GS-A.

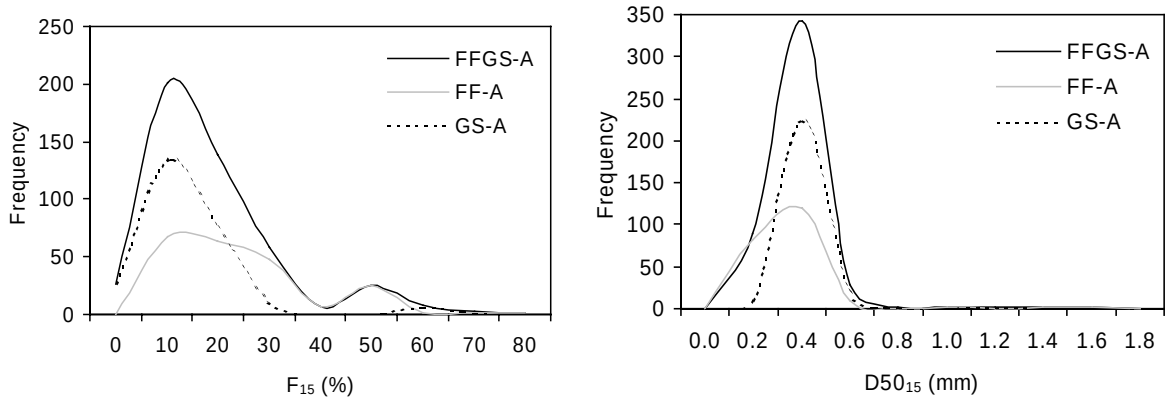

Figure 5-4. Histograms of fine contents F_{15} and mean grain size $D50_{15}$ in data sets FFGS-A, FF-A and GS-A.

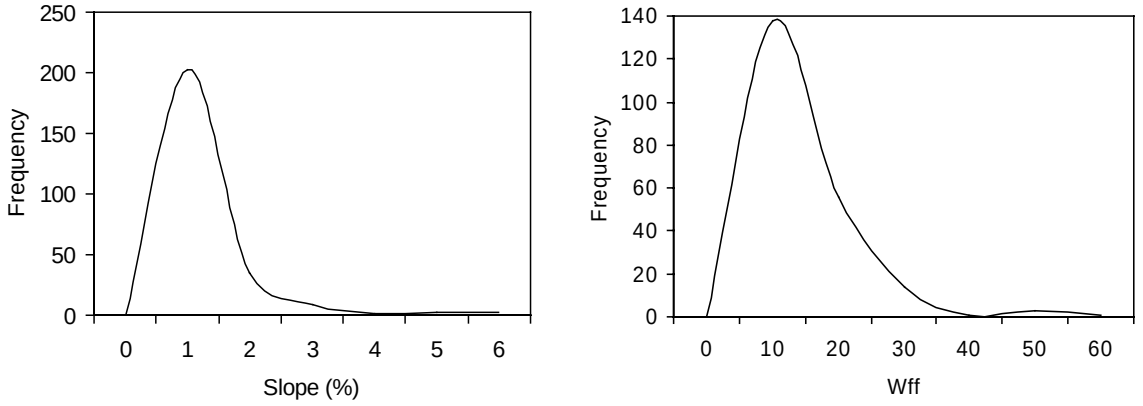

Figure 5-5. Histograms of ground-slope and free-face ratio in data set A.

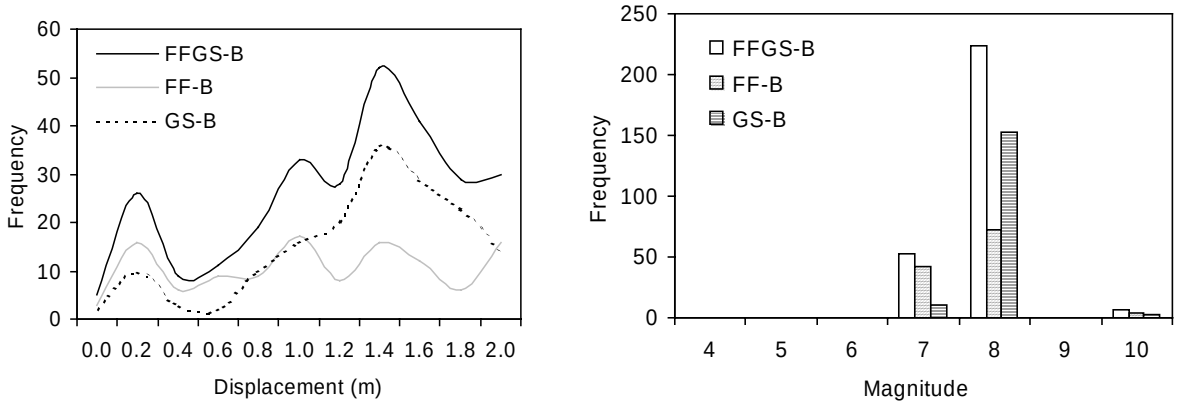

Figure 5-6. Histograms of displacement-amplitude and earthquake magnitude in data sets FFGS-B, FF-B and GS-B.

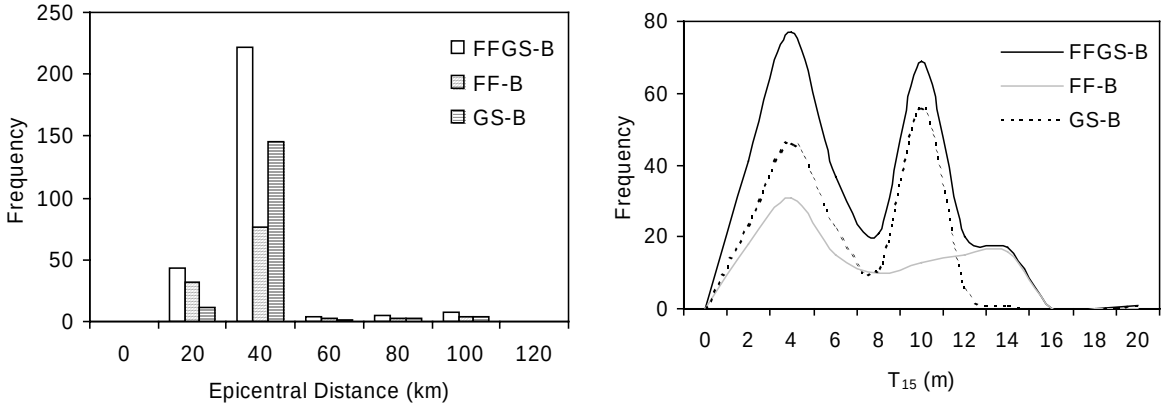

Figure 5-7. Histograms of epicentral distance and thickness T_{15} in data sets FFGS-B, FF-B and GS-B.

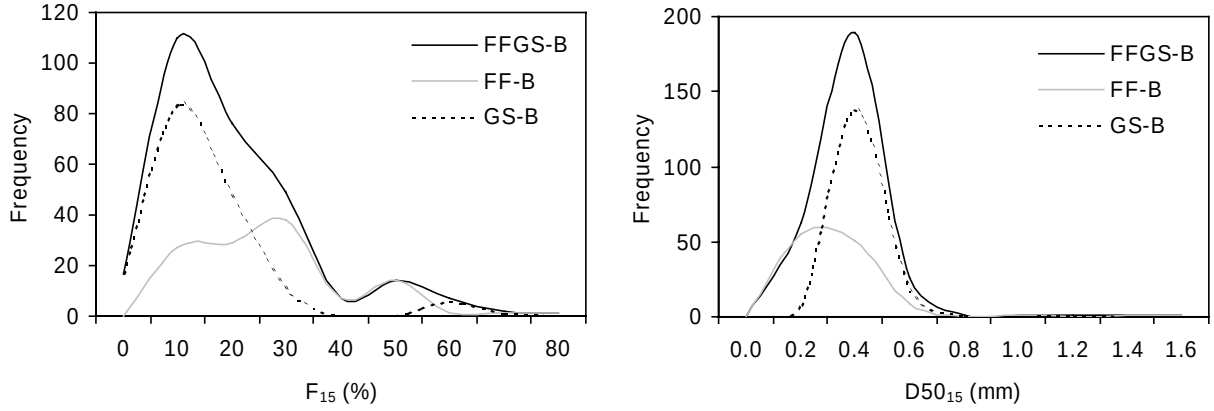

Figure 5-8. Histograms of fine contents F_{15} and mean grain size $D50_{15}$ in data sets FFGS-B, FF-B and GS-B.

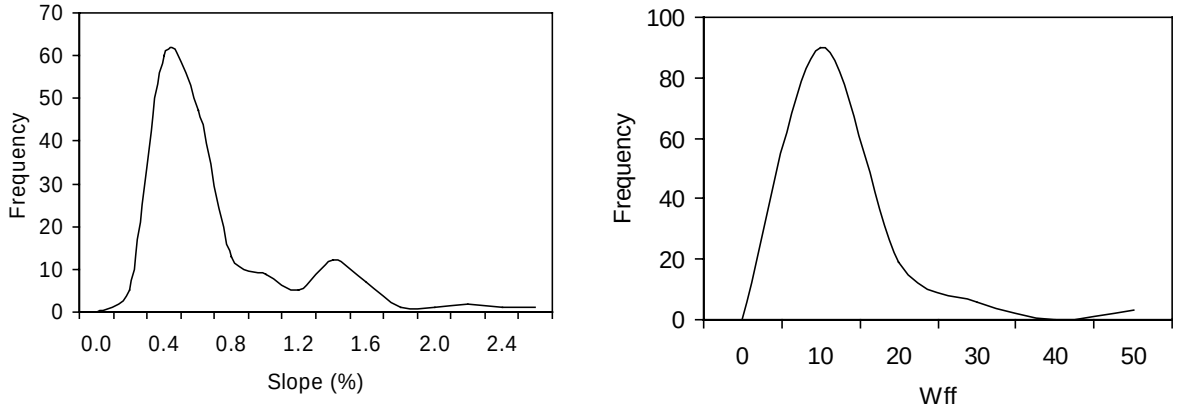

Figure 5-9. Histograms of ground-slope and free-face ratio in data set B.

As shown in Table 4, the variables were combined to form six different MLR models, which are designated *FFGS4, FF6, GS6, FFGS4, FF4*, and *GS4*. As previously defined, *FF, GS* and *FFGS* stand for Free-Face, Ground-Slope, and Free-Face & Ground-Slope, respectively. The variables related to mean grain size and fine contents (i.e., $D50_{15}$ and F_{15}) are average geotechnical parameters, which are rather difficult to determine precisely over large areas. For this reason, simpler MLR models with only 4 variables are proposed. These six models will be calibrated using the data sets A and B, therefore producing a total of 12 different MLR models.

Table 5-4. List of MLR models developed in present study.

Notation	Definition	Number of variables	Variables
FFGS6	Combined Free-Face and Ground-Slope MLR model	6	*M, R, W (*or *S) T_{15}, F_{15},* and *$D50_{15}$*
FF6	Free-Face MLR model	6	*M, R, W, T_{15}, F_{15},* and *$D50_{15}$*
GS6	Ground-Slope MLR model	6	*M, R, S, T_{15}, F_{15},* and *$D50_{15}$*
FFGS4	Combined Free-Face and Ground-Slope MLR model	4	*M, R, W (*or *S), T_{15}*
FF4	Free-Face MLR model	4	*M, R, W, T_{15}*
GS4	Ground-Slope MLR model	4	*M, R, S, T_{15}*

5.3 Six-parameter MLR models

The amplitude D_H of ground deformation will be estimated by using the same generic MLR relations as Barlett and Youd (1992):

$$Log(D_H + 0.01) = b_0 + b_{off} + b_1 M + b_2 Log(R) + b_3 R + b_4 Log(W_{ff}) + b_5 Log(S_{gs}) + b_6 Log(T_{15}) + b_7 Log(100 - F_{15}) + b_8 D50_{15} \quad (5.1)$$

where the variables *M, R, W, S, T_{15}, $D50_{15}$,* and F_{15} are defined in Table 2, and the values of the ten constant coefficients - b_0, b_{off}, and b_1 to b_8 - are given in Table 5. The relation in Eq. 5.1 corresponds to Eq. 4.1.9 in Bartlett and Youd (1992). It is general enough to apply to all types of ground deformation, including free-face and ground-slope cases. In the free-face cases, the term *Log(S)* is set equal to zero. In the ground slope cases, the term *Log(W)* is set equal to zero. The coefficient b_{off} only applies to the free-face cases, and is set equal to zero in the ground slope cases. In order to differentiate the free-field and ground-slope cases in the MLR analysis, the additional discrete variable *X* is introduced. The value of X is set equal to 1 for free-field case (i.e., *Log(S)* = 0) and 0 for ground-slope cases (i.e., *Log(W)* = 0).

The values of the *b*-coefficients were obtained by performing a regression analysis with the regression program Minitab (1989) and the "Data Analysis" tool package of Microsoft Excel (1994). Both methods of analysis gave identical results. The Minitab results of all the analyses are given in Appendix C. As shown in Table 5, the values of the coefficients for FFGS6 model are slightly different from those of Bartlett and Youd (1992) due to the difference of data in the new database and that used by Bartlett and Youd (1992). The coefficient values were found to be exactly identical to those of Bartlett and Youd (1992) when the old database was used.

In the FFGS6 models, the coefficients b_1, b_2, and b_3, which control the magnitude-dependent attenuation of liquefaction-induced displacements with distance, are the same for free-face and ground-slope cases. The attenuation relation for large distance is largely controlled by the additional data points from Ambraseys (1988). The model FFGS6 was calibrated for data sets A and B, therefore producing model FFGS6-A and FFGS6-B. As shown in Table 5, the coefficient values of these two models are similar, and their adjusted R^2 values are 80.6% and 81.1%, respectively. The R^2 coefficient, which measures the accuracy of the multiple linear regression, is adjusted to account for the difference in the number of data points in data sets A and B. Based on the results of Table 5, it is concluded that models FFGS6-A and -B fit data sets A and B with similar accuracy.

Two other MLR models - FF6 and GS6 - were calibrated to examine the free-field and ground-slope cases. The formula for the free-face MLR model (FF6) is:

$$Log(D_H + 0.01) = b_0 + b_1 M + b_2 Log(R) + b_3 R + b_4 Log(W) + b_6 Log(T_{15}) + b_7 Log(100 - F_{15}) + b_8 D50_{15} \quad (5.2)$$

and that of the ground-slope MLR model (GS6) is:

$$Log(D_H + 0.01) = b_0 + b_1 M + b_2 Log(R) + b_3 R + b_5 Log(S) + b_6 Log(T_{15}) + b_7 Log(100 - F_{15}) + b_8 D50_{15} \quad (5.3)$$

The coefficients of each model were obtained by subdividing data set A and B into free-field and ground slope cases. As shown in Table 5, the models FF6-A and GS6-A have slightly different

coefficients, and fit data set A only slightly better than FFGS6-A. The adjusted R^2 values are 82.1% and 82.4%, for models FF6-A and GS6-A, respectively, in comparison to 80.6% for model FFGS6-A. In contrast to models FF6-A and GS6-A, models FF6-B and GS6-B fit the B-data set with different accuracy. The adjusted R^2 values of models FF6-B and GS6-B are 80.2% and 87.9%, respectively. Model GS6-B is much more accurate than model FF6-B. The attenuation curves of these models are also different. From this comparison, it is concluded that model GS6-B predicts reasonably liquefaction-induced displacement in ground-slope cases, and that model FF6-B does not work as well as GS6-A. This implies that there may be alternate sets of controlling variables, which could describe free-face cases better.

Table 5-5. Coefficients of Multiple Linear Regression (MLR) and adjusted R^2 values for models FFGS6, FF6 and GS6.

	Old data	Data set A (all displacements)			Data set B (displacements < 2m)		
Number of data points	467	467	213	254	283	118	165
Model coefficients	Bartlett-Youd (1992)	FFGS6-A	FF6-A	GS6-A	FFGS6-B	FF6-B	GS6-B
b_0	-15.787	-14.551	-17.372	-14.152	-13.261	-15.067	-14.212
b_{off}	-0.579	-0.483	-	-	-0.261	-	-
b_1	1.178	1.096	1.248	0.988	1.050	1.130	0.800
b_2	-0.927	-0.873	-0.923	-1.049	-0.778	-0.738	-1.198
b_3	-0.013	-0.014	-0.014	-0.011	-0.013	-0.012	-0.006
b_4	0.657	0.634	0.685	-	0.370	0.396	-
b_5	0.429	0.275	-	0.318	0.106	-	0.071
b_6	0.348	0.494	0.300	0.619	0.270	0.135	0.373
b_7	4.527	4.053	4.826	4.287	3.481	4.032	5.090
b_8	-0.922	-0.814	-1.091	-0.705	-0.715	-0.908	-0.704
R^2 adjusted	82.60%	80.61%	82.10%	82.41%	81.08%	80.24%	87.88%

Figures 10-12 show the measured displacements plotted against those predicted by models FF6, GS6, and FFGS6 for data sets A and B. These figures also show the lines of slopes 0.5, 1 and 2. The data points should fall on the 1:1 line for an ideal result. The lines of slopes 0.5 and 2 correspond to predicted displacement twice and half their measured values, respectively. As shown in Fig. 10, the points are scattered about the 1:1 line in the case of models FF6-A and -B. As shown in Figs. 11 and 12, with the exception of a few particular points, the GS6 models predict ground-slope displacements more accurately than the FF6-models predict free-face ground displacements. This result was previously established by comparing the adjusted R^2 values of models FF6 and GS6 in Table 5.

Figures 13 and 14 compare the measured displacements in data sets A and B to those predicted by models FF6, GS6, and FFGS6 in a way different from that in Figs. 10-12. The observed and predicted values of displacement are plotted as a function of the entry number in the data sets. This alternate representation indicates that models FFGS6, FF6 and GS6 are capable of modeling the ground displacement over a wide range of displacement amplitude.

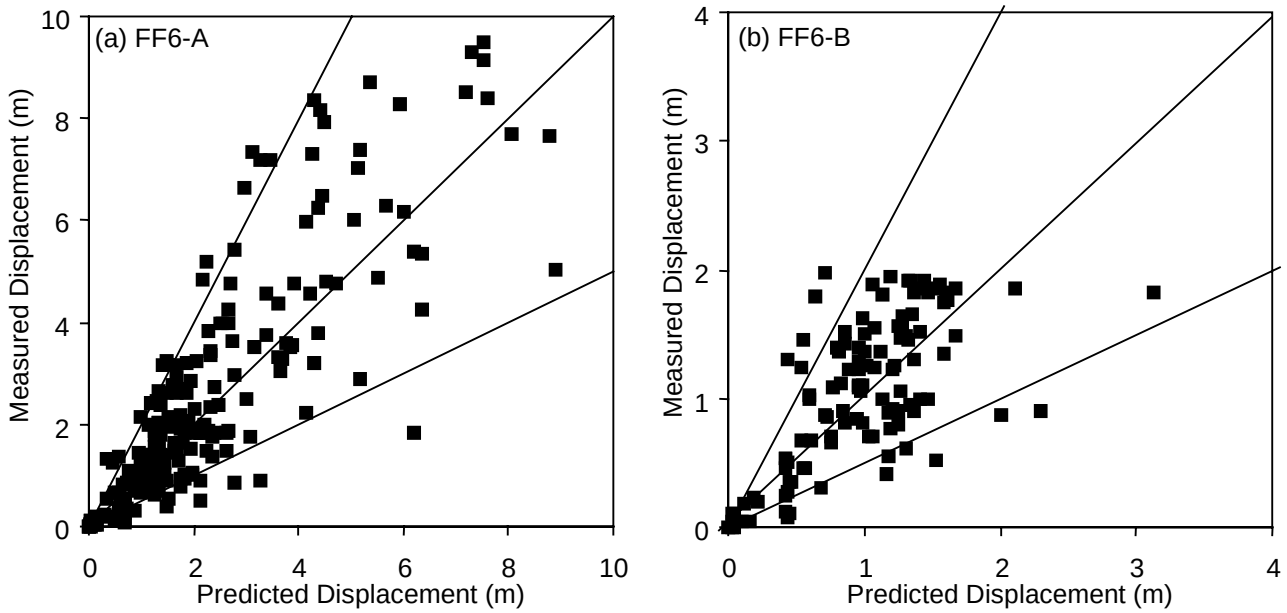

Figure 5-10. Measured versus predicted displacements for six-parameters free-face models (FF6) calibrated from (a) data set A, and (b) data set B.

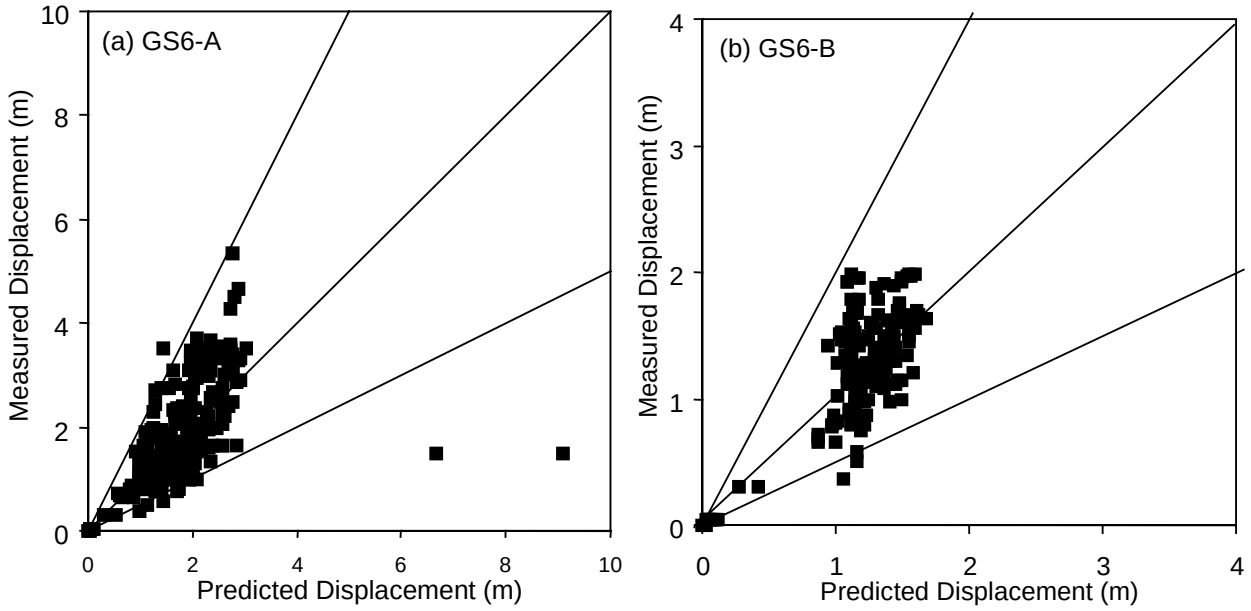

Figure 5-11. Measured versus predicted displacements for six-parameter ground-slope model (GS6) calibrated from (a) data set A, and (b) data set B.

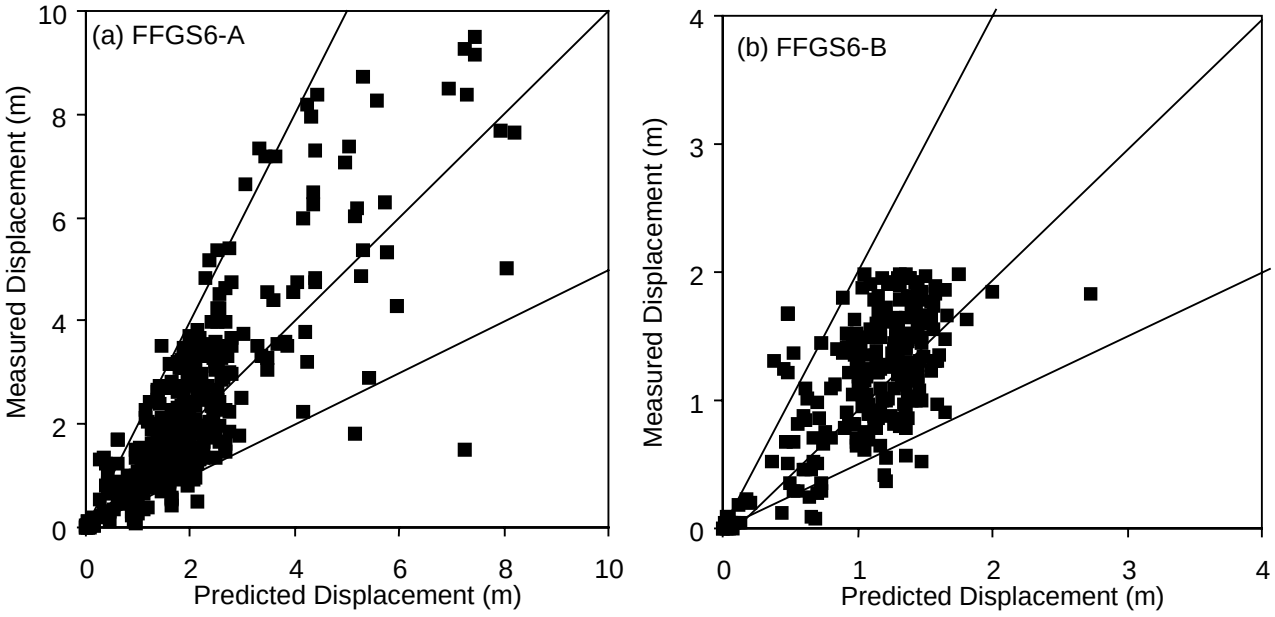

Figure 5-12. Measured versus predicted displacements for six-parameter model (FFGS6) calibrated from (a) data set A, and (b) data set B.

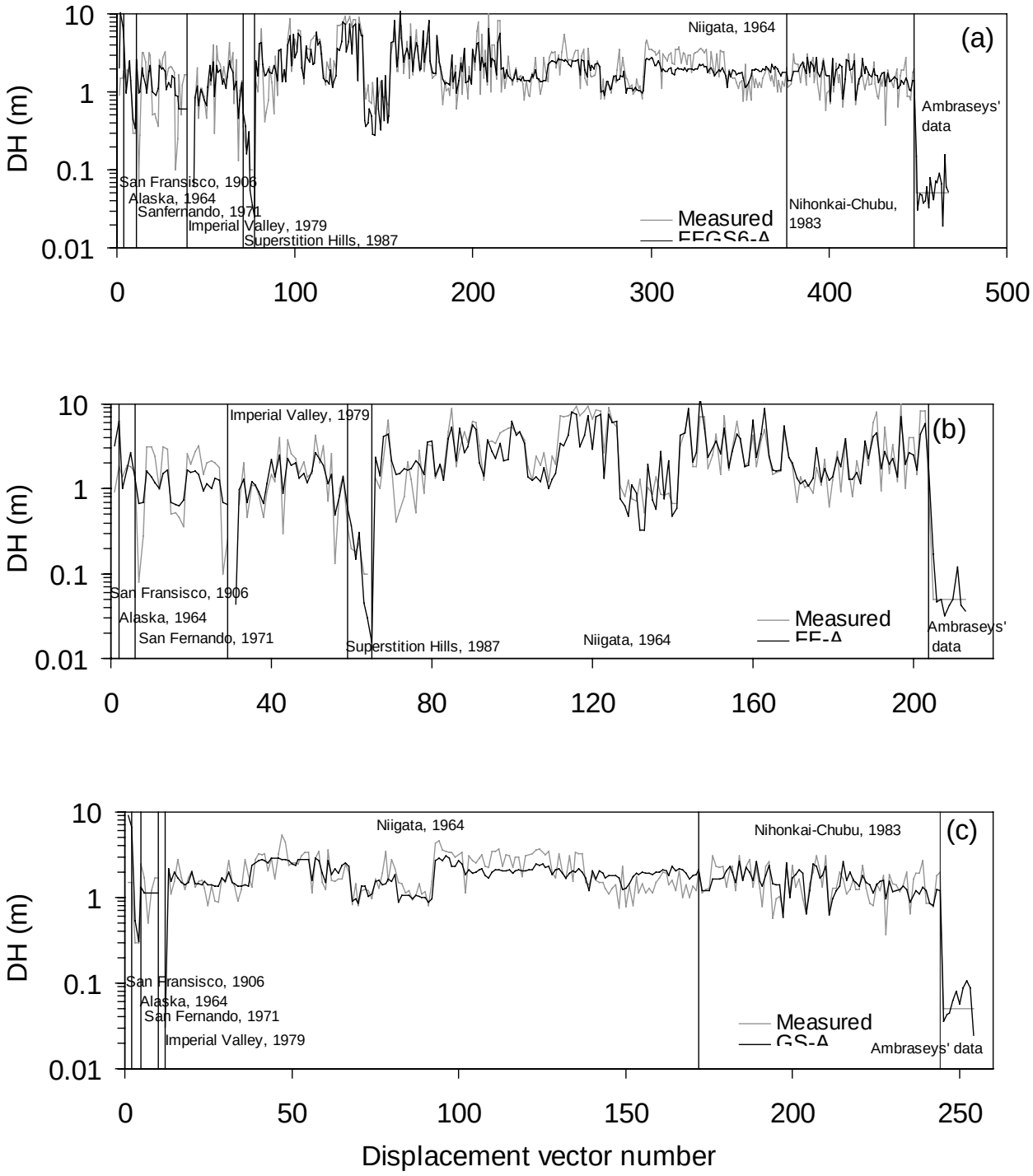

Figure 5-13. Comparison of the amplitudes of liquefaction-induced lateral displacements measured and predicted for data set A (entire database) by 6-parameter models: (a) FFGS6-A, (b) FF6-A, and (c) GS6-A.

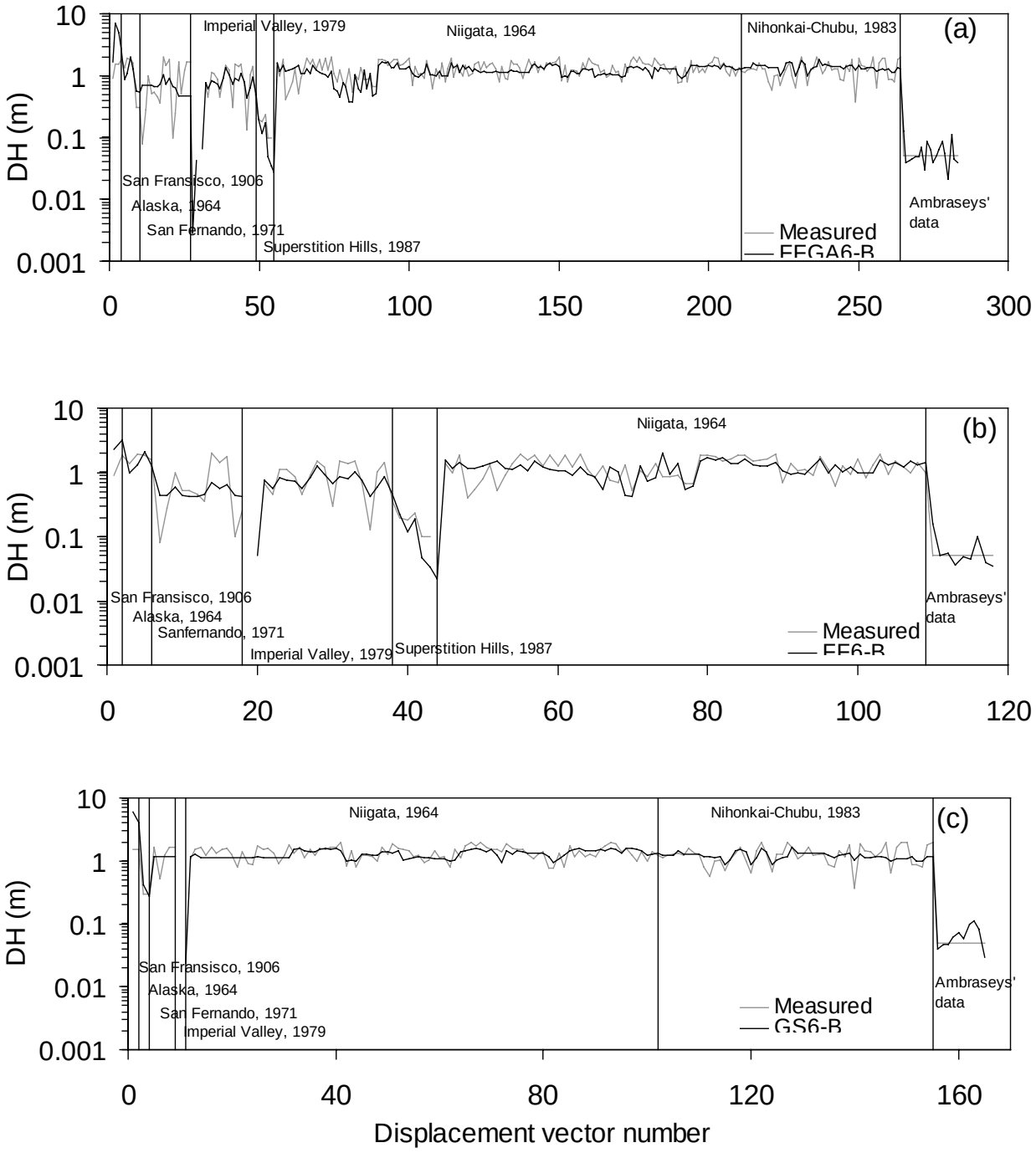

Figure 5-14. Comparison of the amplitudes of liquefaction-induced lateral displacements measured and predicted for data set B (displacement amplitude smaller than 2m) by 6-parameter models: (a) FFGS6-B, (b) FF6-B, and (c) GS6-B.

5.4 Four-parameter MLR model

The parameters F_{15} and $D50_{15}$ of the six-parameter models GS6, FF6 and FFGS6 are rather difficult to obtain from borehole data. They require taking soil sampling from the boreholes, performing grain-size analysis in the laboratory, and computing averages in the layers with a SPT blow count smaller than 15. It is obvious that this task can be formidable, and even impractical when the areas under investigation are large. In the present database (Bartlett, 1998), it is unclear how many values of F_{15} and $D50_{15}$ were actually measured, interpolated, extrapolated, or assumed. The uncertainties on variables F_{15} and $D50_{15}$ are certainly larger than on any other MLR variables.

The four-parameter MLR model was developed to provide a first-order approximation of liquefaction-induced displacement, and to eliminate the errors related to the determination of F_{15} and $D50_{15}$. The model FFGS4 has the following generic equation:

$$Log(D_H + 0.01) = b_0 + b_{off} + b_1 M + b_2 Log(R) + b_3 R + b_4 Log(W_{ff}) + b_5 Log(S_{gs}) + b_6 Log(T_{15}) \quad (5.4)$$

where the variables *M, R, W, S,* and T_{15} are defined in Table 2, and the values of the ten constant coefficients - b_0, b_{off}, and b_1 to b_8 - are given in Table 6. As for the six-parameter models, the free-face and ground-slope case were modeled separately by introducing the four-parameter models FF4 and GS4 and calibrating them from the data sets A and B. The expression of model FF4 is:

$$Log(D_H + 0.01) = b_0 + b_1 M + b_2 Log(R) + b_3 R + b_4 Log(W) + b_6 Log(T_{15}) \quad (5.5)$$

and that of model GS4 is:

$$Log(D_H + 0.01) = b_0 + b_1 M + b_2 Log(R) + b_3 R + b_5 Log(S) + b_6 Log(T_{15}) \quad (5.6)$$

The coefficients of the four-parameter models were calibrated from data sets A and B by using the same regression analysis techniques as for the six-parameter models. The values of the coefficients and adjusted R^2- values for models FFGS4, FF4 and GS4 are listed in Table 6. As shown in Table 6, the adjusted R^2-values are 64.3%, 62.2% and 68.5% for models FFGS4-A, FF4-A, and GS4-A, respectively, and 64.3%, 57.7% and 71.4% for models FFGS4-B, FF4-B, and GS4-B, respectively. Overall, the adjusted R^2-values of the four-parameter models are lower than those of the six-parameters models. As expected, the four-parameter models do not predict measured ground displacement as accurately as the six-parameter models. The adjusted R^2-value is the best (i.e., 71.4%) in the case of model GS4-B, which is remarkable in view of the model simplicity. The four-parameter model predicts the free-face displacements less accurately than ground-slope displacements for both data sets A and B, as was the case for the six-parameters models.

Figures 15 - 17 show the measured displacements plotted against those predicted by models FF4, GS4, and FFGS4 for data sets A and B, as was previously done for models FFGS6, FF6, and GS6. The results of Figs. 15-17 and 10-12 are similar. The points are however more scattered about the 1:1 line than in Figs. 10-12, which corresponds to lower values of adjusted R^2 coefficients.

Figures 18 and 19 compare the measured displacements in data sets A and B to those predicted by models FF4, GS4, and FFGS4 as in Figs. 13 and 14. Overall, this representation indicates that models FFGS4, FF4 and GS4 do not follow the observed displacement amplitude as well as models FF6, GS6, and FFGS6 over a wide range of displacement amplitude.

Table 5-6. Coefficients of Multiple Linear Regression (MLR) model with 4 parameters.

	Data set A (all displacements)			Data set B (displacements < 2m)		
Number of data points	467	213	254	283	118	165
Model coefficients	FFGS4-A	FF4-A	GS4-A	FFGS4-B	FF4-B	GS4-B
b_0	-6.815	-6.968	-7.586	-6.747	-6.034	-8.410
b_{off}	-0.465	-	-	-0.162	-	-
b_1	1.017	0.972	1.109	1.001	0.880	1.239
b_2	-0.278	-0.271	-0.233	-0.289	-0.271	-0.358
b_3	-0.026	-0.027	-0.025	-0.021	-0.018	-0.024
b_4	0.497	0.497	-	0.090	0.013	-
b_5	0.454	-	0.477	0.203	-	0.266
b_6	0.558	0.584	0.579	0.289	0.257	0.373
R^2 adjusted	64.25%	62.22%	68.48%	64.27%	57.71%	71.42%

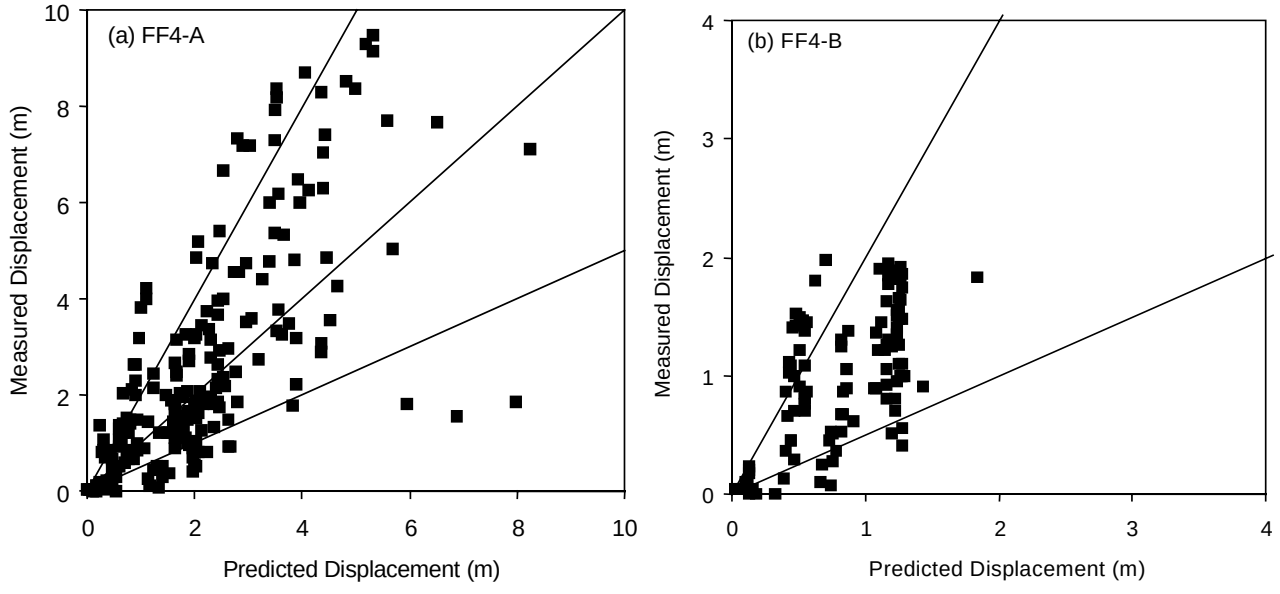

Figure 5-15. Measured versus predicted displacements for four-parameter model FF4 calibrated from (a) data set A, and (b) data set B.

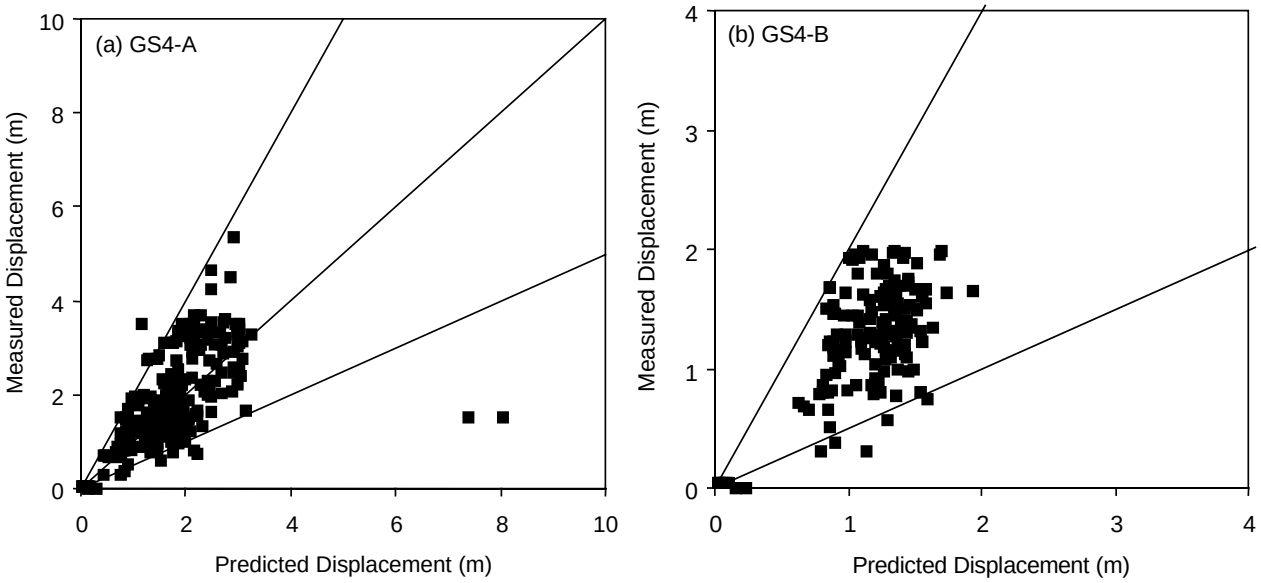

Figure 5-16. Measured versus predicted displacements for four-parameter model FFGS4 calibrated from (a) data set A, and (b) data set B.

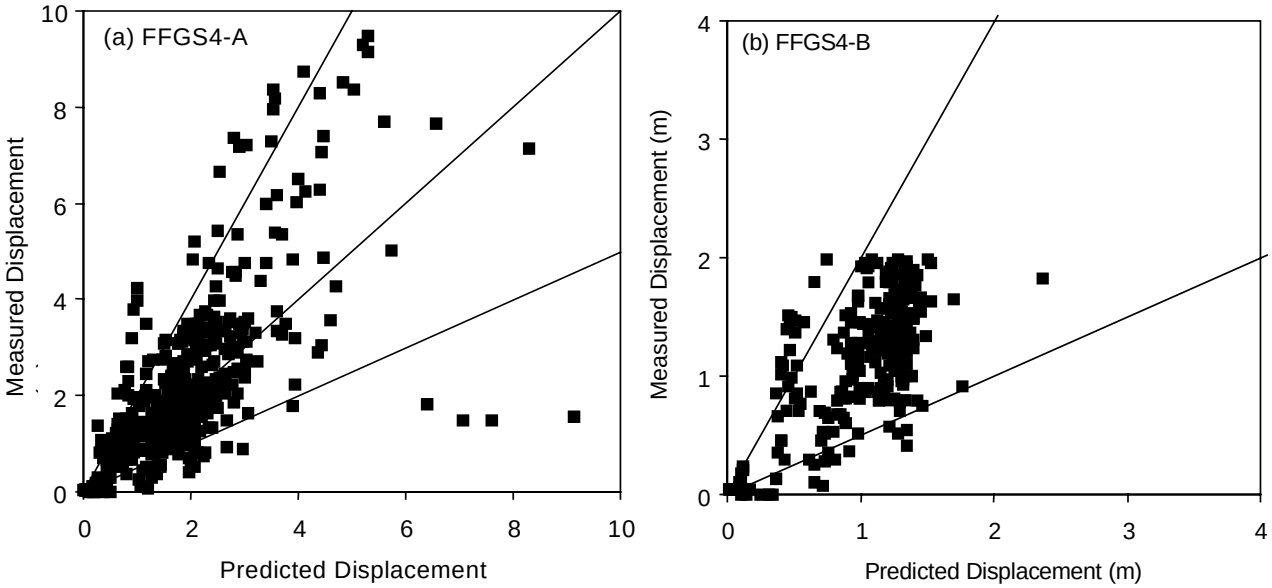

Figure 5-17. Measured versus predicted displacements for four-parameter model FFGS4 calibrated from (a) data set A, and (b) data set B.

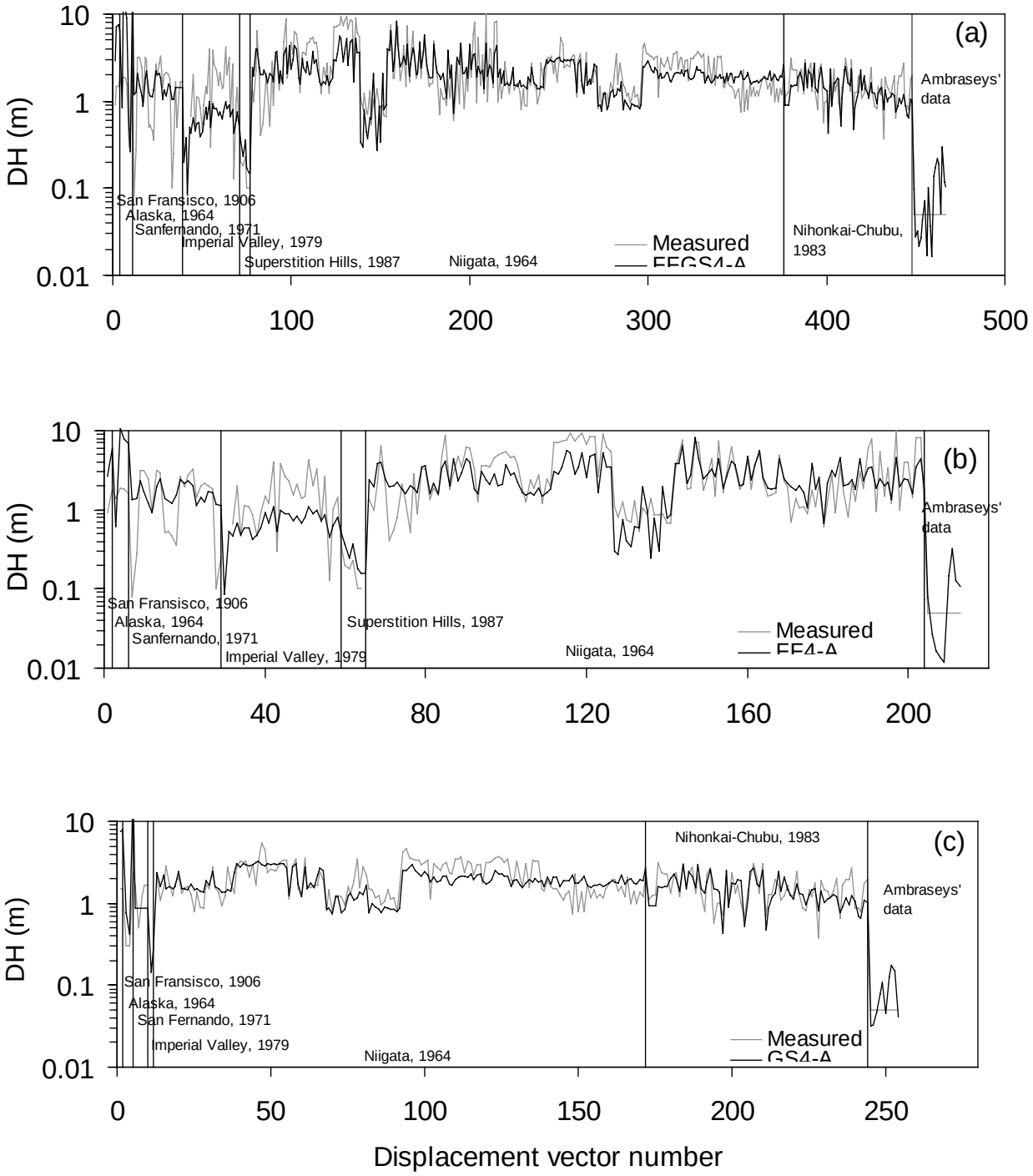

Figure 5-18. Comparison of amplitudes of liquefaction-induced lateral displacements measured and predicted for data set A by 4-parameter models: (a) FFGS4-A, (b) FF4-A, and (c) GS4-A.

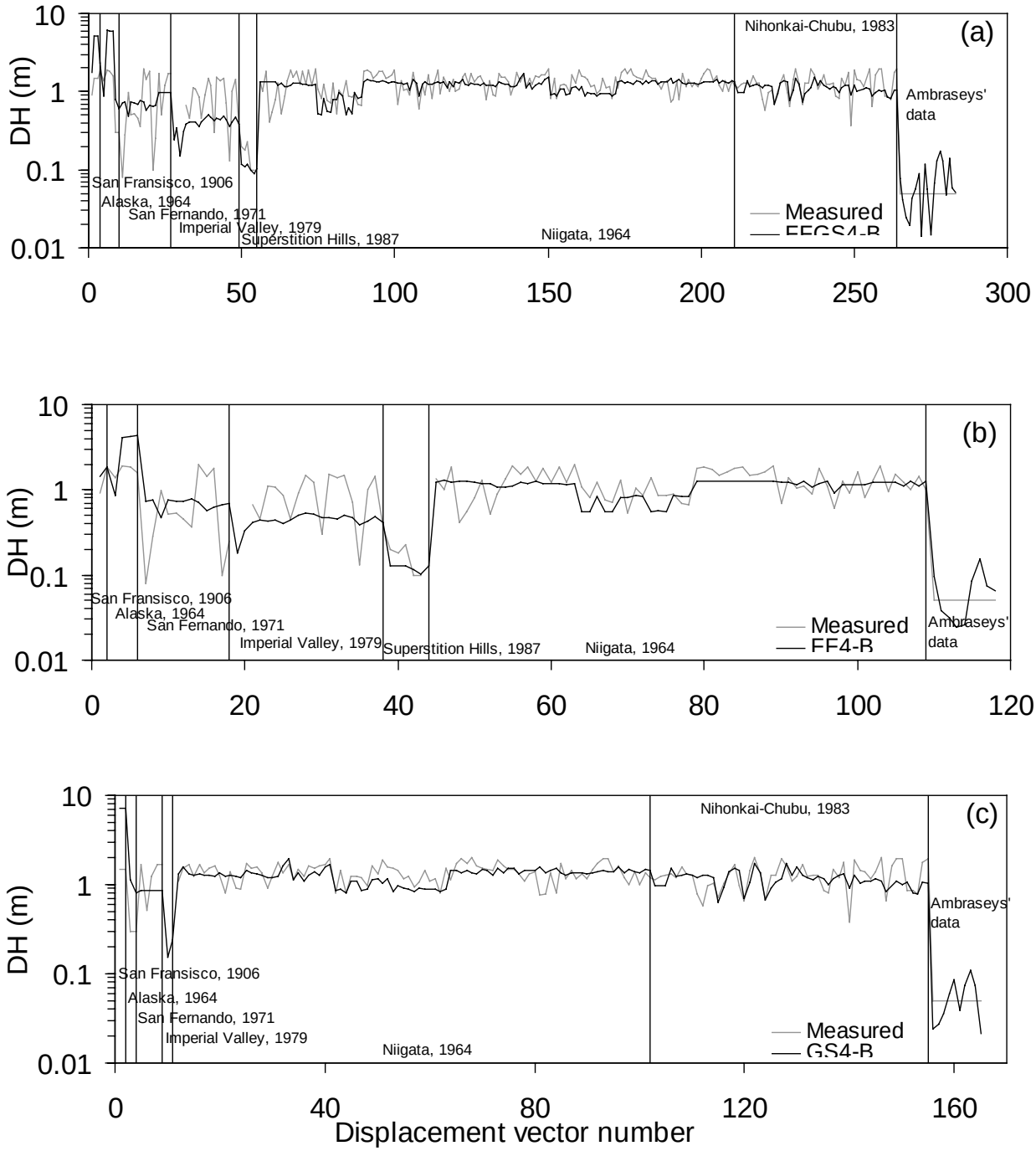

Figure 5-19. Comparison of amplitudes of liquefaction-induced lateral displacements measured and predicted for data set B by 4-parameter models: (a) FFGS4-B, (b) FF4-B, and (c) GS4-B.

5.5 Comparison of MLR models and recommendations

A total of twelve MLR models have been calibrated in this study. Table 7 summarizes the adjusted R^2 coefficients for all these models. It is clear that six-parameter models are systematically more accurate than four-parameter models.

Table 5-7. Comparison of adjusted R^2 for all MLR models

Models	Data set A	Data set B
FFGS4	64.3%	64.3%
FF4	62.2%	57.7%
GS4	68.5%	71.4%
FFGS6	80.6%	81.1%
FF6	82.1%	80.2%
GS6	82.4%	87.9%

These twelve models are compared in Figs. 20 and 21 by plotting the relative error between the measured and predicted displacements. The relative error is defined as follows:

$$\varepsilon = 100\ |DH_m - DH_p| / DH_m\ (\%) \quad (7)$$

where DH_m is the measured displacement amplitude, and DH_p is the predicted displacement amplitude. As shown in Figs. 20 and 21, the six-parameter models are more accurate than the 4-parameter models.

Based on the preceding analysis, some preliminary recommendations can be made regarding the selection of MLR models for predicting liquefaction-induced ground displacement. The choice of a particular model depends on (1) the site conditions (free face or ground slope) and (2) the availability of geotechnical data. For engineering design requiring an estimate of ground displacements, the models calibrated from the data set B are recommended compared to those calibrated from data set A.

When there is information available on the grain-size distribution of soils, the *FFGS6-B* model is recommended in the free-face and ground-slope conditions. The model GS6-B is especially recommended for ground slope conditions.

When there is little information on the soil grain-size distribution, the model FFGS4-B is recommended for free-face and ground-slope conditions, and the model GS4-B for ground-slope conditions.

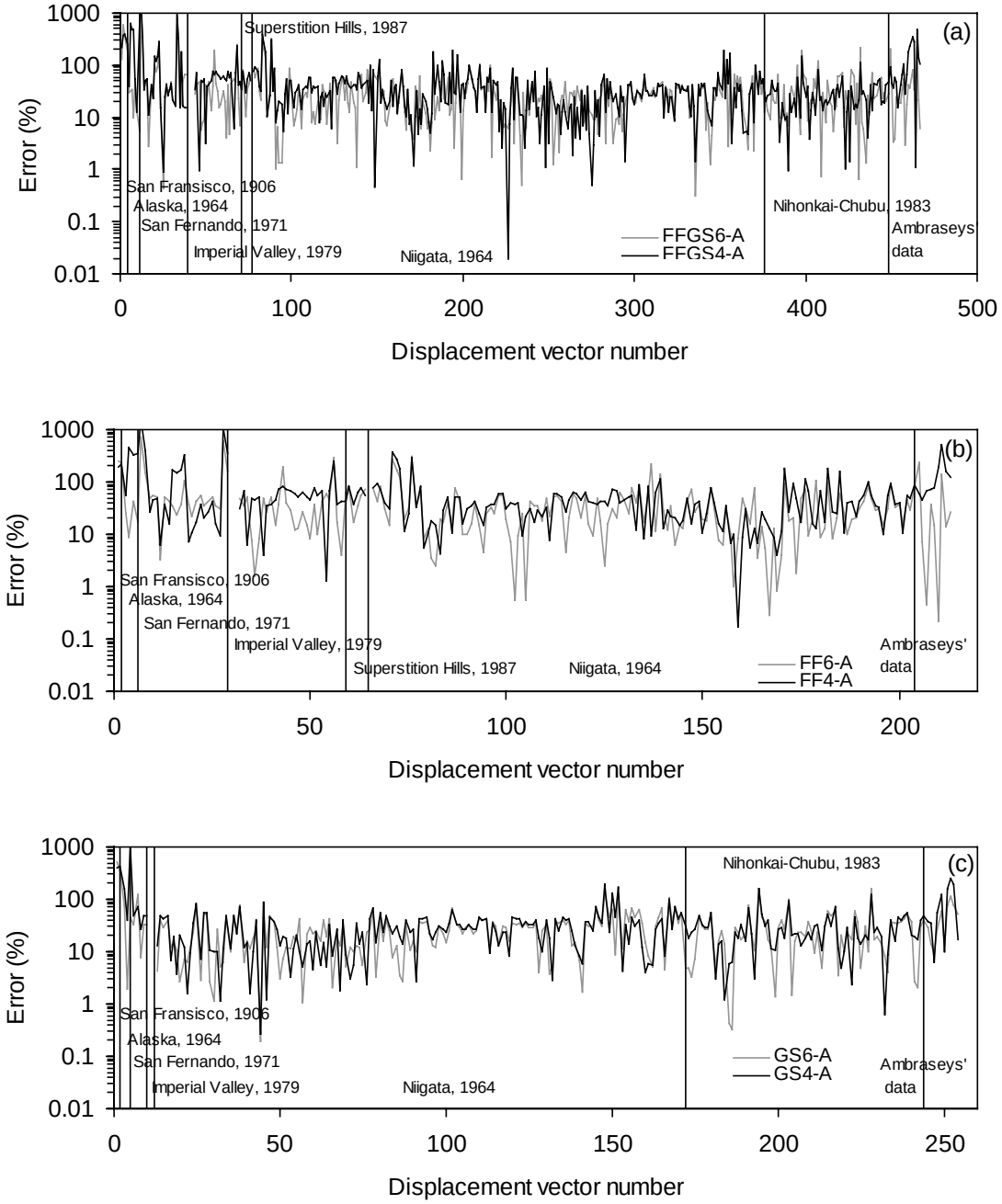

Figure 5-20. Comparison of relative errors between measured displacement and displacement predicted by 6 and 4 parameter models for data set A (all ranges of displacement amplitude): (a) FFGS6-A and FFGS4-A; (b) FF6-A and FF4-A; and (c) GS6-A and GS4-A.

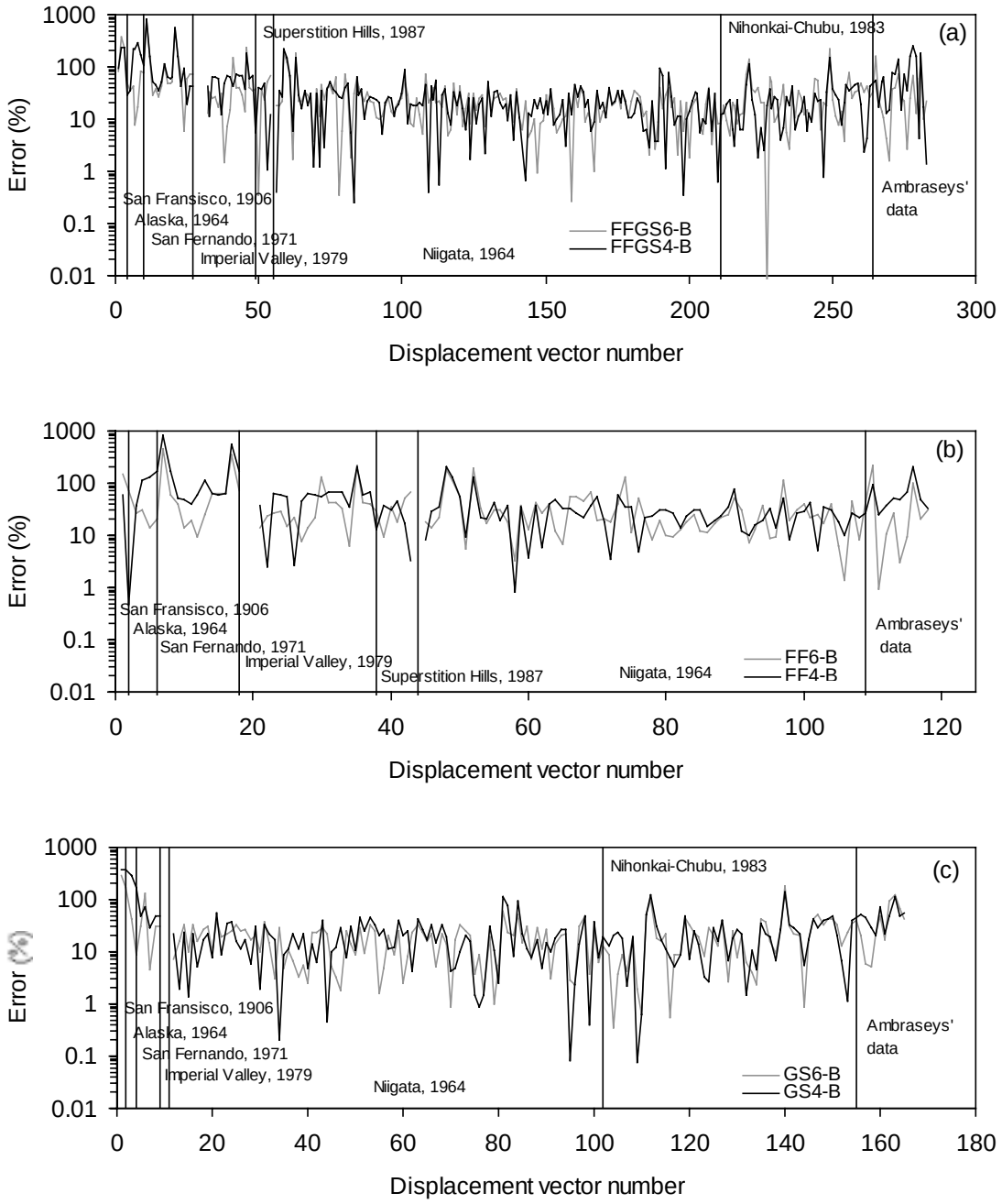

Figure 5-21. Comparison of relative error between measured displacement and displacement predicted by 6 and 4 parameter models in the case of data set B (displacement smaller than 2 m): (a) FFGS6-B and FFGS4-B; (b) FF6-B and FF4-B; and (c) GS6-B and GS4-B.

5.6 Suggestion for future work

There are statistical methods in seismology which could be used for constructing the empirical models of liquefaction-induced ground displacement instead of the multi-linear regression techniques (Abrahamson, private communication, 1998). These methods, which have successfully been used to develop attenuation curves in seismology, have the capabilities of dealing with bias in data. These methods will be applied to deriving new empirical models once the recent data from the 1994 Northridge and 1995 Hyogoken-Nanbu earthquakes has been added to the database of liquefaction-induced displacements.

5.7 Mapping of liquefaction-induced ground deformation

In the previous section, the amplitudes of liquefaction-induced displacements predicted by MLR models were compared to the observed values as individual data points, independently from their spatial distributions over the slide areas. The present section introduces the concepts of spatial distribution and direction of liquefaction-induced displacements, and briefly investigates the ability of MLR models to predict the spatial distribution of liquefaction-induced displacement vectors in two examples of free-face and ground-slope cases. Additional assumptions are required to predict the direction of liquefaction-induced lateral displacement. In the free-face cases, the horizontal displacements are assumed to be perpendicular to the free-face. In the ground slope cases, the horizontal displacements are assumed to be collinear to the average slope gradient direction.

Figure 22 shows the surface elevation and the contours of measured displacement amplitudes for the slide G-10 FF' at Niigata, Japan, during the 1964 Niigata earthquake. The measured displacement amplitudes are the largest on the free face (i.e., the Shinano River), and decrease with the distance from the free face. As shown in Fig. 23, the displacement vectors are oriented perpendicular to the free face, and in the opposite direction to the ground slope gradient. The slide G-10 FF' at Niigata is a clear case of free-face liquefaction-induced slide. As shown in Fig. 24, kriging techniques (Surfer, 1998) are used to predict a continuous spatial distribution of the liquefaction-induced displacements predicted by model FFGS6-A for the slide G-10 FF' at Niigata, Japan, during the 1964 Niigata earthquake. This predicted spatial distribution is obtained from the discrete displacements predicted at the locations of measured displacements. As shown in Figs. 23 and 24, the FFGS6-A model predicts reasonably the amplitude and spatial distribution of liquefaction-induced displacements over the slide area.

In theory, the model FFGS6-A variables could be extrapolated beyond the slide areas to obtain the spatial distributions of predicted displacements over large areas. Figure 24 also shows the continuous spatial distributions of the geotechnical properties, T_{15}, F_{15}, and $D50_{15}$ over the area encompassing slide G-10 FF'. A kriging technique (Surfer, 1998) is used to compute the values of T_{15}, F_{15}, and $D50_1$ in the slide vicinity. Theses values are interpolated or extrapolated at evenly spaced grid nodes (49 x 43) from the variable values at the borehole locations represented as numbered pins in Fig. 24. There are definite uncertainties in extrapolating spatially the averages from borehole data (i.e., T_{15}, F_{15} and $D50_{15}$). This extrapolation was found to overestimate the extent of liquefaction-induced slides. There is a need to collect data outside slide areas for assessing more accurately the spatial extent of liquefaction-induced displacements.

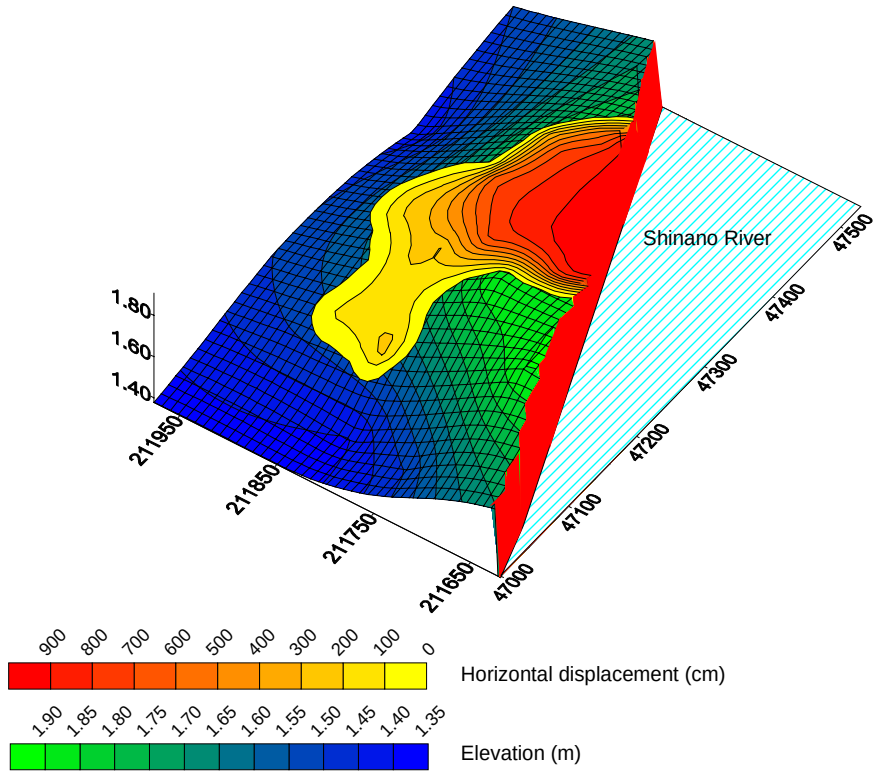

Figure 5-22. Contours of ground surface elevation and measured amplitude of lateral ground displacement for slide G-10 FF' during 1964 Niigata, Japan, earthquake (coordinates are in meters).

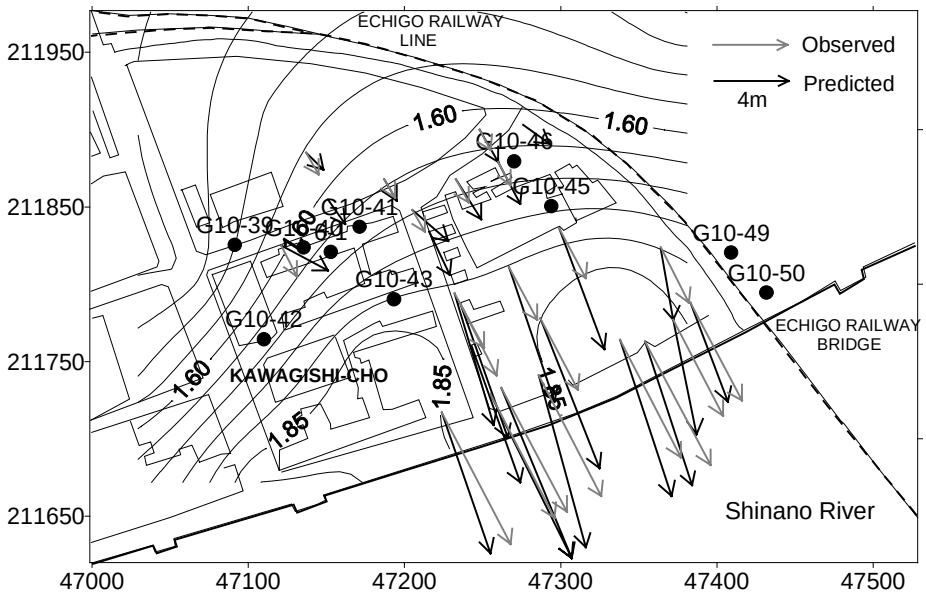

Figure 5-23. Comparison of measured and predicted liquefaction-induced displacements for slide G-10 FF' at Niigata, Japan, during 1964 Niigata earthquake (coordinates are in meters).

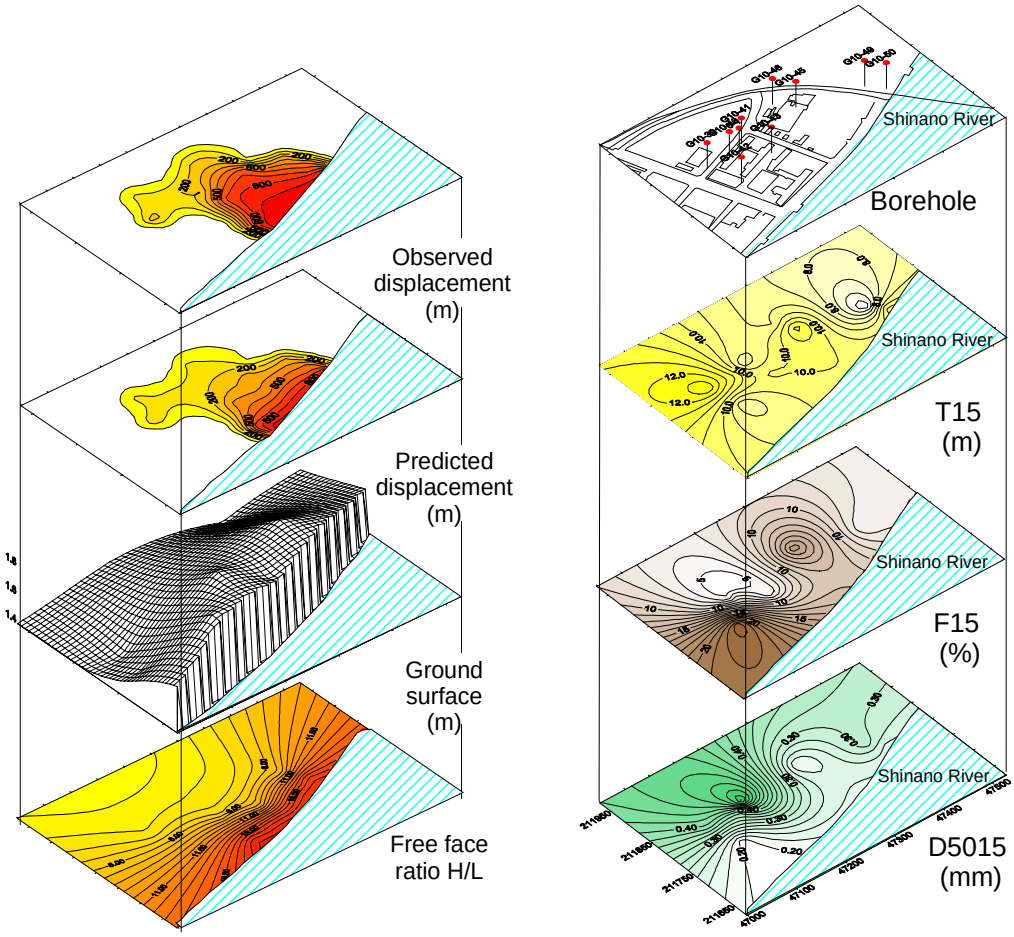

Figure 5-24. Representations of ground surface, spatial distribution of average geotechnical properties, and predicted and measured amplitude of liquefaction-induced lateral ground deformation for slide G10-FF' in Niigata during the 1964 Niigata, Japan, earthquake (coordinates are in meters).

Figure 25 shows the ground surface elevation and the contours of measured displacement amplitudes for the slide H-10 MM' at Niigata, Japan, during the 1964 Niigata earthquake. The magnitudes of the liquefaction-induced displacement vectors are clearly related to the ground slope. This slide, which took place far away from any free-faces, is considered to be a representative example of ground-slope cases. As shown in Fig. 25, the slide boundaries were assumed to be rather abrupt due to the absence of measured displacement vectors. It is likely that there were small deformations around this slide, which were difficult to obtain from aerial photographs. As shown in Fig. 26, the measured displacement vectors have almost the same direction as the average slope direction. Figure 27 shows the continuous spatial distributions of the geotechnical properties, T_{15}, F_{15}, and $D50_{15}$, which were calculated from the discrete boreholes represented as numbered pins. As shown in Figs. 26 and 27, model FFGS6-A predicts reasonably the amplitude and spatial distribution of liquefied displacement within the slide area. There are however uncertainties in extrapolating the results beyond the slide area, and defining the extent of the liquefaction-induced slides, which deserve to be studied in greater detail in the future.

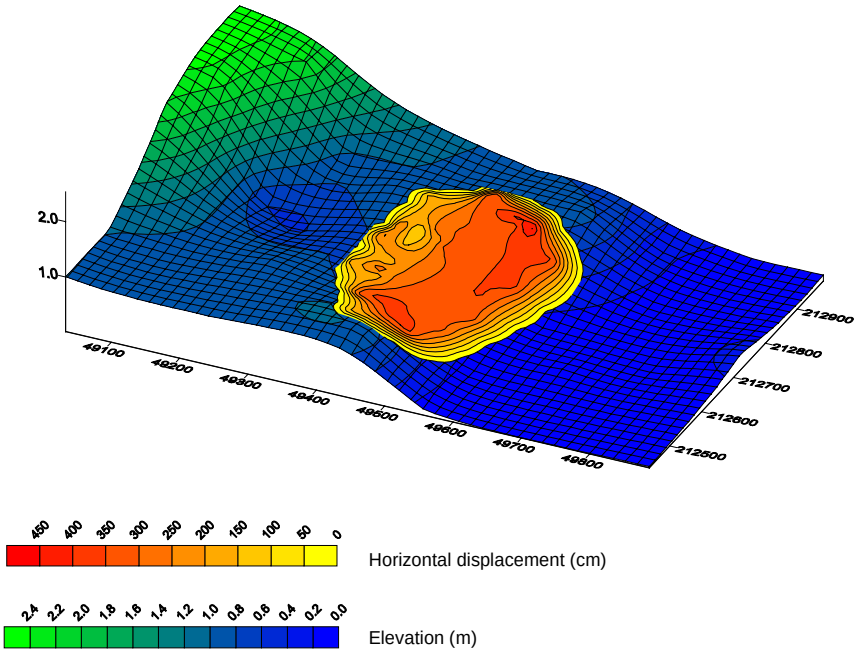

Figure 5-25. Contours of ground surface elevation and measured amplitude of lateral ground displacement measured for slide H10-MM' during 1964 Niigata, Japan, earthquake (coordinates are in meters).

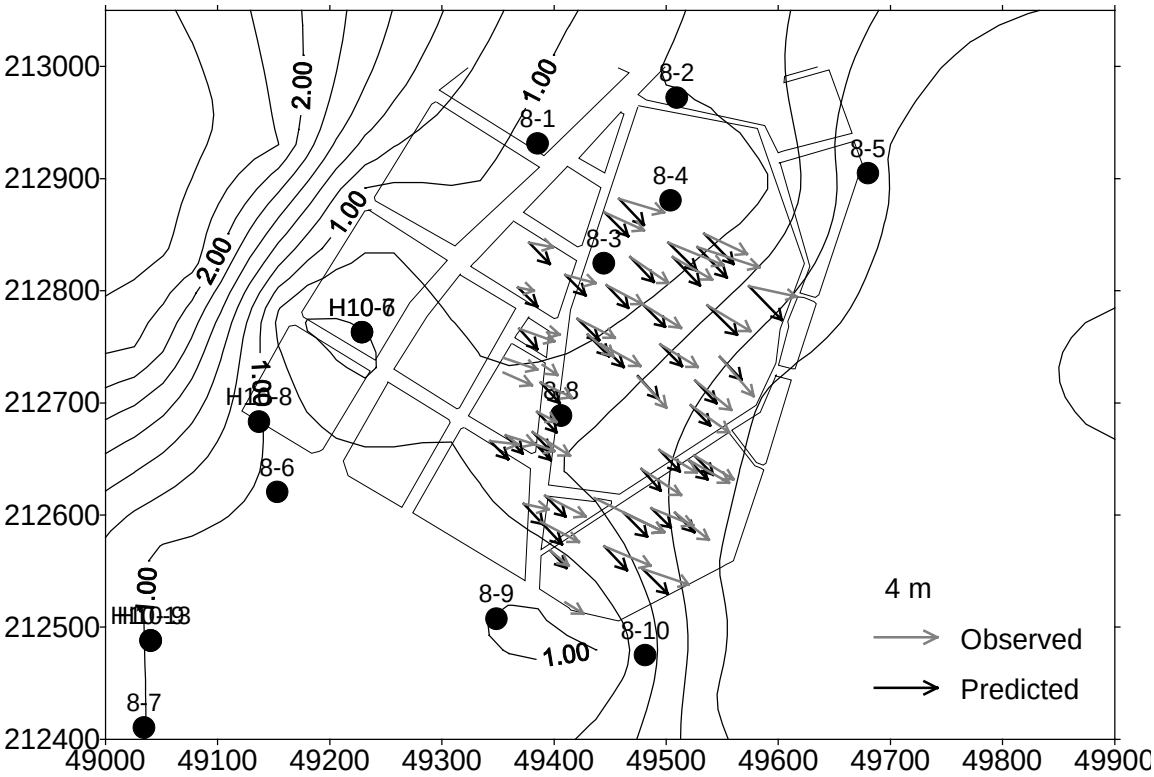

Figure 5-26. Comparison of measured and predicted liquefaction-induced displacements for slide H10-MM' during 1964 Niigata, Japan, earthquake (coordinates are in meters).

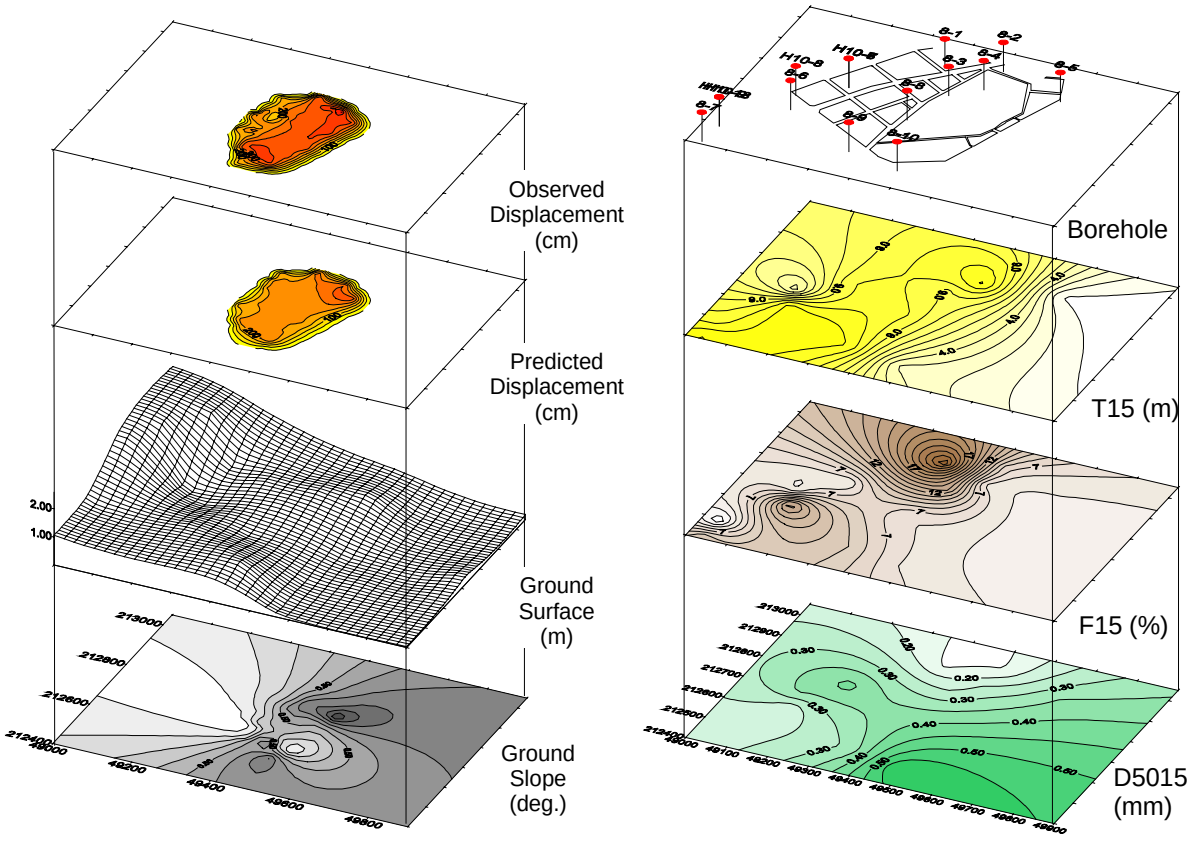

Figure 5-27. Representations of ground surface and gradient, spatial distribution of average geotechnical properties, and predicted and measured amplitude of liquefaction-induced lateral ground deformation for slide H10-MM' in Niigata, Japan, during the 1964 Niigata earthquake (coordinates are in meters).

6. PROBABILISTIC MODEL OF LIQUEFACTION-INDUCED GROUND DEFORMATION

As described previously, twelve MLR models have been calibrated, based on data sets A and B. These MLR models predict the mean values of liquefaction-induced ground deformation. Based on the previously developed MLR models, this section determines (1) the confidence limits for liquefaction-induced ground deformation and (2) the probability of exceeding some level of ground deformation. The reader is referred to Draper and Smith (1981) for details on probability analysis.

6.1 Mean and variance of ground deformation

The MLR models for liquefaction-induced ground deformation predict the mean value of ground deformation $\hat{D}$ as follows:

$$\hat{D} = b_0 + b_1 X_1 + ... + b_p X_p \tag{6.1}$$

where b_0, …, b_p are constant coefficients, X_1 ,…, X_p are the model variables and p the total number of model variables. The variance of $\hat{D}$ is:

$$V(\hat{D}) = V(b_0 + b_1 X_1 + ... + b_p X_p) \tag{6.2}$$

Equation 2 can be expanded as follows:

$$\begin{aligned} V(\hat{D}) = {} & V(b_0) + X_1^2 V(b_1) + ... + X_p^2 V(b_p) \\ & + 2X_1 \text{covar}(b_0, b_1) + ... + 2X_p \text{covar}(b_0, b_p) \\ & + 2X_1 X_2 \text{covar}(b_1, b_2) + ... + 2X_{p-1} X_p \text{covar}(b_{p-1}, b_p) \end{aligned} \tag{6.3}$$

where V(b_i) is the variance of coefficient b_i, and covar(b_i, b_j) is the covariance of coefficient b_i and b_j. Equation 3 can be written in a matrix form as follows:

$$V(\hat{D}) = s^2 \mathbf{X}_0^T \mathbf{C} \mathbf{X}_0 \tag{6.4}$$

s^2 is the residual mean square:

$$s^2 = \frac{1}{n - p - 1} \sum_{i=1}^{n} \left(\hat{D}_i - D_i \right)^2 \tag{6.5}$$

where D_i is the ith observed value of D, and $\hat{D}_i$ is ith predicted value corresponding to D_i (i=1 to n).The variance-covariance matrix $s^2\mathbf{C}$ has p+1 columns and p+1 rows:

$$\mathbf{C} = \left(\mathbf{X}^T\mathbf{X}\right)^{-1} = \begin{pmatrix} c_{00} & c_{01} & \cdots & c_{0p} \\ c_{10} & c_{11} & \cdots & c_{1p} \\ \vdots & & \ddots & \vdots \\ c_{p0} & & & c_{pp} \end{pmatrix} \tag{6.6}$$

The matrix $\mathbf{X}$ with p+1 columns and n rows is defined as:

$$\mathbf{X} = \begin{pmatrix} 1 & X_{1,1} & \cdots & X_{1,p} \\ 1 & X_{2,1} & \cdots & X_{2,p} \\ \vdots & \vdots & \vdots & \vdots \\ 1 & X_{n,1} & \cdots & X_{n,p} \end{pmatrix} \tag{6.7}$$

where $X_{i,j}$ is the value of j^{th} variable of the i^{th} observation. In Eq. 4, the vector $\mathbf{X}_0$ represents the values of the model variables for an individual observation. $\mathbf{X}_0$ has the same type of components as a row of $\mathbf{X}$. The vector $\mathbf{X}_0$ and its transpose $\mathbf{X}_0^T$ are:

$$\mathbf{X}_0 = \begin{pmatrix} 1 \\ X_1 \\ X_2 \\ \vdots \\ X_p \end{pmatrix} \quad \text{and} \quad \mathbf{X}_0^T = \begin{pmatrix} 1 & X_1 & X_2 & \cdots & X_p \end{pmatrix} \tag{6.8}$$

In the case of the six-parameter MLR models of liquefaction-induced ground deformation (e.g., FFGS6-A), the components of $\mathbf{X}_0$ are given in Table 1. For the four-parameter MLR models of liquefaction-induced ground deformation (e.g., FFGS4-A), the last two components (i.e., X_8 and X_9) are omitted.

The variance-covariance matrix $\mathbf{C}$ and residual mean square s^2 for the twelve MLR models were calculated by using the computer program Minitab (1989). Table 2 lists the values of $\mathbf{C}$ and s^2 for model FFGS6-A. All the coefficient values for other models are given in Appendix B. Based on the values of $\mathbf{C}$ and s^2, the confidence limits for ground deformation and probability of exceeding some amplitude threshold can be defined.

Table 6-1 Components of observation vector $\mathbf{X}_0$.

Component	Variable	Definition
1		
X_1	1 for free face and 0 for ground slope	
X_2	*M*	Earthquake moment magnitude
X_3	*R*	Closest distance to source (km)
X_4	*Log R*	
X_5	*Log W*	Free face ratio
X_6	*Log S*	Ground slope (%)
X_7	*Log* T_{15}	Thickness of saturated cohesionless soils with $(N1)_{60}$<15 (m)
X_8	*Log(100 -*F_{15}*)*	Average fines (<75 μm) content in T_{15} (%)
X_9	$D50_{15}$	Average mean grain size D_{50} in T_{15} (mm)

Table 6-2. Parameter values for probabilistic model FFGS6-A.

Covariance matrix **C** (symmetric)

0.001	0.000	0.002	0.000	0.000	-0.001	0.000	0.000	-0.007	0.001
	0.047	0.002	0.000	0.000	-0.040	-0.011	-0.005	-0.011	0.001
		0.029	0.000	-0.001	-0.004	0.004	0.000	-0.104	-0.005
			0.026	-0.001	0.005	-0.003	-0.005	-0.007	-0.014
				0.000	0.000	0.000	0.000	0.002	-0.001
					0.047	0.000	0.000	0.011	0.007
						0.045	0.011	-0.011	0.000
Number of observations (n) =	467						0.022	-0.003	-0.004
Number of degrees of freedom (p) =	9							0.386	0.005
Residual mean square (s^2) =	0.046								0.196

6.2 Confidence limits

The 1-α confidence limits for the predicted mean value of *D* at observation state $\mathbf{X}_0$ are:

$$D_{\pm} = \hat{D} \pm t(n-p-1,1-\tfrac{1}{2}\alpha)s\sqrt{\frac{1}{q}+\frac{1}{n}+\mathbf{X}_0^T\mathbf{C}\mathbf{X}_0} \tag{6.9}$$

where *t* is the *t*-distribution with *n-p-1* degrees of freedom (Fig. 1), α is the significance level, *s* is the residual mean, *q* is the number of values used for the mean predicted value of *D* at state $\mathbf{X}_0$, and *n* is the total number of observations used in the regression. The confidence limit for a single predicted value of *D* is obtained by setting *q* equal to 1 in Eq. 9. The size of the confidence interval decreases when one wishes to obtain a mean value of *D* (i.e., *q* > 1) instead of a single value of *D* (i.e., *q = 1)*. This interval is minimum when one wishes a mean value of *D* based on many values (i.e., $1/q \rightarrow 0$). When *n* becomes large (e.g., n > 500), the *t*-distribution becomes identical to the normal distribution. The probability for the value *D* at state $\mathbf{X}_0$ to be comprised between D_- and D_+ is equal to 1-α, i.e.:

$$p(D_- \le D \le D_+) = 1-\alpha \tag{6.10}$$

In Microsoft Excel (1994), the *t*-distribution is given by the function *TINV* as follows:

$$t(n-p-1,1-\tfrac{1}{2}\alpha) = TINV(\alpha, n-p-1) \tag{6.11}$$

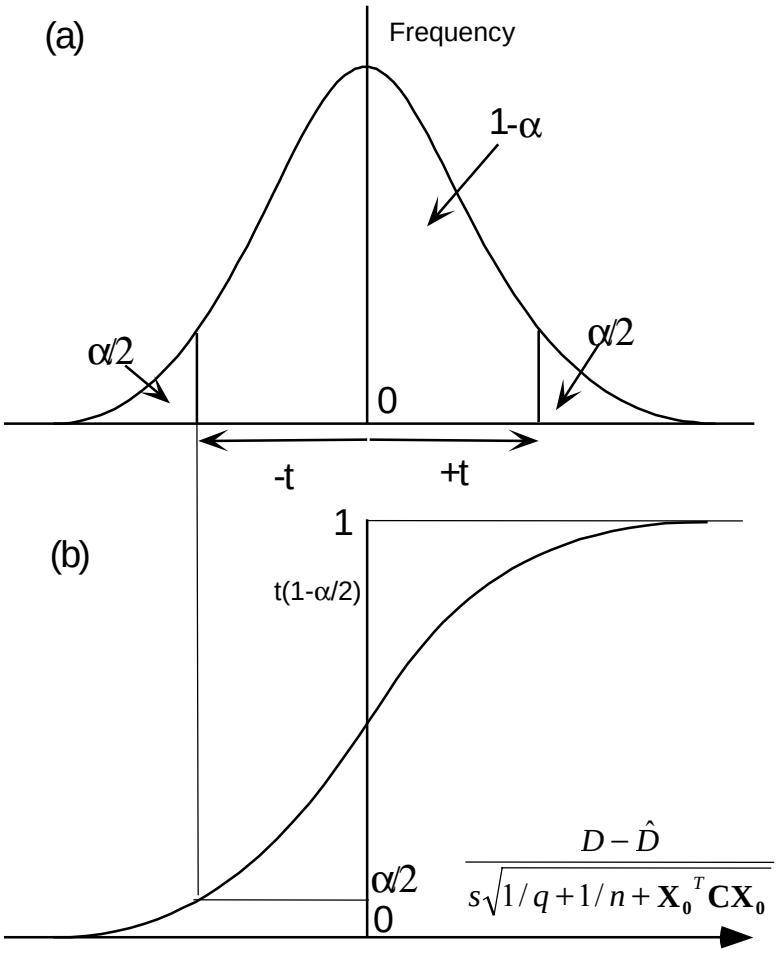

Figure 6-1. Representation of *t*-distribution: (a) probability distribution function of *t*-distribution with two tails, and (b) inverse *t*-distribution.

6.3 Probabilistic model

Based on Eq. 9, the probability $p(D>D^*)$ for the mean deformation D at state $\mathbf{X}_0$ to exceed some value D^* is estimated as follows:

$$p(D > D^*) = \beta \tag{6.13}$$

where β is the area under the *t*-probability distribution curve as shown in Fig. 2a. Using the inverse *t*-distribution t^{-1} (see Fig. 2b), Eq. 13 can be written as follows:

$$p(D > D^*) = \begin{cases} 1 - t^{-1}\left(n - p - 1, \dfrac{\hat{D} - D^*}{s\sqrt{1/q + 1/n + \mathbf{X}_0^T \mathbf{C} \mathbf{X}_0}} \right) & \text{if } D^* < \hat{D} \\ t^{-1}\left(n - p - 1, \dfrac{D^* - \hat{D}}{s\sqrt{1/q + 1/n + \mathbf{X}_0^T \mathbf{C} \mathbf{X}_0}} \right) & \text{if } D^* \geq \hat{D} \end{cases} \tag{6.14}$$

Equation 14 gives the probability that the mean value D of liquefaction-induced ground deformation at state $\mathbf{X}_0$ exceeds some value D^*. The parameter n refers to the total number of observations used in the regression analysis. The parameter q is the number of values used for the mean value of D. The probability for a single value of D to exceed D^* at state $\mathbf{X}_0$ is given by setting q equal to 1. The probability for a mean value of D based on many values is given by setting $1/q$ equal to zero.

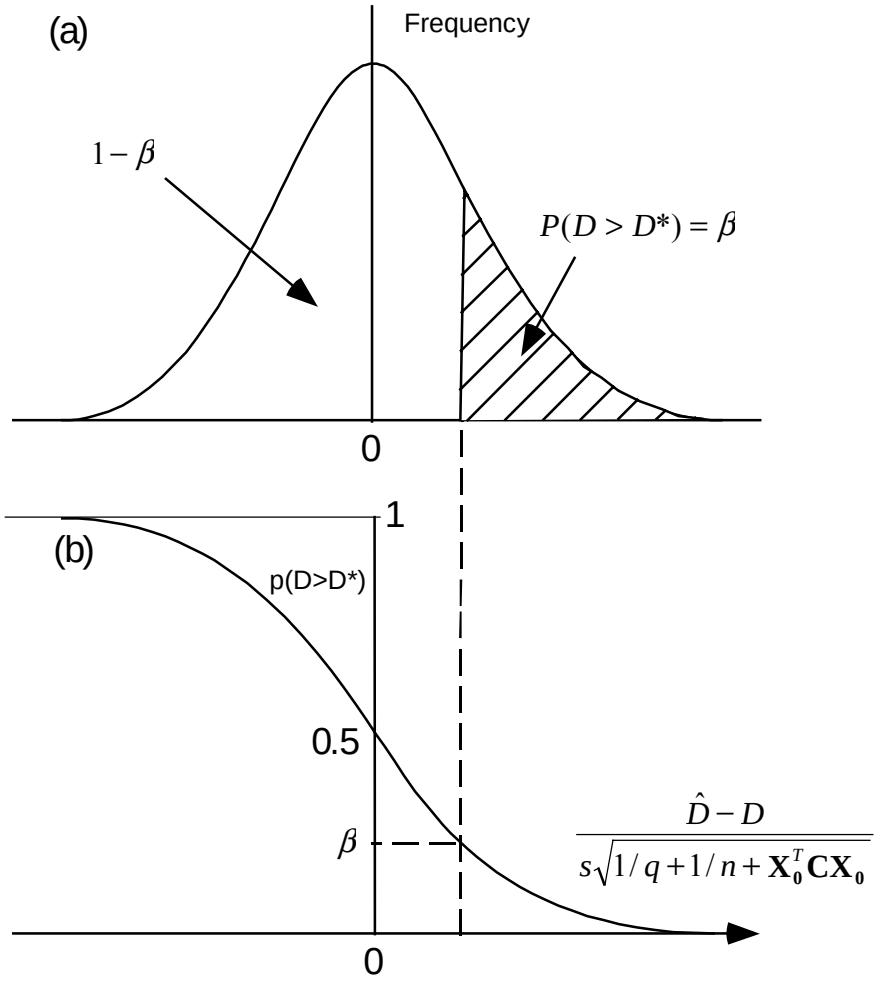

Figure 6-2. Representation of probabilistic model for exceeding a threshold of deformation: (a) probability distribution function of t-distribution with single tail, and (b) inverse t-distribution $D^* < \hat{D}$.

In Microsoft Excel, the inverse *t*-distribution is defined by the function TDIST. Equation 14 can therefore be implemented as follows:

$$p(D > D^*) = \begin{cases} 1 - TDIST\left(\dfrac{\hat{D} - D^*}{s\sqrt{1/q + 1/n + \mathbf{X}_0^T \mathbf{C} \mathbf{X}_0}}, n - p - 1, 1 \right) & if\ D^* < \hat{D} \\ TDIST\left(\dfrac{D^* - \hat{D}}{s\sqrt{1/q + 1/n + \mathbf{X}_0^T \mathbf{C} \mathbf{X}_0}}, n - p - 1, 1 \right) & if\ D^* \geq \hat{D} \end{cases} \quad (6.15)$$

6.4 Confidence intervals for liquefaction-induced ground deformation

Figure 3 shows the confidence limits of liquefaction-induced deformation predicted by model FFGS6-A for $q = 1$. The confidence limits corresponding to 95% confidence are represented by error bars. The numbers along the horizontal axis refer to the numbering system in data set A, which regroups data points by earthquakes. Figure 3 also shows the measured displacement values, and the values of mean displacement predicted by model FFGS6-A as a line centered at the error bars. As shown in Fig. 3, the confidence intervals enclose most of the measured displacement values. In some cases however, these intervals become large and do not encompass the measured displacement.

Figures 4 and 5 show the confidence limits predicted by models FF6-A and GS6-A, respectively. The confidence intervals in the ground-slope model (i.e., GS6-A) are smaller and enclose a little better the measured values than the free-face model (i.e., FF6-A) and the combined model (i.e., FFGS6-A).

Figures 6, 7 and 8 show the confidence limits for the models FFGS6-B, FF6-B, and GS6-B, respectively, which were calibrated from data sets B including only displacements smaller than 2 meters. Overall, the confidence intervals enclose the measured values more accurately than the models based on data set A.

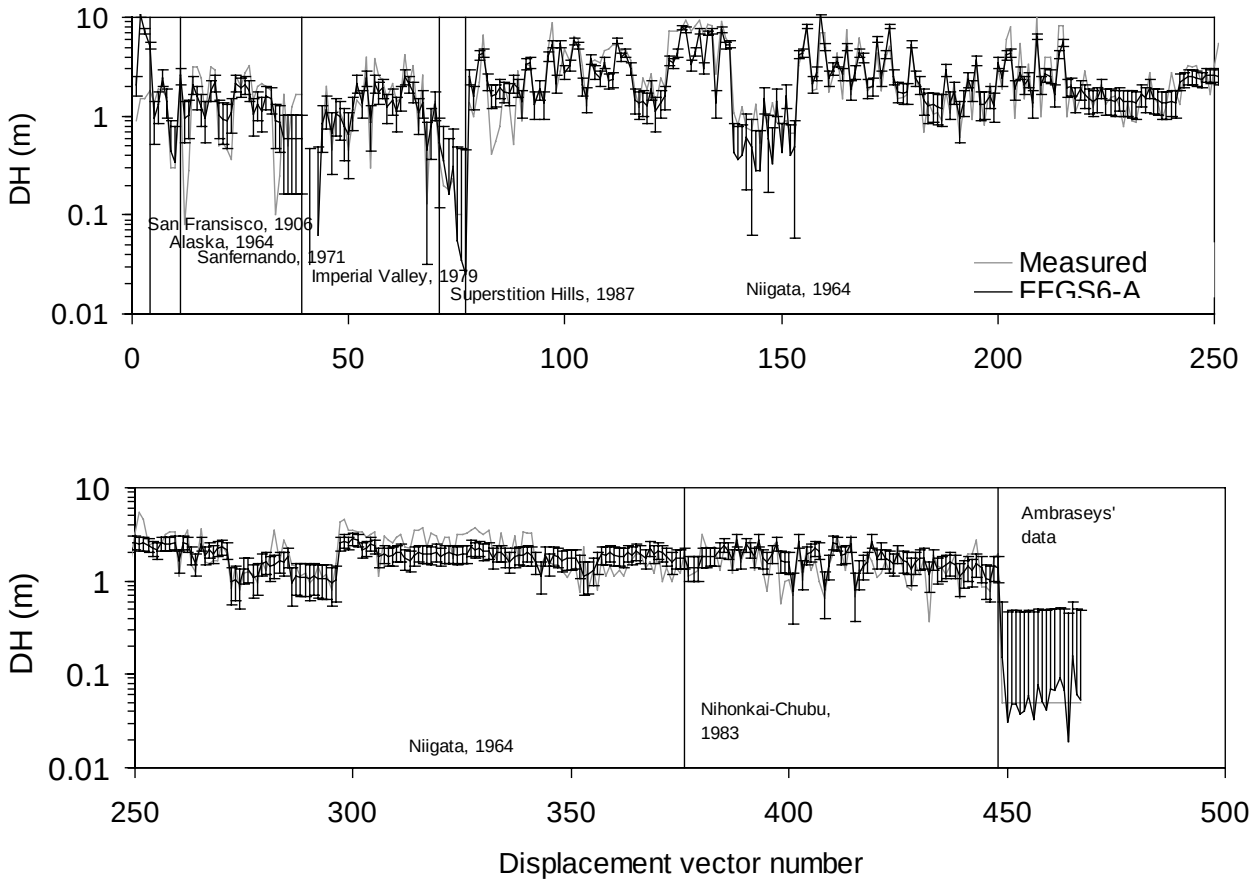

Figure 6-3. Model FFGS6-A for liquefaction-induced lateral displacement: measured displacement, and predicted mean displacement and confidence interval (95% *t*-distribution).

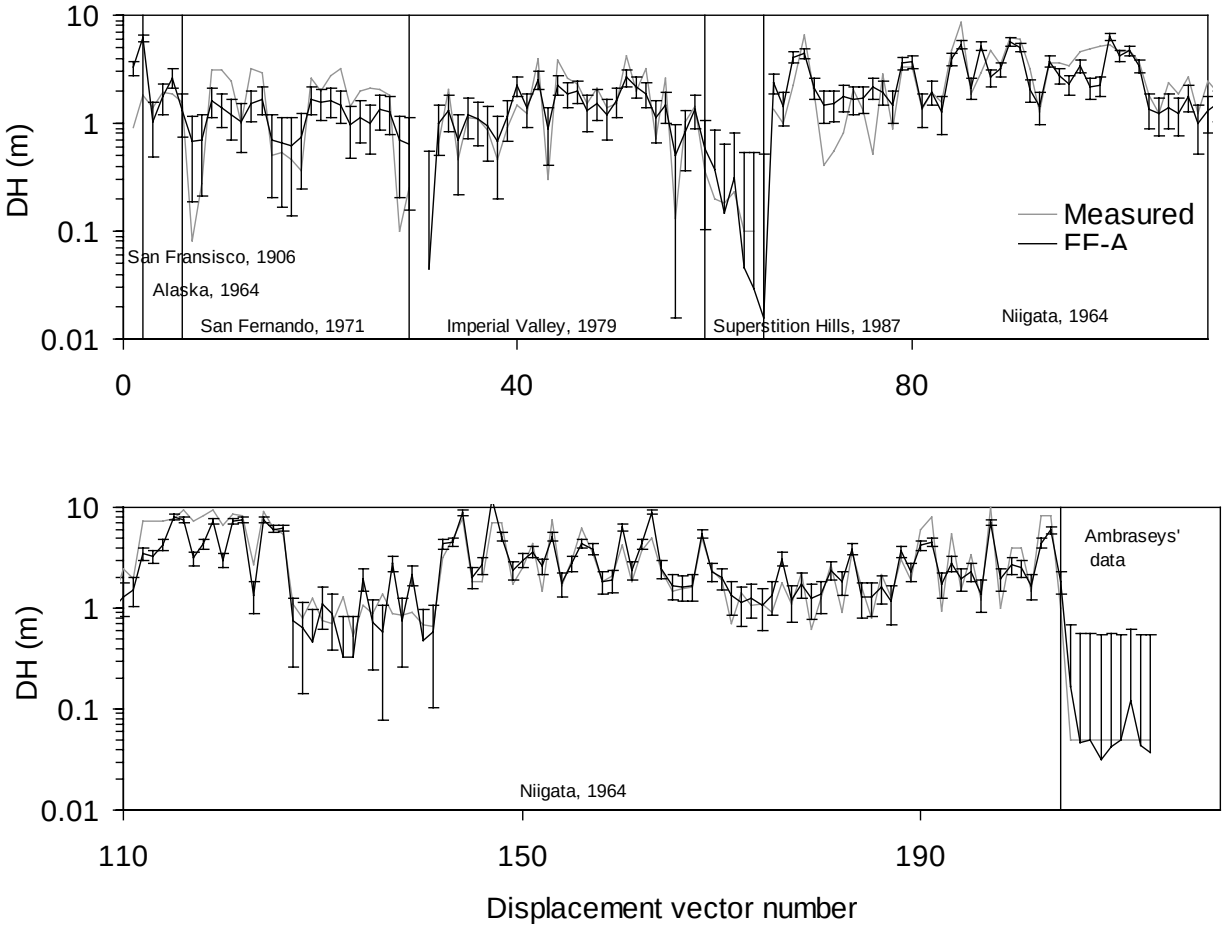

Figure 6-4. Model FF6-A for liquefaction-induced lateral displacement: measured displacement, and predicted mean displacement and confidence interval (95% t-distribution).

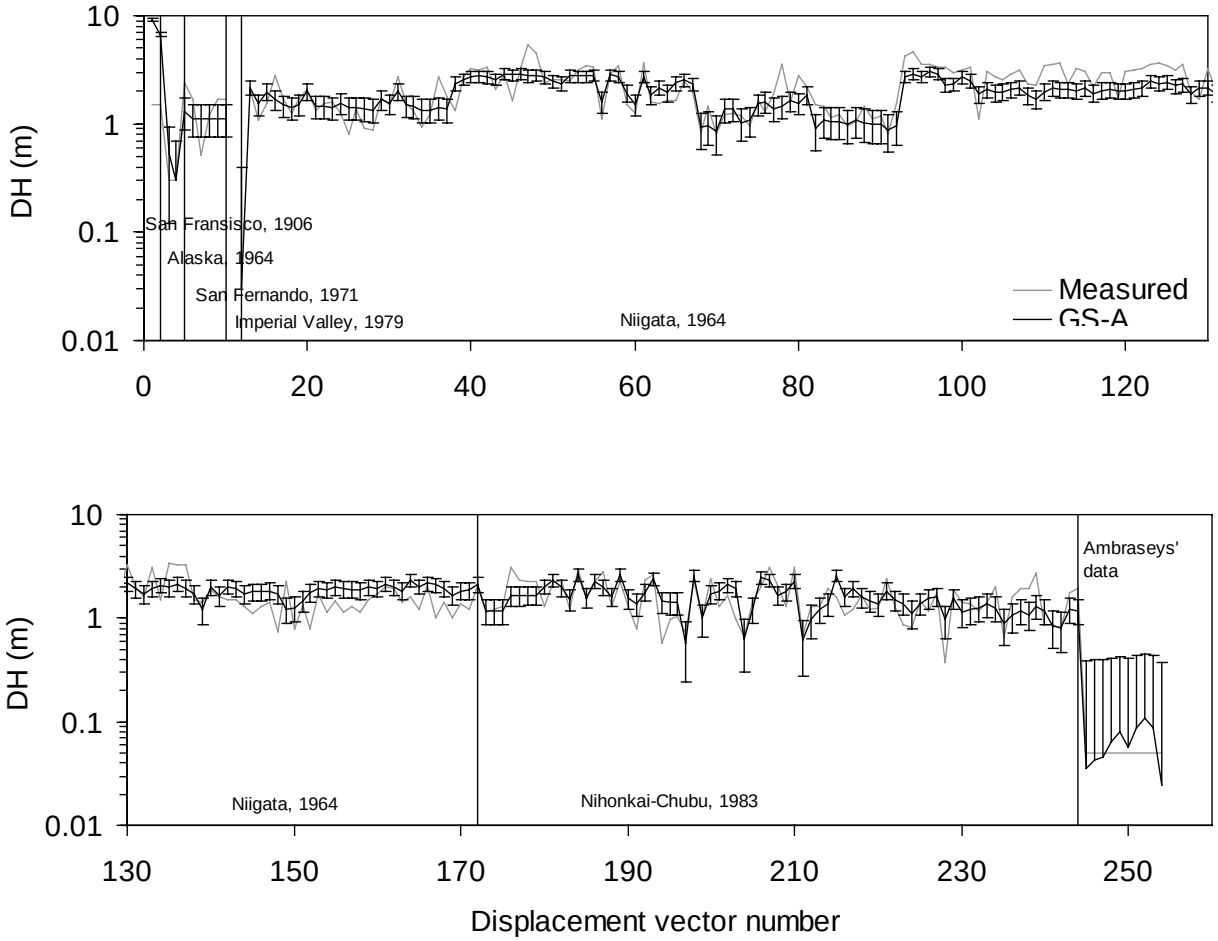

Figure 6-5. Model GS6-A for liquefaction-induced lateral displacement: measured displacement, and predicted mean displacement and confidence interval (95% t-distribution).

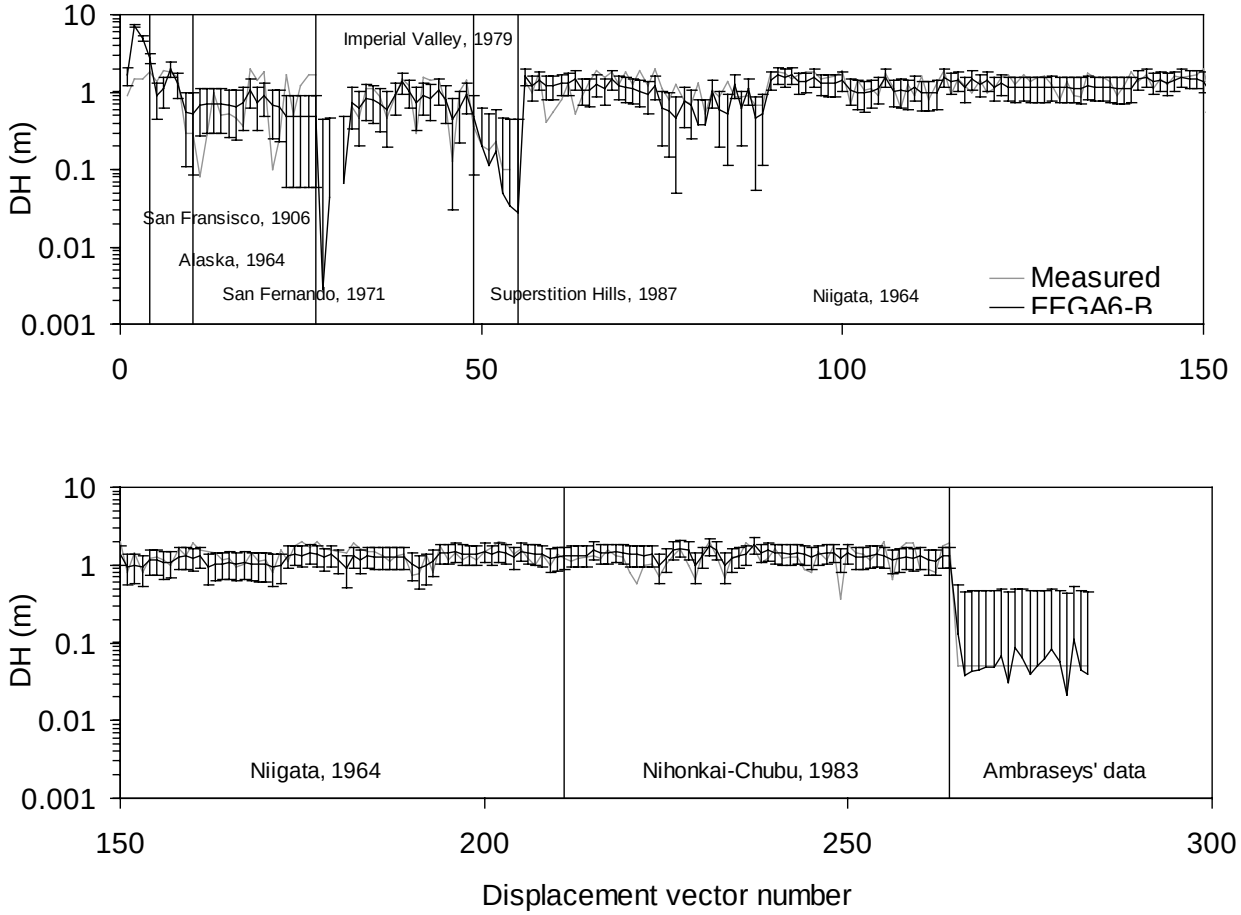

Figure 6-6. Model FFGS6-B for liquefaction-induced lateral displacement: measured displacement, and predicted mean displacement and confidence interval (95% t-distribution).

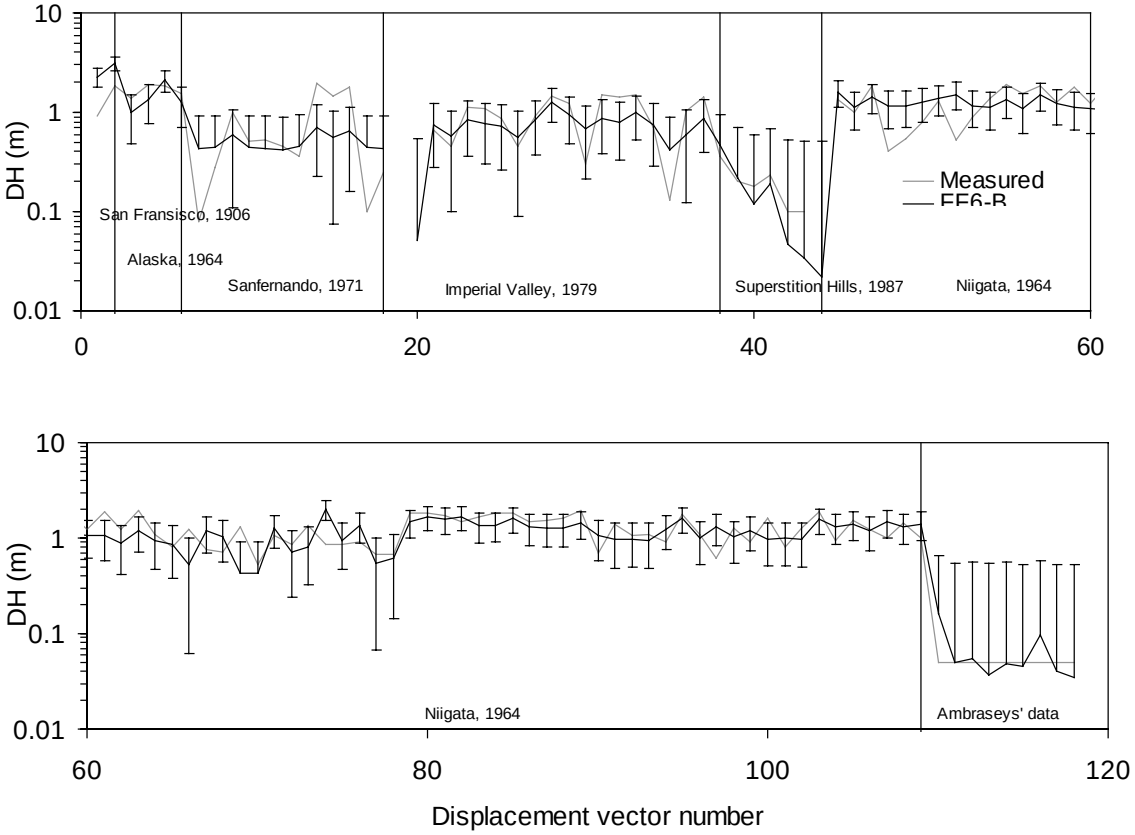

Figure 6-7. Model FF6-B for liquefaction-induced lateral displacement: measured displacement, and predicted mean displacement and confidence interval (95% t-distribution).

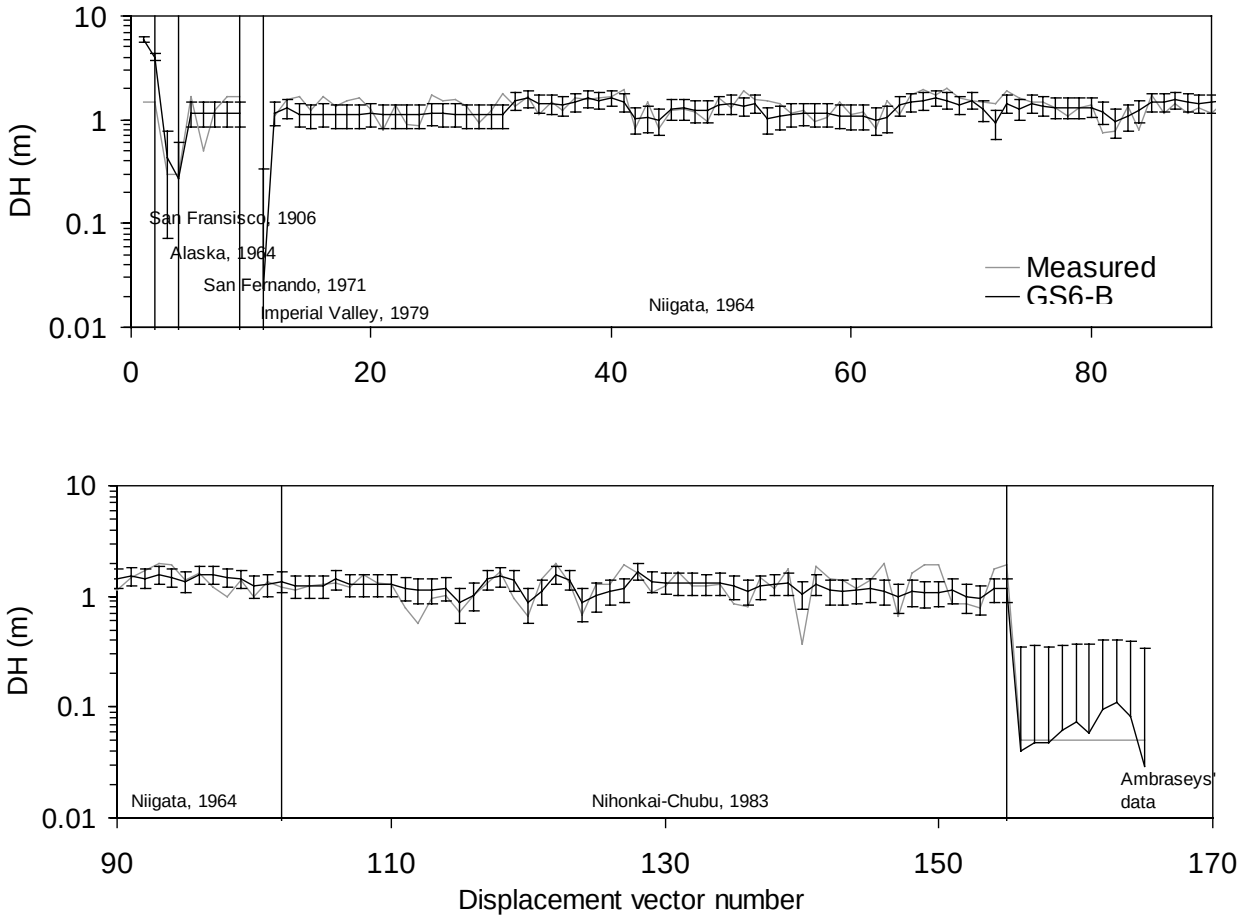

Figure 6-8. Model GS6-B for liquefaction-induced lateral displacement: measured displacement, and predicted mean displacement and confidence interval (95% t-distribution).

6.5 Probability calculation

Equation 14 defines the probabilistic models for assessing the probability of the liquefaction-induced ground deformation to exceed some threshold value D^*, given some local conditions characterized by the parameter values $\mathbf{X}_0$. The value of q should be set equal to 1 for the probability associated to a single event. The calculation of probability at a given site characterized by the parameter values $\mathbf{X}_0$ requires the values of the covariance matrix $\mathbf{C}$, the residual mean square s, the total number n of observations in the regression analysis, the total number p of MLR variables, and the values of the coefficients of the MLR analysis. All the required values are listed in Appendix B. Equation 15 is the Excel implementation of Eq. 14, which permits users to multiply the matrix $\mathbf{C}$ and vector $\mathbf{X}_0$.

Figure 9 shows an example of probability map which was generated by model FFGS6-A for slide G-10 FF' at Niigata, Japan, during 1964 Niigata earthquake. For comparison, Fig. 10 shows the measured displacement vectors in the same area.

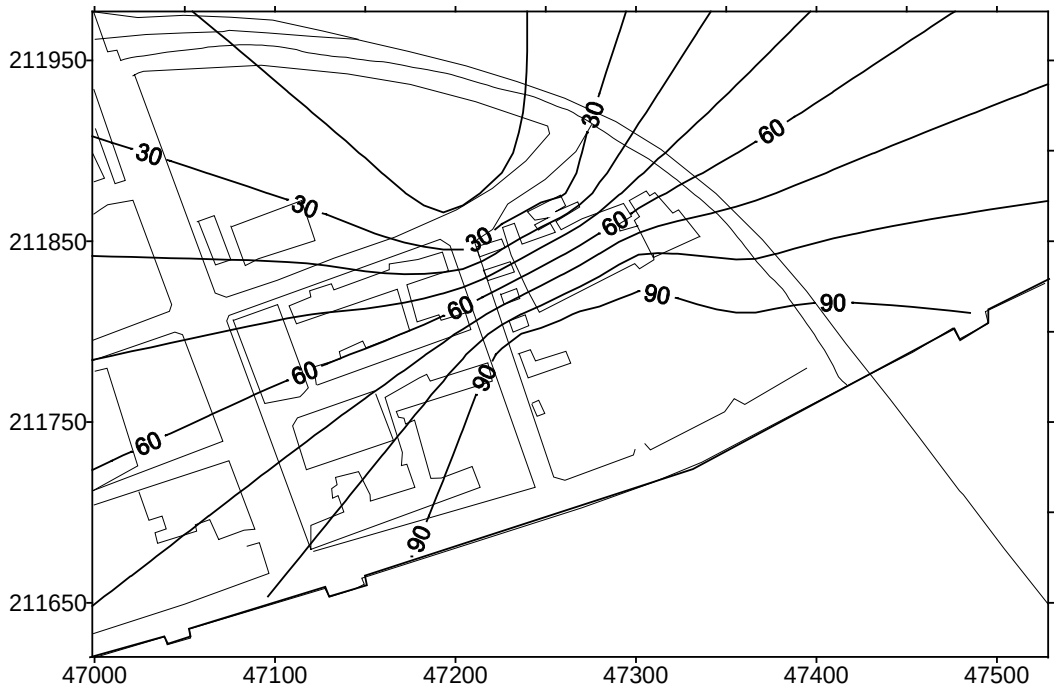

Figure 6-9. Probability of liquefaction-induced lateral spread larger than 2 m for slide G-10 FF' at Niigata, Japan, during 1964 Niigata earthquake (model FFGS6-A).

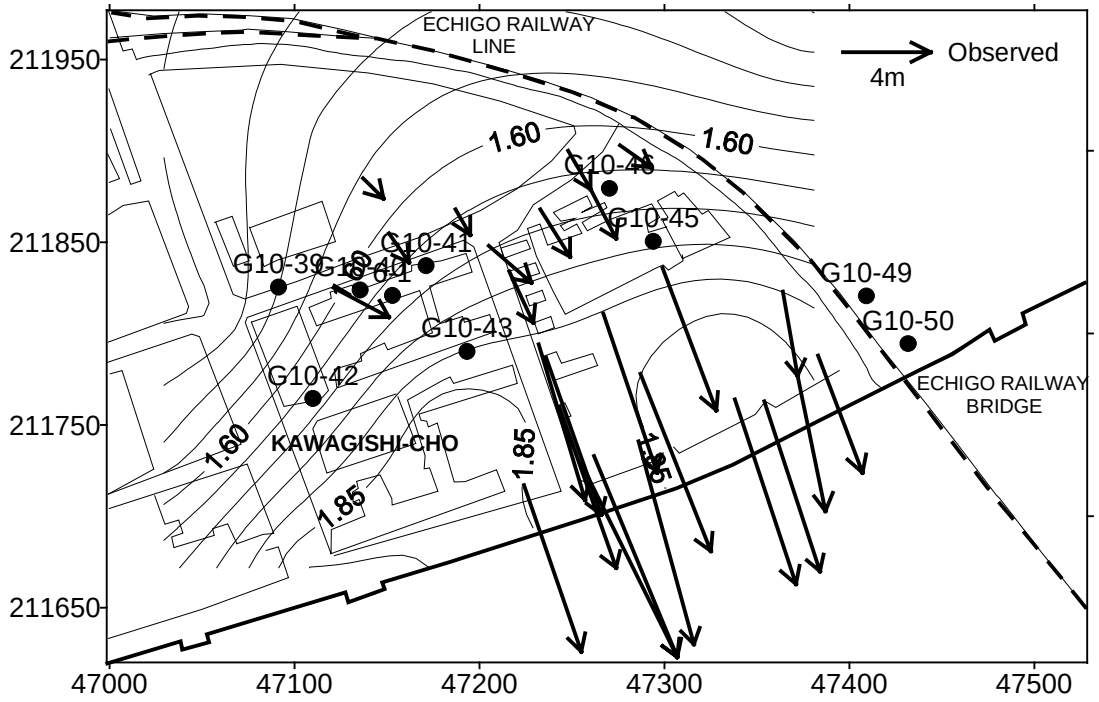

Figure 6-10. Liquefaction-induced displacements measured for slide G-10 FF' during 1964 Niigata, Japan, earthquake.

Mapping the probability of liquefaction-induced displacement amplitudes requires the use of spatial interpolation techniques similar to those used for mapping the predicted mean values of displacement. There are definite uncertainties in extending the probability maps outside the slide areas, which result from the uncertainties of mapping displacement amplitudes, as previously mentioned. Again, there is a need for collecting data outside liquefaction-induced slide area.

6.6 Future work

The MLR and probabilistic models developed in this study are based on a corrected version (Bartlett, 1998) of the database originally collected by Bartlett and Youd (1992). This database was constructed from data collected prior to the 1994 Northridge and 1995 Hyogoken Nanbu earthquakes. The multiple linear regression analyses in this study were based on this database and yielded a MLR model (i.e., FFGS6-A) similar to the original model developed by Bartlett and Youd (1992). There is a need to improve and extend the present database on liquefaction-induced lateral spreads by including the large data sets of high quality which were collected in the vicinity of the Van Norman Complex after the 1994 Northridge earthquake and in Kobe, Japan, after the 1995 Hyogoken Nanbu earthquake. The data should be collected inside and outside the areas where liquefaction-induced displacements were observed to take place. This effort is presently ongoing during the second research phase.

7. CONCLUSION

This report summarizes the findings of the first phase of a long-term research program. It has reviewed the theories and experiments on the mechanisms of liquefaction-induced ground deformation, including past work in the field, laboratory, shaking table tests, centrifuge experiments, and empirical and analytical modeling. Laboratory tests indicate that liquefied soils may deform during and after transient earthquake loadings. The lower amplitude range of liquefaction-induced deformation amplitude correspond mainly to cyclic ratchetting during transient earthquake loading, and is controlled by transient shear stress, number of loading cycles, relative density and stress-dilatancy. The upper amplitude range of liquefaction-induced deformation corresponds to post-liquefaction behavior with a regain of shear strength, which is also induced by a shear strain dependent dilatancy. There are still some disagreements between field observations and experiments in shaking table, centrifuge and laboratory tests about the relative timing of liquefaction-induced ground deformations and earthquake transient ground motions. Analytical models are capable of explaining successfully a few, but not all, aspects of liquefaction-induced deformations. Most of the analytical models require the calibration of numerous parameters for predicting liquefaction-induced deformations, which render them impractical to use over the large areas covered by gas distribution networks. The empirical models calibrated from case histories emerge as the most relevant, immediate and practical approach for predicting liquefaction-induced deformation over large areas.

This report provides some preliminary results and recommendations for estimating (1) the amplitude of liquefaction-induced ground displacement and (2) the probability for liquefaction-induced displacements to exceed some threshold amplitude. The models for assessment of the amplitude and probability of liquefaction-induced ground deformation are based on measured permanent displacements, topographical data, borehole information, and earthquake data prior to the 1994 Northridge and 1995 Hyogoken Nanbu earthquakes. Twelve Multiple Linear Regression (MLR) models have been calibrated from a revised database on liquefaction-induced ground deformations. These MLR models have six and four parameters, respectively, and cover ground-slope and free-face conditions. They have been calibrated from two data sets including all the displacement ranges, and displacements smaller than 2 meters, respectively. As companions to these MLR models, twelve probabilistic models have been proposed for assessing the confidence interval for predicting ground deformation and the probability of exceeding some ground deformation levels. The four-parameter models are recommended for assessing liquefaction-induced ground deformation when only regional geologic data is available. The six-parameter models are to be applied when there is sufficient information from soil boreholes.

Both MLR and probabilistic models are preliminary because they are only based on data collected from earthquakes prior to 1994. The next phase of the research is now focusing on data collection of high-quality case histories of liquefaction-induced ground deformation in the 1994 Northridge and 1995 Hyogoken Nanbu earthquakes. Following the completion of the new database on liquefaction-induced ground deformation, new generations of probabilistic models will be proposed.

8. REFERENCES

1. **Adachi, T., and F. Oka,** 1982, "Constitutive equations for sands and overconsolidated clays and assigned works for sands," *Proceedings of the International Workshop on Constitutive Relations for Soils*, Grenoble, pp. 141-157.

2. **Ambraseys, N. N.,** 1988, "Engineering Seismology," *Earthquake Engineering and Structural Dynamics,* Vol. 17, pp. 1-105.

3. **Arulanandan, K., and R. F. Scott,** 1993-1994, Verification of Numerical procedures for the analysis of soil liquefaction problems," *Proceedings of the International Conference on the Verification of Numerical Procedures for the Analysis of Soil Liquefaction Problems,* Vols. 1 and 2, A. A. Balkema, Rotterdam, the Netherlands.

4. **Arulmoli, K., K. K. Muraleetharan, M. M. Hossain, and L. S. Fruth,** 1992, "VELACS: Verification of Liquefaction Analysis by Centrifuge Studies. Laboratory Testing Program. Soil Data Report," *The Earth Technology Corporation*, Long Beach, CA, report for the National Science Foundation.

5. **Bardet, J. P.,** 1986, "A Bounding Surface Plasticity Model for Sands," *Journal of Engineering Mechanics, ASCE,* Vol. 112, No. 11, pp. 1198 -1217.

6. **Bardet, J. P.,** 1989, "LINOS: a nonlinear finite element program for Geomechanics and Geotechnical Engineering," *University of Southern California, Los Angeles.*

7. **Bardet, J. P.,** 1990, "A Hypoplastic Model for Sand," *Journal of Engineering Mechanics, ASCE,* Vol. 116, No. 9, pp. 1973 -1998.

8. **Bardet, J. P.,** 1995, "A Scaled Memory Model for the Cyclic Behavior of Soils," *Journal of Geotechnical Engineering, ASCE,* Vol. 121, No. 11, pp. 766 - 775.

9. **Bardet, J. P.,** 1995, "A Scaled Memory Model for the Undrained Behavior of Anisotropic Clays," *Journal of Geotechnical Engineering, ASCE,* Vol. 121, No. 1, pp. 755 - 764.

10. **Bardet, J. P., and C. A. Davis,** 1996, " Engineering Observations on Ground Motion At the Van Norman Complex after the 1994 Northridge Earthquake," *Bulletin of the Seismological Society of America,* Vol. 86, No. 1B, pp. S333-S349.

11. **Bardet, J. P., and C. A. Davis,** 1996, . Performance of San Fernando Dams during the 1994 Northridge Earthquake,. *Journal of Geotechnical Engineering,* ASCE, Vol. 122, No. 7, pp. 554-564.

12. **Bardet, J. P., Q. Huang, and S. W. Chi,** 1993, "Numerical Prediction for Model No. 1; Numerical Prediction for Model No. 3; and Numerical Prediction for Model No. 7," *Proceedings of the International Conference on the Verification of Numerical Procedures for the Analysis of Soil Liquefaction Problems,* K. Arulanandan and R. F. Scott eds., A. A. Balkema pub., pp. 67 - 86, 483 - 488, and 829 - 834.

13. **Bartlett, S. F. and T. L. Youd,** 1992, . Empirical analysis of horizontal ground displacement generated by liquefaction-induced lateral spreads,. *Technical report NCEER-92-0021*, National Center for Earthquake Engineering Research, State University of New York, Buffalo, pp. 5-14-15.

14. **Bartlett, S. F.,** 1998, Revised liquefaction-induced database, *Private communication.*

15. **Bartlett, S. F. and T. L. Youd,** 1995, . Empirical prediction of Lateral Spread Displacement,. *Journal of Geotechnical Engineering*, ASCE, Vol. 121, No. 4, pp. 316-329.

16. **Baziar, M. H., R. Dobry, and A. W. M. Elgamal,** 1992, . Engineering evaluation of permanent ground deformation due to seismically-induced liquefaction," Technical report NCEER-92-0007, *National Center for Earthquake Engineering Research*, State University of New York, Buffalo, 2 Vol.

17. **Byrne, P. M.,** 1991, . A model for predicting liquefaction induced displacement," *Proceedings of the second international conference on recent advances in geotechnical earthquake engineering and soil dynamics*, St. Louis, Missouri, Vol. 2, pp. 1027-1035.

18. **Byrne, P. M.,** 1997, . Liquefaction-induced displacements*," NCEER Workshop on Post-liquefaction Ground Deformation*, Presentation Notes, August.

19. **Cao, Y. L., and K. T. Law,** 1992, "Energy dissipation and dynamic behaviour of clay under cyclic loading," *Canadian Geotechnical Journal,* Vol. 29, pp. 103-111.

20. **Dafalias, Y.F., and L. R. Herrmann,** 1982, "Bounding surface formulation of soil plasticity," *Soil Mechanics - Transient and cyclic loads,* G. Pande and O. C. Zienkiewicz, eds., John Wiley and Sons, London, UK., pp. 253-282.

21. **Davis, C., and J. P. Bardet,** 1996, "Performance of two reservoirs during the 1994 Northridge Earthquake," *Journal of Geotechnical Engineering, ASCE,* Vol. 122, No. 8, pp. 613-622.

22. **Dobry, R., Taboada, V., and L. Liu,** 1995, . Centrifuge modeling of liquefaction effects during earthquakes,. *Proceedings of the 1rst International Conference on Earthquake Geotechnical Engineering, IS-Tokyo*, Keynote and Theme lectures, pp. 129-162.

23. **Draper, N. R., and H. Smith**, 1981, *Applied Regression Analysis*, 2nd edition, John Wiley & Sons, New York, p 709.

24. **FLAC,** 1995, "Fast Lagrangian Analysis of Continua," Version 3.3, Itasca Consulting Group Inc, Minneapolis, Minesota.

25. **Hamada, M., H. Sato, T. Kawakami,** 1994, "A consideration for the mechanism for liquefaction-related large ground displacement," *Proceedings of the 5th U.S. Japan Workshop on Earthquake Resistant Design of Lifeline Facilities and Countermeasures for Soil Liquefaction*, NCEER Report 94-0026, T. D. O'Rourke and M. Hamada, Eds., pp. 217-232.

26. **Hamada, M., and K. Wakamatsu,** 1998, "Liquefaction-induced ground displacement triggered by quaywall movement," *Soils and Foundations, Special Issue Vol. 2, Japanese Geotechnical Society*, pp. 85-96.

27. **Hamada, M., and T. D. O'Rourke**, 1992, "Case histories of liquefaction and lifeline performance during past earthquakes," Technical report NCEER-92-0001, National Center for Earthquake Engineering Research, State University of New York, Buffalo, 2 Vols.

28. **Hamada, M., R. Isoyama. and K. Wakamatsu,** 1996, "Liquefaction-induced ground displacement and its related damage to lifeline facilities," *Soils and Foundations*, Special Issue on Geotechnical Aspects of the January 17 1995 Hyogoken-Nanbu Earthquake, Japanese Geotechnical Society, pp. 81- 97.

29. **Hamada, M., R. Isoyama. and K. Wakamatsu,** 1996, "The 1995 Hyogoken-Nanbu (Kobe) Earthquake, Liquefaction, Ground Displacement and Soil Condition in Hanshin Area," *Association for Development of Earthquake Prediction*, The School of Science and Engineering, Waseda University, Japan Engineering Consultants.

30. **Hamada, M., S. Yasuda, R. Isoyama, and K. Emoto,** 1986, . Study on Liquefaction induced permanent ground displacement*," Report for the Association for the Development of Earthquake Prediction.*

31. **Harder, L.,** 1991, "Evaluation of Liquefaction Potential Using the SPT," *Seismic Short Course, Evaluation and Mitigation of Earthquake Induced Liquefaction Hazards*, University of Southern California, Los Angeles, February.

32. **Holzer, T. L., J. C. Tinsley, III, M. J. Bennett, and C. S. Mueller,** 1994, . Observed and predicted ground deformation - Miller Farm lateral spread, Watsonville, California, " *Proceedings of the 6th U.S. Japan Workshop on Earthquake Resistant Design of Lifeline Facilities and Countermeasures for Soil Liquefaction*, NCEER, M. Hamada and T. D. O'Rourke, Eds., pp. 79-98.

33. **Holzer, T. L., M. J. Bennett, D. J. Ponti, and J. C. Tinsley, III,** 1998, . Permanent ground deformation in alluvium during the 194 Northridge, California, earthquake," *USGS Open-file report 98-118,* Menlo Park, CA.

34. **Holzer, T. L., M. J. Bennett, J. C. Tinsley, III, D. J. Ponti, and R. V. Sharp,** 1996, "Causes of ground failure in alluvium during the Northridge," California, earthquake of January 17,1994" *Proceedings of the 6th U.S. Japan Workshop on Earthquake Resistant Design of Lifeline Facilities and Countermeasures for Soil Liquefaction*, NCEER, M. Hamada and T. D. O'Rourke, Eds., pp. 345-360.

35. **Ishihara, K.,** 1993, "Liquefaction and flow failure during earthquakes," The 33rd Rankine lecture, *Geotechnique*, Vol. 43, No. 3, pp. 351 - 415.

36. **Ishihara, K.,** 1996, *Soil Behavior in Earthquake Geotechnics*, Oxford Science Publications, Clarendon Press, Oxford, UK.

37. **Ishihara, K., K. Yoshida, and M. Kato**, 1997, "Characteristics of lateral Spreading in Liquefied Deposits during the 1995 Hanshin-Awaji Earthquake, *Journal of Earthquake Engineerin*g, Vol. 1, No. 1, pp. 23-55.

38. **Ishihara, K., S. Yasuda, and H. Nagase**, 1996, "Soil characteristics and ground damage," Soils and Foundations, *Special Issue on Geotechnical Aspects of the January 17 1995 Hyogoken-Nanbu Earthquake*, Japanese Geotechnical Society, pp. 109-118.

39. **Isoyama , R.,** 1994, "Liquefaction-Induced Ground Failures and Displacements Along the Shiribeshi-toshibetsu River Caused by the 1993 Hokkaido Nansei-oki Earthquake," *Proceedings of the 5th U.S. Japan Workshop on Earthquake Resistant Design of Lifeline Facilities and Countermeasures for Soil Liquefa*ction, NCEER, T. D. O'Rourke and M.. Hamada, Eds., pp. 1-26.

40. **Jibson, R.,** 1994, "Predicting earthquake-induced landslide displacement using Newmark's sliding block analysis," Transportation Research Record 1411, Transportation Research Board, Washington, D.C., pp. 9-17.

41. **Karube, D., and M. Kimura**, 1996, . Damage to Foundation of Railways Structures,. Soils and Foundations, *Special Issue on Geotechnical Aspects of the January 17 1995 Hyogoken Nanbu Earthquake*, Japanese Geotechnical Society, pp. 201-210.

42. **Ko, H.Y.,** 1988, "Summary of the state-of-the-art in centrifuge model testing," *In Centrifuges in Soil Mechanics* (eds Craig, W.H., James, R.G. and Schofield, A.N.), Balkema, Rotterdam, pp. 11-18.

43. **Kokusho, T., K. Watanabe, and T. Sawano,** 1998, "Effect of water film on lateral flow failure of liquefied sand," *Proceedings of the 11th European Conference on Earthquake Engineering*, A. A. Balkema, Rotterdam, The Netherlands, pp. 1-8.

44. **Kramer, S. L.,** 1996, *Geotechnical Earthquake Engineering*, Prentice-Hall, Upper Saddle River, NJ, pp. 451-453.

45. **Law, K. T., and Y. L. Cao,** 1990, "An energy approach for assessing seismic liquefaction potential," *Canadian Geotechnical Journal,* Vol. 27, pp. 320 -329.

46. **Liao, S. S. C.,** 1986, "Statistical modeling of earthquake-induced liquefaction," *Ph.D. Thesis*, Department of Civil Engineering, Massachusetts Institute of Technology, 470 p.

47. **Matsui, T., and K. Oda,** 1996, "Foundation Damage of Structures," *Soils and Foundations, Special Issue on Geotechnical Aspects of the January 17 1995 Hyogoken Nanbu Earthquake*, Japanese Geotechnical Society, pp. 189-200.

48. **Microsoft Excel,** 1994, *Microsoft Excel, Version 5.0*, Microsoft Corporation.

49. **Minitab,** 1989, *Minitab Statistical Software, Release 7*, Minitab Inc., 3081 Enterprise Drive, State College, PA 16801.

50. **Nakase, H., A. Hiro-oka, and T. Yanagihata,** 1997, "Deformation characteristics of liquefied loose sand by triaxial compression tests," *Proceedings of IS-Nagoya 97, Deformation and Progressive Failure in Geomechanics*, A. Asaoka, T. Adachi, and F. Oka, eds., Pergamon, Elsevier Science, pp. 559-564.

51. **Newmark, N. M.,** 1965, "Effects of Earthquakes on Embankments and Dams," *Géotechnique,* 15, No.2, pp.139-160.

52. **O'Rourke, T. D., and P. A. Lane,** 1989, . Liquefaction hazards and their effects on buried pipelines,. Technical report NCEER-89-0007, National Center for Earthquake Engineering Research, State University of New York, Buffalo.

53. **Para-Colmenares, E. J.,** 1996, "Numerical modeling of liquefaction and lateral ground deformation including cyclic mobility and dilation response in soil systems," *Ph.D. Thesis,* Rensselaer Polytechnic Institute, Troy, NY.

54. **Pastor, M., O. C. Zienkiewicz, and K. H. Leung**, 1985, "Simple model for transient soil loading in earthquake analysis," *International Journal of Analytical Numerical Methods in Geomechanics,* Vol. 9, pp. 453-498.

55. **Pease, J. W., and T. D. O'Rourke,** 1993, . Liquefaction Hazards in the Mission District and South of Market Stress Areas, San Francisco, California," *U.S. Geological Survey*, External Contract No. 14-08-001-G2128.

56. **Peiris, T. A. and Yoshida, N.,** 1995, "Dilatancy characteristics of sand under cyclic loading," *Proc. Of First International Conference on Earthquake Geotechnical Engineering*, Tokyo, pp. 265-270.

57. **Peiris, T. A. and Yoshida, N.,** 1996, "Modeling of Volume Change Characteristics of Sand under Cyclic Loading*," Proc. of Eleventh World Conference on Earthquake Engineering*, Acapulco, Mexico, Paper No. 1087.

58. **Robertson, P. K., and R. G. Campanella,** 1985, Liquefaction Potential of Sands Using the Cone Penetration Test*," Journal of Geotechnical Engineering*, ASCE, Vol. 111, No. 3, pp. 298-307.

59. **Rauch, A. F.,** 1997, EPOLLS: An empirical method for predicting surface displacement due to liquefaction-induced lateral spreading in earthquakes, *PhD thesis*, Virginia Polytechnic Institute, Virginia.

60. **Sasaki, Y., I. Towahata, K. Tokida, K. Yamada, H. Matsumoto, Y. Tamari, and S. Saya,** 1992, "Mechanism of permanent displacement of ground caused by seismic liquefaction," *Soils and Foundations*, Vol. 32, No. 3, pp. 76-96.

61. **Scott, R.F., and B. Hushmand, 1995,** . Piezometer performance at Wildlife liquefaction site, California," Journal of Geotechnical Engineering Division, ASCE, Discussion, Vol. 121, No. 12, pp. 912-919.

62. **Seed, H. B., and P. De Alba,** 1986, "Use of SPT and CPT Tests for evaluating the liquefaction resistance of sands," *Use of In-Situ Tests in Geotechnical Engineering*, ASCE, Geotechnical Special Publication No. 6, pp. 281-302.

63. **Seed, H. B., and I. M. Idriss,** 1971, "Simplified procedure for evaluating soil liquefaction potential," *Journal of the Soil Mechanics and Foundation Division, ASCE,* Vol. 97, No. 9, pp. 1249-1274.

64. **Seed, H. B., Tokimatsu, F. K., Harder, L. F. and R. M. Chung,** 1985, "Influence of SPT Procedures in Soil Liquefaction Resistance Evaluation," *Journal of Geotechnical Engineering Division*, ASCE, No. 12, pp. 1425-1445.

65. **Shamoto, Y. J.-M. Zhang, and S. Goto,** 1997, "Mechanism of large Post-Liquefaction Deformation in Saturated sand," *Soils and Foundations*, *Japanese Geotechnical Society*, Vol. 37, No. 2, pp. 71-80.

66. **Shamoto, Y., J.-M. Zhang, and K. Tokimatsu**, 1997, "New charts for predicting large residual post-liquefaction ground deformation," Extended abstract for *the 8th International Conference on Soil Dynamics and Earthquake Engineering* (SDEE-97), 2 p.

67. **Shamoto, Y., J.-M. Zhang, and K. Tokimatsu**, 1998, "Methods for evaluating residual post-liquefaction ground settlement and horizontal displacement," *Soils and Foundations, Special Issue Vol. 2, Japanese Geotechnical Society*, pp. 69-84.

68. **Smith, I. M.,** 1994, "An overview of numerical procedures used in the VELACS project," *Proceedings of the international conference on the Verification of Numerical Procedures for the Analysis of Soil Liquefaction Problems*, Vol. 2, K. Arulanandan and R. F. Scott, eds., A. A. Balkema, Rotterdam, pp. 1321 - 1337.

69. **Stokoe, K. H. II, J. M. Roesset, J. G. Biecherwale, and M. Aoouad,** 1988, "Liquefaction potential of sands from shear wave velocity," *Proceedings of the 9th world conference on earthquake engineering*, Tokyo, Japan, Vol. III, pp. 213-218.

70. **Surfer**, 1998, *Surfer for Windows, User's guide, Version 6*, Golden Software, Inc., Golden, Colorado.

71. **Taguchi, Y., A. Tateishi, F. Oka, and A. Yashima,** 1995, "A cyclic elasto-plastic model for sand based on the generalized flow rule and its application," *Proceedings of the 5th International Symposium on Numerical Methods in Geomechanics*, Davos, pp. 57-62.

72. **Tokimatsu, K., and H. B. Seed,** 1987, "Evaluation of settlements in sand due to earthquake shaking," *Journal of Geotechnical Engineering, ASCE,* Vol. 113, No. 8, pp. 861-878.

73. **Tokimatsu, K., H. Mizumo, and M. Kakurai**, 1996, "Building Damage Associated with Geotechnical Problems," *Soils and Foundations*, *Special Issue on Geotechnical Aspects of the January 17 1995 Hyogoken-Nanbu Earthquake*, Japanese Geotechnical Society, pp. 219-234.

74. **Towhata, I., H. Toyota, and W. M. Vargas,** 1995**,** "Dynamics in lateral flow of liquefied ground," *Proceedings of the 10th Asian Regional Conference on Soil Mechanics and Foundation Engineering, Beijing,* Vol. 2, pp. 245-247.

75. **Towhata, I., H. Toyota, and W. M. Vargas,** 1996**,** "A transient study on lateral flow on liquefied ground," *Proceedings of the 7th International Symposium on Landslides,* Trondheim, Norway, A. A. Balkema, The Netherlands, Vol. 2, pp. 1047-1054.

76. **Towhata, I., R. P. Orense, and H. Toyota,** 1997**,** . Mathematical principles in prediction of lateral ground displacement induced by seismic liquefaction," *Soils and Foundations,* Accepted for publication.

77. **Orense, R. P., and I. Towhata,** 1996**,** . Three-dimensional analysis on lateral displacement of liquefied subsoil," *Soils and Foundations,* Accepted for publication.

78. **Towhata, I., Y. Kogai, K. Amimoto, and H. G. Putra,** 1996, . Theory and model tests on mitigation measures against lateral flow of liquefied ground," *Proceedings of the 6th U.S. Japan Workshop on Earthquake Resistant Design of Lifeline Facilities and Countermeasures for Soil Liquefaction*, NCEER, M. Hamada and T. D. O'Rourke, Eds., pp. 403-419.

79. **Towhata, I., Y. Kogai, K. Amimoto, and H. G. Putra,** 1996, . Mitigation of lateral flow of liquefied ground," *Proceedings of the 28th Joint Meeting, Panels for Earthquake Engineering and Wind Engineering*, UJNR, Gaithersburg, Maryland, US, pp. 39-51.

80. **Yashima, A., F. Oka, J. M. Konrad, R. Uzuoka, and Y. Taguchi,** 1997, "Analysis of a progressive flow failure in an embankment of compacted fill," *Proceedings of IS-Nagoya, A.* Asaoka, T. Adachi, and F. Oka, eds., *Pergamon,* pp. 599-604.

81. **Yasuda, S., K. Ishihara, and S. Iai,** 1997, "A simple procedure to predict ground flow due to liquefaction behind quaywalls," *Extended abstract for the 8th International Conference on Soil Dynamics and Earthquake Engineering* (SDEE-97), 2 p.

82. **Yasuda, S., Masuda, T., Yoshida, N., Kiku, H., Itafuji, S., Mine, K. and Sato, K.,** 1994, "Torsional shear and triaxial compression tests on deformation characteristics of sands before and after liquefaction," *Proc., 5th U.S.-Japan Workshop on Earthquake Resistant Design of Lifeline Facilities and Countermeasures Against Soil Liquefaction*, Salt Lake City, Technical Report NCEER-94-0026, National Center for Earthquake Engineering Research, U.S.A., pp. 249-266.

83. **Yegian, M. K., E. A. Marciano, and V. G. Gharaman,** 1991, "Earthquake-induced permanent deformation: probabilistic approach," *Journal of Geotechnical Engineering, ASCE,* Vol. 117, No. 1, pp. 35-50.

84. **Yoshida, N.,** 1994, "Applicability of conventional computer code SHAKE to nonlinear problem," *Proceedings of the Symposium on Amplification of Ground Shaking in Soft Ground,* JSSMFE, pp.14-31 (in Japanese).

85. **Yoshida, N.,** 1996, "Initial Stress Effect on Response of Level Ground," *Eleventh World Conference on Earthquake Engineering,* Acapulco, Mexico, Paper No. 102.3.

86. **Yoshida, N., Tsujino, S. and Inadomaru,K.,** 1995, "Preliminary study on the settlement of ground after liquefaction," *Proc., The 29th Japan National Conference of Soil Mechanics and Foundation Engineering*, pp.859-860 (in Japanese).

87. **Youd, T. L., and D. M. Perkins,** 1987, . Mapping of Liquefaction Severity Index,. *Journal of Geotechnical Engineering Division*, ASCE, No. 11, pp. 1374-1392.

88. **Youd, T. L., and I. M. Idriss,** 1998, *Proceedings of NCEER workshop on evaluation of liquefaction resistance of soils*, National Center for Earthquake Engineering Research, State University of New York, Buffalo.

89. **Youd, T. L., and S. J. Kiehl,** 1996, "Ground deformation characteristics caused by lateral spreading during the 1995 Hanshin-Awaji earthquake," *Proceedings of the 6th U.S. Japan Workshop on Earthquake Resistant Design of Lifeline Facilities and Countermeasures for Soil Liquefaction*, NCEER, M. Hamada and T. D. O'Rourke, Eds., pp. 221-242.

90. **Youd, T. L., and T. L. Holzer,** 1994, "Piezometer performance at Wildlife liquefaction site, California," Journal of Geotechnical Engineering Division, ASCE, Vol. 120, No. 6.

91. **Youd, T. L., E. L. Harp, D. K. Keefer, and R. C. Wilson,** 1985, "The Borah peak, Idaho earthquake of October 28, 1983 - liquefaction," Earthquake Spectra, Vol. 2, No. 6.

92. **Zienkiewicz, O. C. and T. Shiomi,** 1984, "Dynamic behavior of saturated porous media: the generalized Biot formulation and its numerical solution," *International Journal of Numerical and Analytical Methods in Geomechanics*, Vol. 8, pp. 71-96.

93. **Zienkiewicz, O. C., A. H. C. Chan, M. Pastor, D. K. Paul, and T. Shiomi,** 1990, "Static and dynamic behavior of soils: a rational approach to quantitative solutions: Part I-fully saturated problems," *Proc. Roy. Soc. A.,* 429, pp. 285-309.

APPENDIX A: LIQUEFACTION DATABASES

The following databases have been used in the course of this research:

- Database of liquefaction occurrence (Harder, 1991).
- Database of liquefaction-induced ground deformation (Bartlett and Youd, 1992).
- Database of liquefaction-induced ground deformation (Bartlett, 1998).

All these databases are available as EXCEL files from http://rccg03.usc.edu/gees/

APPENDIX B: COEFFICIENTS FOR MLR AND PROBALISTIC MODELS

Appendix B provides the values of the coefficients required for calculating (1) MLR mean values of liquefaction-induced ground displacement, (2) confidence intervals on predicted displacement, and (3) probability of exceeding some amplitude of liquefaction-induced ground deformation. There is a total of twelve probabilistic models corresponding to the twelve MLR models FFGS6-A, FF6-A, GS6-A, FFGS6-B, FF6-B, GS6-B, FFGS4-A, FF4-A, GS4-A, FFGS4-B, FF4-B, and GS4-B. The model variables are defined by the vector **X**, as introduced in Chapter 6. Appendix B provides for each model the MLR coefficients, the covariance matrix **C**, the total number n of observations, the total number p of degrees of freedom, and the residual mean square s^2.

Table B1. Values of coefficients for MLR and probabilistic models FFGS6-A.

Components of **X**									
1.0	*0 or 1*	M_w	*LOG(R)*	*R*	*LOG(W_{ff})*	*LOG(S)*	*LOG(T_{15})*	*LOG(100-F_{15})*	*D50$_{15}$*
MLR coefficients									
b_0	b_{off}	b_1	b_2	b_3	b_4	b_5	b_6	b_7	b_8
-14.551	-0.483	1.096	-0.873	-0.014	0.634	0.275	0.494	4.053	-0.814
Covariance matrix **C** (symmetric)									
0.001	0.000	0.002	0.000	0.000	-0.001	0.000	0.000	-0.007	0.001
	0.047	0.002	0.000	0.000	-0.040	-0.011	-0.005	-0.011	0.001
		0.029	0.000	-0.001	-0.004	0.004	0.000	-0.104	-0.005
			0.026	-0.001	0.005	-0.003	-0.005	-0.007	-0.014
				0.000	0.000	0.000	0.000	0.002	-0.001
					0.047	0.000	0.000	0.011	0.007
						0.045	0.011	-0.011	0.000
Number of observations (n) = 467							0.022	-0.003	-0.004
Number of degrees of freedom (p) = 9								0.386	0.005
Residual mean square (s^2) = 0.046									0.196

Table B2. Values of coefficients for MLR and probabilistic models FF6-A.

Components of **X**							
1.0	M_w	*LOG(R)*	*R*	*LOG(W_{ff})*	*LOG(T_{15})*	*LOG(100-F_{15})*	*D50$_{15}$*
MLR coefficients							
b_0	b_1	b_2	b_3	b_4	b_6	b_7	b_8
-17.372	1.248	-0.923	-0.014	0.685	0.300	4.826	-1.091
Covariance matrix **C** (symmetric)							
11.171	-0.701	0.720	-0.008	-0.204	0.260	-3.712	1.371
	0.084	-0.050	0.000	0.006	-0.015	0.097	-0.113
		0.088	-0.001	0.000	0.005	-0.233	0.078
			0.000	0.000	0.000	0.004	-0.002
				0.052	-0.005	0.068	-0.003
Number of observations (n) = 213					0.049	-0.102	0.017
Number of degrees of freedom (p) = 7						1.727	-0.383
Residual mean square (s^2) = 0.058							0.466

Table B3. Values of coefficients for MLR and probabilistic models GS6-A.

Components of **X**							
1.0	M_w	*LOG(R)*	*R*	*LOG(S)*	*LOG(T_{15})*	*LOG(100-F_{15})*	*D50*$_{15}$
MLR coefficients							
b_0	b_1	b_2	b_3	b_5	b_6	b_7	b_8
-14.152	0.988	-1.049	-0.011	0.318	0.619	4.287	-0.705
Covariance matrix **C** (symmetric)							
12.655	-0.528	1.218	-0.015	0.173	-0.121	-5.293	1.635
	0.097	-0.030	-0.001	0.005	0.006	-0.068	-0.048
		0.209	-0.003	0.022	-0.014	-0.625	0.115
			0.000	0.000	0.000	0.012	-0.004
				0.058	0.025	-0.130	0.045
Number of observations (n) =	254				0.052	0.030	-0.003
Number of degrees of freedom (p) =	7					3.362	-0.819
Residual mean square (s^2) =	0.028						0.841

Table B4. Values of coefficients for MLR and probabilistic models FFGS6-B.

Components of **X**									
1.0	*0 or 1*	M_w	*LOG(R)*	*R*	*LOG(W_{ff})*	*LOG(S)*	*LOG(T_{15})*	*LOG(100-F_{15})*	*D50*$_{15}$
MLR coefficients									
b_0	b_{off}	b_1	b_2	b_3	b_4	b_5	b_6	b_7	b_8
-13.261	-0.261	1.050	-0.778	-0.013	0.370	0.106	0.270	3.481	-0.715
Covariance matrix **C** (symmetric)									
6.232	0.070	-0.359	0.429	-0.004	-0.248	0.082	0.000	-2.169	0.776
	0.081	-0.003	0.004	0.000	-0.076	-0.029	-0.016	-0.034	0.005
		0.053	-0.024	0.000	0.011	-0.003	0.000	0.009	-0.065
			0.064	-0.001	-0.010	0.007	-0.001	-0.165	0.037
				0.000	0.000	0.000	0.000	0.003	-0.001
					0.104	0.004	0.011	0.095	-0.016
						0.085	0.020	-0.032	0.014
Number of observations (n) =	467						0.035	-0.007	-0.004
Number of degrees of freedom (p) =	9							1.183	-0.211
Residual mean square (s^2) =	0.046								0.320

Table B5. Values of coefficients for MLR and probabilistic models FF6-B.

Components of **X**							
1.0	M_w	LOG(R)	R	LOG(W_{ff})	LOG(T_{15})	LOG(100-F_{15})	$D50_{15}$
MLR coefficients							
b_0	b_1	b_2	b_3	b_4	b_6	b_7	b_8
-15.067	1.130	-0.738	-0.012	0.396	0.135	4.032	-0.908
Covariance matrix **C** (symmetric)							
15.080	-0.854	0.795	-0.004	-0.690	0.130	-5.121	1.706
	0.094	-0.054	0.000	0.029	-0.007	0.135	-0.131
		0.106	-0.002	-0.014	0.004	-0.265	0.082
			0.000	-0.001	0.000	0.003	-0.001
				0.132	0.014	0.220	-0.042
Number of observations (n) = 118					0.063	-0.071	0.005
Number of degrees of freedom (p) = 7						2.309	-0.486
Residual mean square (s^2) = 0.054							0.518

Table B6. Values of coefficients for MLR and probabilistic models GS6-B.

Components of **X**							
1.0	M_w	LOG(R)	R	LOG(S)	LOG(T_{15})	LOG(100-F_{15})	$D50_{15}$
MLR coefficients							
b_0	b_1	b_2	b_3	b_5	b_6	b_7	b_8
-14.212	0.800	-1.198	-0.006	0.071	0.373	5.090	-0.704
Covariance matrix **C** (symmetric)							
13.595	-0.359	1.381	-0.019	0.199	-0.121	-6.501	1.778
	0.187	0.031	-0.002	0.022	0.011	-0.513	-0.100
		0.255	-0.004	0.041	-0.006	-0.955	0.103
			0.000	-0.001	0.000	0.021	-0.003
				0.118	0.055	-0.217	0.067
Number of observations (n) = 165					0.089	0.000	0.001
Number of degrees of freedom (p) = 7						5.780	-0.717
Residual mean square (s^2) = 0.021							1.017

Table B7. Values of coefficients for MLR and probabilistic models FFGS4-A.

Components of **X**							
1.0	*0 or 1*	M_w	*LOG(R)*	*R*	*LOG(W_{ff})*	*LOG(S)*	*LOG(T_{15})*
MLR coefficients							
b_0	b_{off}	b_1	b_2	b_3	b_4	b_5	b_6
-6.815	-0.465	1.017	-0.278	-0.026	0.497	0.454	0.558
Covariance matrix **C** (symmetric)							
0.0005	0.0001	0.0000	0.0001	0.0000	-0.0004	0.0000	0.0000
	0.0465	-0.0008	-0.0003	0.0001	-0.0399	-0.0113	-0.0051
		0.0006	-0.0023	0.0000	-0.0004	0.0006	-0.0012
			0.0247	-0.0005	0.0061	-0.0027	-0.0056
				0.0000	-0.0002	0.0001	0.0001
Number of observations (n) = 467					0.0468	0.0000	-0.0002
Number of degrees of freedom (p) = 7						0.0443	0.0106
Residual mean square (s^2) = 0.084							0.0223

Table B8. Values of coefficients for MLR and probabilistic models FF4-A.

Components of **X**						
1.0	M_w	*LOG(R)*	*R*	*LOG(W_{ff})*	*LOG(T_{15})*	
MLR coefficients						
b_0	b_1	b_2	b_3	b_4	b_6	
-6.968	0.972	-0.271	-0.027	0.497	0.584	
Covariance matrix **C** (symmetric)						
2.403	-0.362	0.183	0.003	-0.075	0.050	
	0.056	-0.031	0.000	0.005	-0.011	
		0.055	-0.001	0.008	-0.008	
			0.000	0.000	0.000	
				0.049	-0.001	
Number of observations (n) = 213					0.043	
Number of degrees of freedom (p) = 5						
Residual mean square (s^2) = 0.123						

Table B9. Values of coefficients for MLR and probabilistic models GS4-A.

Components of **X**					
1.0	M_w	LOG(R)	R	LOG(S)	$LOG(T_{15})$
MLR coefficients					
b_0	b_1	b_2	b_3	b_5	b_6
-7.586	1.109	-0.233	-0.025	0.477	0.579
Covariance matrix **C** (symmetric)					
4.137	-0.600	0.255	0.004	-0.039	-0.076
	0.089	-0.046	-0.001	0.004	0.007
		0.091	-0.001	-0.001	-0.009
			0.000	0.000	0.000
				0.052	0.026
					0.051

Number of observations (n) =	254
Number of degrees of freedom (p) =	5
Residual mean square (s^2) =	0.051

Table B10. Values of coefficients for MLR and probabilistic models FFGS4-B.

Components of **X**							
1.0	0 or 1	M_w	LOG(R)	R	$LOG(W_{ff})$	LOG(S)	$LOG(T_{15})$
MLR coefficients							
b_0	b_{off}	b_1	b_2	b_3	b_4	b_5	b_6
-6.747	-0.162	1.001	-0.289	-0.021	0.090	0.203	0.289
Covariance matrix **C** (symmetric)							
1.718	0.009	-0.254	0.115	0.002	-0.076	0.012	-0.005
	0.080	-0.003	0.000	0.000	-0.073	-0.030	-0.016
		0.038	-0.021	0.000	0.011	0.000	-0.001
			0.041	0.000	0.003	0.002	-0.002
				0.000	-0.001	0.000	0.000
					0.096	0.006	0.011
						0.084	0.020
							0.035

Number of observations (n) =	283
Number of degrees of freedom (p) =	7
Residual mean square (s^2) =	0.079

Table B11. Values of coefficients for MLR and probabilistic models FF4-B.

Components of **X**					
1.0	M_w	*LOG(R)*	*R*	*LOG(W_{ff})*	*LOG(T_{15})*
MLR coefficients					
b_0	b_1	b_2	b_3	b_4	b_6
-6.034	0.880	-0.271	-0.018	0.013	0.257
Covariance matrix **C** (symmetric)					
2.770	-0.398	0.167	0.005	-0.209	-0.011
	0.060	-0.031	-0.001	0.017	-0.005
		0.073	-0.001	0.011	-0.003
			0.000	-0.001	0.000
				0.111	0.020
					0.061

Number of observations (n) = 118

Number of degrees of freedom (p) = 5

Residual mean square (s^2) = 0.116

Table B12. Values of coefficients for MLR and probabilistic models GS4-B.

Components of **X**					
1.0	M_w	*LOG(R)*	*R*	*LOG(S)*	*LOG(T_{15})*
MLR coefficients					
b_0	b_1	b_2	b_3	b_5	b_6
-8.410	1.239	-0.358	-0.024	0.266	0.373
Covariance matrix **C** (symmetric)					
5.264	-0.765	0.324	0.005	-0.088	-0.121
	0.113	-0.057	-0.001	0.010	0.012
		0.097	-0.001	0.005	-0.006
			0.000	0.000	0.000
				0.108	0.055
					0.089

Number of observations (n) = 165

Number of degrees of freedom (p) = 5

Residual mean square (s^2) = 0.049

APPENDIX C: OUTPUTS OF MINITAB REGRESSION ANALYSES

Appendix C contains the outputs of Minitab regression analyses of:

- the Bartlett and Youd (1992) model calibrated from the original database of Bartlett and Youd (1992), and

- the twelve MLR models developed in this study from the corrected database of Bartlett (1998) including data sets A and B.

Minitab regression analysis from the original database by Bartlett and Youd (1992)

```
MTB > Regress 'log(Dh)' 9 'B0ff' 'M' 'log R' 'R' 'log Wff' 'log Sgs'  &
CONT>     'log T15' 'log (100-F15)' 'D5015';
SUBC>   Constant.

Regression Analysis


The regression equation is
log(Dh) = - 15.8 - 0.579 B0ff + 1.18 M - 0.927 log R - 0.0133 R + 0.657 log Wff
           + 0.429 log Sgs + 0.348 log T15 + 4.53 log (100-F15) - 0.922 D5015

Predictor       Coef       Stdev    t-ratio        p
Constant    -15.7869      0.4752     -33.22    0.000
B0ff        -0.57883     0.04504     -12.85    0.000
M            1.17817     0.04274      27.57    0.000
log R       -0.92745     0.04819     -19.24    0.000
R          -0.013289    0.001231     -10.79    0.000
log Wff      0.65716     0.04570      14.38    0.000
log Sgs      0.42932     0.04484       9.57    0.000
log T15      0.34834     0.03140      11.09    0.000
log (100-F15) 4.5270      0.2005      22.58    0.000
D5015        -0.9223      0.1092      -8.45    0.000

s = 0.2086      R-sq = 82.6%     R-sq(adj) = 82.3%

Analysis of Variance

SOURCE       DF          SS          MS         F        p
Regression    9      94.633      10.515    241.75    0.000
Error       457      19.877       0.043
Total       466     114.510

SOURCE       DF      SEQ SS
B0ff          1       0.477
M             1      11.604
log R         1      13.880
R             1      28.419
log Wff       1       5.538
log Sgs       1       4.681
log T15       1       7.841
log (100      1      19.087
D5015         1       3.105

Unusual Observations
Obs.     B0ff    log(Dh)        Fit  Stdev.Fit   Residual    St.Resid
  1      1.00   -0.03621    0.43331    0.04353   -0.46952      -2.30R
```

2	0.00	0.17898	1.16221	0.03632	-0.98323	-4.79R
3	0.00	0.17898	0.99454	0.02609	-0.81556	-3.94R
4	1.00	0.26482	0.74533	0.03425	-0.48051	-2.34R
5	1.00	0.13988	0.05827	0.07990	0.08161	0.42 X
6	1.00	0.28330	0.17724	0.10318	0.10606	0.59 X
7	1.00	0.26951	0.47337	0.10022	-0.20386	-1.11 X
8	1.00	0.19866	0.20391	0.11030	-0.00525	-0.03 X
9	0.00	-0.50864	-0.40477	0.08985	-0.10387	-0.55 X
10	0.00	-0.50864	-0.52308	0.08487	0.01444	0.08 X
11	0.00	0.38917	0.34106	0.09785	0.04811	0.26 X
12	1.00	-1.04576	-0.08656	0.03592	-0.95920	-4.67R
13	1.00	-0.53760	-0.07156	0.03604	-0.46604	-2.27R
33	1.00	-0.95861	-0.08889	0.03378	-0.86972	-4.23R
34	1.00	-0.58503	-0.11530	0.03467	-0.46973	-2.28R
35	0.00	0.22789	-0.17577	0.05433	0.40366	2.00RX
36	0.00	-0.28400	-0.17577	0.05433	-0.10823	-0.54 X
37	0.00	0.08991	-0.17577	0.05433	0.26568	1.32 X
38	0.00	0.22789	-0.17577	0.05433	0.40366	2.00RX
39	0.00	0.22789	-0.17577	0.05433	0.40366	2.00RX
40	0.00	-2.00000	-2.22700	0.08273	0.22700	1.19 X
41	0.00	-2.00000	-1.42365	0.05572	-0.57635	-2.87RX
42	1.00	-2.00000	-2.56716	0.09161	0.56716	3.03RX
43	1.00	-2.00000	-1.20942	0.05097	-0.79058	-3.91R
55	1.00	-0.50864	-0.03466	0.02983	-0.47398	-2.30R
68	1.00	-0.85387	-0.28663	0.02810	-0.56724	-2.74R
76	1.00	-0.95861	-1.37847	0.05107	0.41986	2.08R
77	1.00	-2.00000	-1.54092	0.04939	-0.45908	-2.27R
83	1.00	-0.37675	0.17807	0.02442	-0.55482	-2.68R
84	1.00	-0.25181	0.18622	0.02417	-0.43803	-2.11R
88	1.00	-0.27572	0.32843	0.01904	-0.60415	-2.91R
141	1.00	0.09691	-0.34849	0.03532	0.44540	2.17R
144	1.00	0.12057	-0.49544	0.04114	0.61601	3.01R
148	1.00	0.13988	-0.29365	0.04561	0.43353	2.13R
149	1.00	-0.05552	0.35686	0.04815	-0.41238	-2.03R
432	0.00	-0.14267	0.27199	0.02443	-0.41466	-2.00R
449	1.00	-1.22185	-0.74737	0.05403	-0.47448	-2.36RX
450	0.00	-1.22185	-1.33730	0.05470	0.11545	0.57 X
451	1.00	-1.22185	-1.21864	0.05780	-0.00321	-0.02 X
452	1.00	-1.22185	-1.19877	0.06710	-0.02308	-0.12 X
453	0.00	-1.22185	-1.24779	0.06019	0.02594	0.13 X
456	1.00	-1.22185	-1.34545	0.06456	0.12360	0.62 X
458	0.00	-1.22185	-1.12997	0.05941	-0.09188	-0.46 X
459	1.00	-1.22185	-1.25156	0.07015	0.02971	0.15 X

R denotes an obs. with a large st. resid.
X denotes an obs. whose X value gives it large influence.

Minitab regression analysis for FFGS6-A model

```
The regression equation is
LOG(Dhc+ = - 14.6 - 0.483 B0ff + 1.10 M - 0.873 log R - 0.0140 R
           + 0.635 log Wff + 0.276 log Sgs + 0.494 log T15 + 4.05 Log(100-F15)- 0.814 D5015

Predictor       Coef       Stdev    t-ratio        p
Constant    -14.5511      0.4871     -29.87    0.000
B0ff        -0.48266     0.04618     -10.45    0.000
M            1.09594     0.04382      25.01    0.000
log R       -0.87266     0.04941     -17.66    0.000
R          -0.014013    0.001263     -11.10    0.000
log Wff      0.63455     0.04685      13.54    0.000
log Sgs      0.27569     0.04597       6.00    0.000
log T15      0.49438     0.03219      15.36    0.000
Log(F15       4.0527      0.2056      19.71    0.000
D5015        -0.8141      0.1119      -7.27    0.000

s = 0.2138      R-sq = 81.0%     R-sq(adj) = 80.6%

Analysis of Variance

SOURCE       DF          SS          MS         F        p
Regression    9     88.9562      9.8840    216.21    0.000
Error       457     20.8919      0.0457
Total       466    109.8481

SOURCE       DF      SEQ SS
B0ff          1      0.0239
M             1      9.3503
log R         1     13.0621
R             1     28.5023
log Wff       1      5.4340
log Sgs       1      0.8981
log T15       1     13.8932
Log(F15       1     15.3734
D5015         1      2.4189

Unusual Observations
Obs.     B0ff   LOG(Dhc+        Fit  Stdev.Fit   Residual    St.Resid
  2      0.00    0.17900    1.02157    0.03724   -0.84257      -4.00R
  3      0.00    0.17900    0.86004    0.02675   -0.68104      -3.21R
  4      1.00    0.26500    0.71380    0.03511   -0.44880      -2.13R
  5      1.00    0.14000   -0.01138    0.08191    0.15138       0.77 X
  6      1.00    0.28300    0.12139    0.10578    0.16161       0.87 X
  7      1.00    0.27000    0.39488    0.10275   -0.12488      -0.67 X
  8      1.00    0.19900    0.15536    0.11308    0.04364       0.24 X
  9      0.00   -0.50900   -0.33908    0.09212   -0.16992      -0.88 X
 10      0.00   -0.50900   -0.45469    0.08701   -0.05431      -0.28 X
 11      0.00    0.38900    0.41125    0.10032   -0.02225      -0.12 X
 12      1.00   -1.04600   -0.01035    0.03683   -1.03565      -4.92R
 13      1.00   -0.53800    0.00864    0.03695   -0.54664      -2.60R
 23      1.00   -0.43200    0.04282    0.03738   -0.47482      -2.26R
 33      1.00   -0.95900   -0.04101    0.03463   -0.91799      -4.35R
 34      1.00   -0.58500   -0.05981    0.03555   -0.52519      -2.49R
 35      0.00    0.22800   -0.21593    0.05570    0.44393       2.15RX
 36      0.00   -0.28400   -0.21593    0.05570   -0.06807      -0.33 X
 37      0.00    0.09000   -0.21593    0.05570    0.30593       1.48 X
 38      0.00    0.22800   -0.21593    0.05570    0.44393       2.15RX
 39      0.00    0.22800   -0.21593    0.05570    0.44393       2.15RX
 40      0.00   -2.00000   -2.18570    0.08481    0.18570       0.95 X
 41      0.00   -2.00000   -1.37956    0.05712   -0.62044      -3.01RX
 42      1.00   -2.00000   -2.55267    0.09392    0.55267       2.88RX
 43      1.00   -2.00000   -1.14361    0.05226   -0.85639      -4.13R
 55      1.00   -0.50900   -0.05965    0.03058   -0.44935      -2.12R
 68      1.00   -0.85400   -0.33133    0.02881   -0.52267      -2.47R
 77      1.00   -2.00000   -1.45376    0.05064   -0.54624      -2.63R
 83      1.00   -0.37700    0.21374    0.02503   -0.59074      -2.78R
 84      1.00   -0.25200    0.22206    0.02478   -0.47406      -2.23R
```

88	1.00	-0.27600	0.33513	0.01952	-0.61113	-2.87R
141	1.00	0.09700	-0.39161	0.03621	0.48861	2.32R
144	1.00	0.12100	-0.53217	0.04218	0.65317	3.12R
148	1.00	0.14000	-0.47125	0.04676	0.61125	2.93R
398	0.00	-0.23400	0.21876	0.02345	-0.45276	-2.13R
432	0.00	-0.41600	0.07806	0.02504	-0.49406	-2.33R
449	1.00	-1.22200	-0.79597	0.05540	-0.42603	-2.06RX
450	0.00	-1.22200	-1.39036	0.05608	0.16836	0.82 X
451	1.00	-1.22200	-1.23435	0.05926	0.01235	0.06 X
452	1.00	-1.22200	-1.23629	0.06880	0.01429	0.07 X
453	0.00	-1.22200	-1.32074	0.06171	0.09874	0.48 X
456	1.00	-1.22200	-1.36423	0.06619	0.14223	0.70 X
458	0.00	-1.22200	-1.21115	0.06091	-0.01085	-0.05 X
459	1.00	-1.22200	-1.29048	0.07192	0.06848	0.34 X
465	1.00	-1.22200	-0.77743	0.04372	-0.44457	-2.12R

R denotes an obs. with a large st. resid.
X denotes an obs. whose X value gives it large influence.

Minitab regression analysis for model FF6-A

```
The regression equation is
LOG(Dhc+ = - 17.4 + 1.25 M - 0.923 log R - 0.0140 R + 0.685 log Wff
           + 0.300 log T15 + 4.83 log (100-F15) - 1.09 D5015

Predictor       Coef       Stdev    t-ratio        p
Constant    -17.3724      0.8063     -21.55    0.000
M            1.24779     0.06974      17.89    0.000
log R       -0.92338     0.07176     -12.87    0.000
R          -0.014032    0.001957      -7.17    0.000
log Wff      0.68539     0.05490      12.48    0.000
log T15      0.30041     0.05356       5.61    0.000
log (F15      4.8257      0.3170      15.22    0.000
D5015        -1.0912      0.1647      -6.62    0.000

s = 0.2412      R-sq = 82.7%     R-sq(adj) = 82.1%

Analysis of Variance

SOURCE       DF          SS          MS         F        p
Regression    7     56.9659      8.1380    139.83    0.000
Error       205     11.9305      0.0582
Total       212     68.8964

SOURCE       DF      SEQ SS
M             1      7.0852
log R         1      9.2075
R             1     13.8422
log Wff       1      5.4487
log T15       1      7.8966
log (F15      1     10.9317
D5015         1      2.5539

Unusual Observations
Obs.        M   LOG(Dhc+        Fit  Stdev.Fit   Residual    St.Resid
  1      7.90    -0.0360     0.5157     0.0655    -0.5517      -2.38R
  2      7.90     0.2650     0.7922     0.0452    -0.5272      -2.22R
  3      9.20     0.1400     0.0114     0.1215     0.1286       0.62 X
  4      9.20     0.2830     0.2434     0.1500     0.0396       0.21 X
  5      9.20     0.2700     0.4227     0.1348    -0.1527      -0.76 X
  6      9.20     0.1990     0.1215     0.1493     0.0775       0.41 X
  7      6.40    -1.0460    -0.1648     0.0526    -0.8812      -3.74R
 28      6.40    -0.9590    -0.1559     0.0475    -0.8031      -3.40R
 30      6.60    -2.0000    -2.6293     0.1301     0.6293       3.10RX
 31      6.60    -2.0000    -1.2647     0.0764    -0.7353      -3.21R
 56      6.50    -0.8540    -0.2945     0.0368    -0.5595      -2.35R
 71      7.50    -0.3770     0.1733     0.0301    -0.5503      -2.30R
 76      7.50    -0.2760     0.3334     0.0229    -0.6094      -2.54R
132      7.50     0.1210    -0.4704     0.0539     0.5914       2.51R
137      7.50    -0.0560     0.4448     0.0794    -0.5008      -2.20R
205      7.80    -1.2220    -0.7497     0.0852    -0.4723      -2.09RX
206      7.40    -1.2220    -1.2488     0.0892     0.0268       0.12 X
207      7.60    -1.2220    -1.2237     0.1058     0.0017       0.01 X
208      7.40    -1.2220    -1.3807     0.1004     0.1587       0.72 X
209      7.60    -1.2220    -1.2787     0.1108     0.0567       0.26 X

R denotes an obs. with a large st. resid.
X denotes an obs. whose X value gives it large influence.
```

Minitab regression analysis for model GS6-A

```
The regression equation is
LOG(Dhc+ = - 14.2 + 0.988 M - 1.05 log R - 0.0108 R + 0.319 log Sgs
           + 0.619 log T15 + 4.29 Log(100-F15) - 0.705 D5015

Predictor       Coef       Stdev    t-ratio        p
Constant    -14.1525      0.6001     -23.58    0.000
M            0.98784     0.05253      18.81    0.000
log R       -1.04910     0.07707     -13.61    0.000
R          -0.010841    0.001643      -6.60    0.000
log Sgs      0.31865     0.04046       7.87    0.000
log T15      0.61931     0.03838      16.13    0.000
Log(F15       4.2871      0.3093      13.86    0.000
D5015        -0.7049      0.1547      -4.56    0.000

s = 0.1687      R-sq = 82.9%     R-sq(adj) = 82.4%

Analysis of Variance

SOURCE       DF          SS          MS         F        p
Regression    7     33.9285      4.8469    170.35    0.000
Error       246      6.9993      0.0285
Total       253     40.9279

SOURCE       DF      SEQ SS
M             1      2.2741
log R         1      4.2227
R             1     14.3698
log Sgs       1      0.9079
log T15       1      6.5082
Log(F15       1      5.0553
D5015         1      0.5905

Unusual Observations
Obs.        M   LOG(Dhc+        Fit  Stdev.Fit   Residual    St.Resid
  1      7.90     0.1790     0.9597     0.0418    -0.7807      -4.78R
  2      7.90     0.1790     0.8252     0.0308    -0.6462      -3.90R
  3      9.20    -0.5090    -0.2663     0.1213    -0.2427      -2.07RX
  4      9.20    -0.5090    -0.5007     0.0924    -0.0083      -0.06 X
  5      9.20     0.3890     0.1192     0.1314     0.2698       2.55RX
  6      6.40     0.2280     0.0555     0.0748     0.1725       1.14 X
  7      6.40    -0.2840     0.0555     0.0748    -0.3395      -2.25RX
  8      6.40     0.0900     0.0555     0.0748     0.0345       0.23 X
  9      6.40     0.2280     0.0555     0.0748     0.1725       1.14 X
 10      6.40     0.2280     0.0555     0.0748     0.1725       1.14 X
 11      6.60    -2.0000    -2.2883     0.1169     0.2883       2.37RX
 12      6.60    -2.0000    -1.3915     0.0731    -0.6085      -4.00RX
 78      7.50     0.5450     0.1607     0.0178     0.3843       2.29R
148      7.50    -0.1190     0.2372     0.0405    -0.3562      -2.18R
152      7.50    -0.0920     0.2483     0.0288    -0.3403      -2.05R
194      7.70    -0.2340     0.1662     0.0199    -0.4002      -2.39R
228      7.70    -0.4160    -0.0073     0.0249    -0.4087      -2.45R
245      7.50    -1.2220    -1.3432     0.0651     0.1212       0.78 X
246      7.70    -1.2220    -1.2774     0.0709     0.0554       0.36 X
247      7.50    -1.2220    -1.2584     0.0593     0.0364       0.23 X
250      7.80    -1.2220    -1.1786     0.0694    -0.0434      -0.28 X
251      6.40    -1.2220    -1.0124     0.0553    -0.2096      -1.32 X
253      6.40    -1.2220    -1.0089     0.0580    -0.2131      -1.35 X
254      6.60    -1.2220    -1.4647     0.0616     0.2427       1.55 X

R denotes an obs. with a large st. resid.
X denotes an obs. whose X value gives it large influence.
```

Minitab regression analysis for model FFGS6-B

```
The regression equation is
LOG(Dhc+ = - 13.3 - 0.261 B0ff + 1.05 M - 0.778 log R - 0.0126 R
           + 0.370 log Wff + 0.106 log Sgs + 0.270 log T15 + 3.48 log (100-F15)
           - 0.715 D5015

Predictor       Coef       Stdev    t-ratio        p
Constant    -13.2613      0.5100     -26.00    0.000
B0ff        -0.26103     0.05811      -4.49    0.000
M            1.05006     0.04696      22.36    0.000
log R       -0.77763     0.05176     -15.02    0.000
R          -0.012555    0.001263      -9.94    0.000
log Wff      0.36999     0.06575       5.63    0.000
log Sgs      0.10633     0.05965       1.78    0.076
log T15      0.27042     0.03830       7.06    0.000
log (F15      3.4809      0.2222      15.67    0.000
D5015        -0.7151      0.1156      -6.19    0.000

s = 0.2043      R-sq = 81.7%     R-sq(adj) = 81.1%

Analysis of Variance

SOURCE       DF          SS          MS         F        p
Regression    9     50.7979      5.6442    135.24    0.000
Error       273     11.3933      0.0417
Total       282     62.1912

SOURCE       DF      SEQ SS
B0ff          1      2.1261
M             1      7.0842
log R         1     12.2982
R             1     16.6171
log Wff       1      0.0000
log Sgs       1      0.0171
log T15       1      2.3814
log (F15      1      8.6758
D5015         1      1.5981

Unusual Observations
Obs.     B0ff   LOG(Dhc+        Fit  Stdev.Fit   Residual    St.Resid
  2      0.00     0.1790     0.8582     0.0414    -0.6792      -3.40R
  3      0.00     0.1790     0.6958     0.0317    -0.5168      -2.56R
  5      1.00     0.1400    -0.0480     0.0803     0.1880       1.00 X
  6      1.00     0.2830     0.0413     0.1229     0.2417       1.48 X
  7      1.00     0.2700     0.3021     0.1048    -0.0321      -0.18 X
  8      1.00     0.1990     0.1193     0.1133     0.0797       0.47 X
  9      0.00    -0.5090    -0.2501     0.0923    -0.2589      -1.42 X
 10      0.00    -0.5090    -0.2710     0.0931    -0.2380      -1.31 X
 11      1.00    -1.0460    -0.1586     0.0413    -0.8874      -4.44R
 21      1.00    -0.9590    -0.1732     0.0402    -0.7858      -3.92R
 23      0.00     0.2280    -0.3099     0.0631     0.5379       2.77R
 25      0.00     0.0900    -0.3099     0.0631     0.3999       2.06R
 26      0.00     0.2280    -0.3099     0.0631     0.5379       2.77R
 27      0.00     0.2280    -0.3099     0.0631     0.5379       2.77R
 28      0.00    -2.0000    -1.8922     0.0924    -0.1078      -0.59 X
 29      0.00    -2.0000    -1.2732     0.0611    -0.7268      -3.73R
 30      1.00    -2.0000    -2.1124     0.1025     0.1124       0.64 X
 31      1.00    -2.0000    -1.1203     0.0518    -0.8797      -4.45R
 46      1.00    -0.8540    -0.3495     0.0327    -0.5045      -2.50R
 54      1.00    -0.9590    -1.3566     0.0520     0.3976       2.01R
 55      1.00    -2.0000    -1.4309     0.0493    -0.5691      -2.87R
 59      1.00    -0.3770     0.0811     0.0295    -0.4581      -2.27R
 63      1.00    -0.2760     0.1729     0.0250    -0.4489      -2.21R
 77      1.00     0.0970    -0.3288     0.0395     0.4258       2.12R
 80      1.00     0.1210    -0.4157     0.0480     0.5367       2.70R
 84      1.00     0.1400    -0.2690     0.0531     0.4090       2.07R
249      0.00    -0.4160     0.0860     0.0261    -0.5020      -2.48R
268      1.00    -1.2220    -1.2626     0.0672     0.0406       0.21 X
```

```
275      1.00    -1.2220    -1.3111     0.0701     0.0891       0.46 X
R denotes an obs. with a large st. resid.
X denotes an obs. whose X value gives it large influence.
```

Minitab regression analysis for model FF6-B

```
The regression equation is
LOG(Dhc+ = - 15.1 + 1.13 M - 0.738 log R - 0.0124 R + 0.396 log Wff
           + 0.135 log T15 + 4.03 log (100-F15) - 0.908 D5015

Predictor       Coef       Stdev    t-ratio        p
Constant    -15.0668      0.9054     -16.64    0.000
M            1.13037     0.07130      15.85    0.000
log R       -0.73793     0.07576      -9.74    0.000
R          -0.012366    0.002006      -6.17    0.000
log Wff      0.39563     0.08471       4.67    0.000
log T15      0.13451     0.05865       2.29    0.024
log (F15      4.0315      0.3543      11.38    0.000
D5015        -0.9079      0.1678      -5.41    0.000

s = 0.2332      R-sq = 81.4%     R-sq(adj) = 80.2%

Analysis of Variance

SOURCE       DF          SS          MS         F        p
Regression    7     26.2002      3.7429     68.85    0.000
Error       110      5.9803      0.0544
Total       117     32.1805

SOURCE       DF      SEQ SS
M             1      4.8734
log R         1      6.6454
R             1      6.4996
log Wff       1      0.0515
log T15       1      1.0820
log (F15      1      5.4568
D5015         1      1.5914

Unusual Observations
Obs.        M   LOG(Dhc+        Fit  Stdev.Fit   Residual    St.Resid
  3      9.20     0.1400     0.0032     0.1193     0.1368       0.68 X
  4      9.20     0.2830     0.1238     0.1588     0.1592       0.93 X
  5      9.20     0.2700     0.3267     0.1352    -0.0567      -0.30 X
  6      9.20     0.1990     0.1025     0.1486     0.0965       0.54 X
  7      6.40    -1.0460    -0.3536     0.0623    -0.6924      -3.08R
 17      6.40    -0.9590    -0.3415     0.0583    -0.6175      -2.74R
 19      6.60    -2.0000    -2.1774     0.1524     0.1774       1.01 X
 20      6.60    -2.0000    -1.2185     0.0779    -0.7815      -3.56R
 35      6.50    -0.8540    -0.3671     0.0416    -0.4869      -2.12R
 44      6.60    -2.0000    -1.4913     0.0756    -0.5087      -2.31R
 69      7.50     0.1210    -0.3567     0.0606     0.4777       2.12R
110      7.80    -1.2220    -0.7666     0.0826    -0.4554      -2.09R
114      7.60    -1.2220    -1.2332     0.1078     0.0112       0.05 X

R denotes an obs. with a large st. resid.
X denotes an obs. whose X value gives it large influence.
```

Minitab regression analysis for model GS6-B

```
The regression equation is
LOG(Dhc+ = - 14.2 + 0.800 M - 1.20 log R - 0.00584 R + 0.0713 log Sgs
           + 0.373 log T15 + 5.09 log (100-F15) - 0.704 D5015

Predictor       Coef       Stdev    t-ratio        p
Constant    -14.2122      0.5295     -26.84    0.000
M            0.80003     0.06217      12.87    0.000
log R       -1.19836     0.07252     -16.52    0.000
R          -0.005839    0.001646      -3.55    0.001
log Sgs      0.07132     0.04936       1.44    0.150
log T15      0.37276     0.04292       8.68    0.000
log (F15      5.0903      0.3452      14.74    0.000
D5015        -0.7038      0.1448      -4.86    0.000

s = 0.1436      R-sq = 88.4%     R-sq(adj) = 87.9%

Analysis of Variance

SOURCE       DF          SS          MS         F        p
Regression    7     24.6471      3.5210    170.75    0.000
Error       157      3.2376      0.0206
Total       164     27.8846

SOURCE       DF      SEQ SS
M             1      2.2109
log R         1      5.7259
R             1     10.6486
log Sgs       1      0.0169
log T15       1      1.5560
log (F15      1      4.0015
D5015         1      0.4872

Unusual Observations
Obs.        M   LOG(Dhc+        Fit  Stdev.Fit   Residual    St.Resid
  1      7.90     0.1790     0.7741     0.0447    -0.5951      -4.36R
  2      7.90     0.1790     0.6046     0.0362    -0.4256      -3.06R
  3      9.20    -0.5090    -0.3607     0.1077    -0.1483      -1.56 X
  4      9.20    -0.5090    -0.5475     0.0905     0.0385       0.35 X
  5      6.40     0.2280     0.0701     0.0640     0.1579       1.23 X
  6      6.40    -0.2840     0.0701     0.0640    -0.3541      -2.75RX
  7      6.40     0.0900     0.0701     0.0640     0.0199       0.15 X
  8      6.40     0.2280     0.0701     0.0640     0.1579       1.23 X
  9      6.40     0.2280     0.0701     0.0640     0.1579       1.23 X
 10      6.60    -2.0000    -2.3642     0.1188     0.3642       4.52RX
 11      6.60    -2.0000    -1.4739     0.0707    -0.5261      -4.21RX
112      7.70    -0.2340     0.0654     0.0229    -0.2994      -2.11R
140      7.70    -0.4160     0.0270     0.0235    -0.4430      -3.13R
156      7.50    -1.2220    -1.3053     0.0568     0.0833       0.63 X
157      7.70    -1.2220    -1.2434     0.0615     0.0214       0.17 X
161      7.80    -1.2220    -1.1634     0.0600    -0.0586      -0.45 X
162      6.40    -1.2220    -0.9720     0.0551    -0.2500      -1.89 X
163      6.60    -1.2220    -0.9244     0.0461    -0.2976      -2.19R
164      6.40    -1.2220    -1.0304     0.0575    -0.1916      -1.46 X
165      6.60    -1.2220    -1.4103     0.0584     0.1883       1.44 X

R denotes an obs. with a large st. resid.
X denotes an obs. whose X value gives it large influence.
```

Minitab regression analysis for model FFGS4-A

```
The regression equation is
LOG(Dhc+ = - 6.82 - 0.465 B0ff + 1.02 M - 0.278 log R - 0.0257 R
           + 0.497 log Wff + 0.454 log Sgs + 0.558 log T15

Predictor       Coef       Stdev    t-ratio        p
Constant     -6.8155      0.3511     -19.41    0.000
B0ff        -0.46505     0.06268      -7.42    0.000
M            1.01716     0.05305      19.17    0.000
log R       -0.27811     0.05303      -5.24    0.000
R          -0.025741    0.001493     -17.24    0.000
log Wff      0.49685     0.06282       7.91    0.000
log Sgs      0.45441     0.06117       7.43    0.000
log T15      0.55795     0.04346      12.84    0.000

s = 0.2903      R-sq = 64.8%     R-sq(adj) = 64.2%

Analysis of Variance

SOURCE       DF          SS          MS         F        p
Regression    7      71.164      10.166    120.63    0.000
Error       459      38.684       0.084
Total       466     109.848

SOURCE       DF      SEQ SS
B0ff          1       0.024
M             1       9.350
log R         1      13.062
R             1      28.502
log Wff       1       5.434
log Sgs       1       0.898
log T15       1      13.893

Unusual Observations
Obs.     B0ff   LOG(Dhc+        Fit  Stdev.Fit   Residual    St.Resid
  2      0.00     0.1790     0.8498     0.0369    -0.6708      -2.33R
  3      0.00     0.1790     0.8819     0.0361    -0.7029      -2.44R
  5      1.00     0.1400    -0.0650     0.1048     0.2050       0.76 X
  6      1.00     0.2830     1.1521     0.0979    -0.8691      -3.18RX
  7      1.00     0.2700     1.0258     0.0891    -0.7558      -2.74RX
  8      1.00     0.1990     0.9609     0.0852    -0.7619      -2.75RX
  9      0.00    -0.5090    -0.3202     0.1097    -0.1888      -0.70 X
 10      0.00    -0.5090    -0.5672     0.1168     0.0582       0.22 X
 11      0.00     0.3890     1.2926     0.0921    -0.9036      -3.28RX
 12      1.00    -1.0460     0.0823     0.0496    -1.1283      -3.94R
 13      1.00    -0.5380     0.1020     0.0497    -0.6400      -2.24R
 33      1.00    -0.9590     0.0276     0.0468    -0.9866      -3.44R
 34      1.00    -0.5850     0.0201     0.0479    -0.6051      -2.11R
 35      0.00     0.2280     0.1559     0.0710     0.0721       0.26 X
 36      0.00    -0.2840     0.1559     0.0710    -0.4399      -1.56 X
 37      0.00     0.0900     0.1559     0.0710    -0.0659      -0.23 X
 38      0.00     0.2280     0.1559     0.0710     0.0721       0.26 X
 39      0.00     0.2280     0.1559     0.0710     0.0721       0.26 X
 40      0.00    -2.0000    -0.6740     0.0493    -1.3260      -4.63R
 41      0.00    -2.0000    -0.4078     0.0387    -1.5922      -5.53R
 42      1.00    -2.0000    -1.0153     0.0710    -0.9847      -3.50RX
 43      1.00    -2.0000    -0.2852     0.0391    -1.7148      -5.96R
 54      1.00     0.6020     0.0008     0.0314     0.6012       2.08R
 56      1.00     0.5820    -0.0298     0.0314     0.6118       2.12R
 63      1.00     0.6280     0.0022     0.0312     0.6258       2.17R
 72      1.00    -0.6780    -0.4455     0.0687    -0.2325      -0.82 X
 74      1.00    -0.6200    -0.4383     0.0686    -0.1817      -0.64 X
 77      1.00    -2.0000    -0.7929     0.0512    -1.2071      -4.22R
 83      1.00    -0.3770     0.2991     0.0334    -0.6761      -2.34R
 88      1.00    -0.2760     0.3175     0.0258    -0.5935      -2.05R
148      1.00     0.1400    -0.5494     0.0629     0.6894       2.43R
449      1.00    -1.2220    -0.9709     0.0713    -0.2511      -0.89 X
450      0.00    -1.2220    -1.4208     0.0746     0.1988       0.71 X
```

451	1.00	-1.2220	-1.3777	0.0792	0.1557	0.56	X
452	1.00	-1.2220	-1.5001	0.0898	0.2781	1.01	X
453	0.00	-1.2220	-1.4353	0.0804	0.2133	0.76	X
454	0.00	-1.2220	-1.2840	0.0680	0.0620	0.22	X
456	1.00	-1.2220	-1.5681	0.0880	0.3461	1.25	X
458	0.00	-1.2220	-1.3336	0.0785	0.1116	0.40	X
459	1.00	-1.2220	-1.5812	0.0937	0.3592	1.31	X
462	0.00	-1.2220	-0.6420	0.0492	-0.5800	-2.03	R
465	1.00	-1.2220	-0.5112	0.0515	-0.7108	-2.49	R

R denotes an obs. with a large st. resid.
X denotes an obs. whose X value gives it large influence.

Minitab regression analysis for model FF4-A

```
The regression equation is
LOG(Dhc+ = - 6.97 + 0.972 M - 0.272 log R - 0.0266 R + 0.497 log Wff
           + 0.584 log T15

Predictor       Coef       Stdev    t-ratio        p
Constant     -6.9684      0.5432     -12.83    0.000
M            0.97233     0.08312      11.70    0.000
log R       -0.27154     0.08241      -3.29    0.001
R          -0.026572    0.002541     -10.46    0.000
log Wff      0.49732     0.07741       6.42    0.000
log T15      0.58413     0.07284       8.02    0.000

s = 0.3504      R-sq = 63.1%     R-sq(adj) = 62.2%

Analysis of Variance

SOURCE       DF          SS          MS         F        p
Regression    5     43.4803      8.6961     70.82    0.000
Error       207     25.4160      0.1228
Total       212     68.8963

SOURCE       DF      SEQ SS
M             1      7.0852
log R         1      9.2075
R             1     13.8422
log Wff       1      5.4487
log T15       1      7.8966

Unusual Observations
Obs.        M   LOG(Dhc+        Fit  Stdev.Fit   Residual    St.Resid
  3      9.20     0.1400    -0.2081     0.1713     0.3481       1.14 X
  4      9.20     0.2830     1.0274     0.1462    -0.7444      -2.34RX
  5      9.20     0.2700     0.9020     0.1375    -0.6320      -1.96 X
  6      9.20     0.1990     0.8382     0.1333    -0.6392      -1.97 X
  7      6.40    -1.0460     0.1257     0.0708    -1.1717      -3.41R
 28      6.40    -0.9590     0.0663     0.0655    -1.0253      -2.98R
 30      6.60    -2.0000    -1.0169     0.1094    -0.9831      -2.95RX
 31      6.60    -2.0000    -0.2616     0.0556    -1.7384      -5.02R
 65      6.60    -2.0000    -0.7718     0.0758    -1.2282      -3.59R
136      7.50     0.1400    -0.5899     0.0971     0.7299       2.17R
205      7.80    -1.2220    -1.0435     0.1154    -0.1785      -0.54 X
206      7.40    -1.2220    -1.4324     0.1275     0.2104       0.64 X
207      7.60    -1.2220    -1.5733     0.1471     0.3513       1.10 X
208      7.40    -1.2220    -1.6283     0.1429     0.4063       1.27 X
209      7.60    -1.2220    -1.6568     0.1539     0.4348       1.38 X
211      6.60    -1.2220    -0.4848     0.0754    -0.7372      -2.15R

R denotes an obs. with a large st. resid.
X denotes an obs. whose X value gives it large influence.
```

Minitab regression analysis for model GS4-A

```
The regression equation is
LOG(Dhc+ = - 7.59 + 1.11 M - 0.233 log R - 0.0254 R + 0.477 log Sgs
           + 0.579 log T15

Predictor       Coef       Stdev    t-ratio        p
Constant     -7.5863      0.4593     -16.52    0.000
M            1.10888     0.06738      16.46    0.000
log R       -0.23274     0.06793      -3.43    0.001
R          -0.025354    0.001654     -15.33    0.000
log Sgs      0.47691     0.05162       9.24    0.000
log T15      0.57886     0.05124      11.30    0.000

s = 0.2258      R-sq = 69.1%     R-sq(adj) = 68.5%

Analysis of Variance

SOURCE       DF          SS          MS         F        p
Regression    5     28.2828      5.6566    110.94    0.000
Error       248     12.6451      0.0510
Total       253     40.9279

SOURCE       DF      SEQ SS
M             1      2.2741
log R         1      4.2227
R             1     14.3698
log Sgs       1      0.9079
log T15       1      6.5082

Unusual Observations
Obs.        M   LOG(Dhc+        Fit  Stdev.Fit   Residual    St.Resid
  1      7.90     0.1790     0.8683     0.0416    -0.6893      -3.11R
  2      7.90     0.1790     0.9055     0.0404    -0.7265      -3.27R
  3      9.20    -0.5090    -0.1130     0.1220    -0.3960      -2.08RX
  4      9.20    -0.5090    -0.3709     0.1230    -0.1381      -0.73 X
  5      9.20     0.3890     1.4469     0.1059    -1.0579      -5.30RX
  6      6.40     0.2280    -0.0487     0.0997     0.2767       1.37 X
  7      6.40    -0.2840    -0.0487     0.0997    -0.2353      -1.16 X
  8      6.40     0.0900    -0.0487     0.0997     0.1387       0.68 X
  9      6.40     0.2280    -0.0487     0.0997     0.2767       1.37 X
 10      6.40     0.2280    -0.0487     0.0997     0.2767       1.37 X
 11      6.60    -2.0000    -0.8106     0.0689    -1.1894      -5.53RX
 12      6.60    -2.0000    -0.5344     0.0536    -1.4656      -6.68R
 78      7.50     0.5450     0.0624     0.0217     0.4826       2.15R
148      7.50    -0.1190     0.3488     0.0200    -0.4678      -2.08R
245      7.50    -1.2220    -1.3794     0.0836     0.1574       0.75 X
246      7.70    -1.2220    -1.3704     0.0892     0.1484       0.72 X
247      7.50    -1.2220    -1.2458     0.0762     0.0238       0.11 X
248      7.50    -1.2220    -1.0580     0.0660    -0.1640      -0.76 X
250      7.80    -1.2220    -1.2596     0.0866     0.0376       0.18 X
251      6.40    -1.2220    -0.8619     0.0701    -0.3601      -1.68 X
252      6.60    -1.2220    -0.7346     0.0605    -0.4874      -2.24RX
253      6.40    -1.2220    -0.8022     0.0723    -0.4198      -1.96 X
254      6.60    -1.2220    -1.2892     0.0804     0.0672       0.32 X

R denotes an obs. with a large st. resid.
X denotes an obs. whose X value gives it large influence.
```

Minitab regression analysis for model FFGS4-B

```
The regression equation is
LOG(Dhc+ = - 6.75 - 0.162 B0ff + 1.00 M - 0.289 log R - 0.0215 R
           + 0.0904 log Wff + 0.203 log Sgs + 0.289 log T15

Predictor       Coef       Stdev    t-ratio        p
Constant     -6.7472      0.3679     -18.34    0.000
B0ff        -0.16205     0.07937      -2.04    0.042
M            1.00124     0.05503      18.19    0.000
log R       -0.28932     0.05679      -5.09    0.000
R          -0.021456    0.001546     -13.88    0.000
log Wff      0.09041     0.08693       1.04    0.299
log Sgs      0.20319     0.08141       2.50    0.013
log T15      0.28872     0.05252       5.50    0.000

s = 0.2807      R-sq = 65.2%     R-sq(adj) = 64.3%

Analysis of Variance

SOURCE       DF          SS          MS         F        p
Regression    7     40.5240      5.7891     73.48    0.000
Error       275     21.6672      0.0788
Total       282     62.1912

SOURCE       DF      SEQ SS
B0ff          1      2.1261
M             1      7.0842
log R         1     12.2982
R             1     16.6171
log Wff       1      0.0000
log Sgs       1      0.0171
log T15       1      2.3814

Unusual Observations
Obs.     B0ff   LOG(Dhc+        Fit  Stdev.Fit   Residual    St.Resid
  5      1.00     0.1400    -0.0519     0.1048     0.1919       0.74 X
  6      1.00     0.2830     0.7950     0.1187    -0.5120      -2.01RX
  7      1.00     0.2700     0.7795     0.1028    -0.5095      -1.95 X
  8      1.00     0.1990     0.7768     0.0950    -0.5778      -2.19RX
  9      0.00    -0.5090    -0.0894     0.1127    -0.4196      -1.63 X
 10      0.00    -0.5090    -0.2076     0.1253    -0.3014      -1.20 X
 11      1.00    -1.0460    -0.1383     0.0568    -0.9077      -3.30R
 21      1.00    -0.9590    -0.1819     0.0552    -0.7771      -2.82R
 23      0.00     0.2280    -0.0033     0.0823     0.2313       0.86 X
 24      0.00    -0.2840    -0.0033     0.0823    -0.2807      -1.05 X
 25      0.00     0.0900    -0.0033     0.0823     0.0933       0.35 X
 26      0.00     0.2280    -0.0033     0.0823     0.2313       0.86 X
 27      0.00     0.2280    -0.0033     0.0823     0.2313       0.86 X
 28      0.00    -2.0000    -0.5888     0.0545    -1.4112      -5.13R
 29      0.00    -2.0000    -0.4510     0.0418    -1.5490      -5.58R
 30      1.00    -2.0000    -0.7998     0.0803    -1.2002      -4.46R
 31      1.00    -2.0000    -0.4883     0.0447    -1.5117      -5.45R
 50      1.00    -0.6780    -0.8927     0.0849     0.2147       0.80 X
 52      1.00    -0.6200    -0.8889     0.0849     0.2689       1.01 X
 55      1.00    -2.0000    -0.9488     0.0525    -1.0512      -3.81R
268      1.00    -1.2220    -1.5356     0.0878     0.3136       1.18 X
269      0.00    -1.2220    -1.2702     0.0822     0.0482       0.18 X
272      1.00    -1.2220    -1.6215     0.0862     0.3995       1.50 X
275      1.00    -1.2220    -1.6040     0.0915     0.3820       1.44 X

R denotes an obs. with a large st. resid.
X denotes an obs. whose X value gives it large influence.
```

Minitab regression analysis for model FF4-B

```
The regression equation is
LOG(Dhc+ = - 6.03 + 0.880 M - 0.271 log R - 0.0184 R + 0.013 log Wff
           + 0.257 log T15

Predictor       Coef       Stdev    t-ratio        p
Constant     -6.0349      0.5677     -10.63    0.000
M            0.87989     0.08364      10.52    0.000
log R       -0.27137     0.09243      -2.94    0.004
R          -0.018443    0.002804      -6.58    0.000
log Wff       0.0127      0.1137       0.11    0.911
log T15      0.25658     0.08413       3.05    0.003

s = 0.3411      R-sq = 59.5%     R-sq(adj) = 57.7%

Analysis of Variance

SOURCE       DF          SS          MS         F        p
Regression    5     19.1520      3.8304     32.93    0.000
Error       112     13.0285      0.1163
Total       117     32.1805

SOURCE       DF      SEQ SS
M             1      4.8734
log R         1      6.6454
R             1      6.4996
log Wff       1      0.0515
log T15       1      1.0820

Unusual Observations
Obs.        M   LOG(Dhc+        Fit  Stdev.Fit   Residual    St.Resid
  3      9.20     0.1400    -0.0552     0.1704     0.1952       0.66 X
  4      9.20     0.2830     0.6186     0.1632    -0.3356      -1.12 X
  5      9.20     0.2700     0.6251     0.1454    -0.3551      -1.15 X
  6      9.20     0.1990     0.6351     0.1370    -0.4361      -1.40 X
  7      6.40    -1.0460    -0.1243     0.0859    -0.9217      -2.79R
 17      6.40    -0.9590    -0.1693     0.0823    -0.7897      -2.39R
 19      6.60    -2.0000    -0.7208     0.1205    -1.2792      -4.01R
 20      6.60    -2.0000    -0.4708     0.0609    -1.5292      -4.56R
 44      6.60    -2.0000    -0.8675     0.0760    -1.1325      -3.41R
112      7.60    -1.2220    -1.3833     0.1456     0.1613       0.52 X
113      7.40    -1.2220    -1.4605     0.1411     0.2385       0.77 X
114      7.60    -1.2220    -1.4424     0.1528     0.2204       0.72 X

R denotes an obs. with a large st. resid.
X denotes an obs. whose X value gives it large influence.
```

Minitab regression analysis for model GS4-B

```
The regression equation is
log(Dhc+ = - 8.41 + 1.24 M - 0.358 log R - 0.0243 R + 0.266 log Sgs
           + 0.373 log T15

Predictor       Coef       Stdev    t-ratio        p
Constant     -8.4104      0.5057     -16.63    0.000
M            1.23887     0.07417      16.70    0.000
log R       -0.35833     0.06861      -5.22    0.000
R          -0.024273    0.001641     -14.79    0.000
log Sgs      0.26553     0.07252       3.66    0.000
log T15      0.37286     0.06588       5.66    0.000

s = 0.2204      R-sq = 72.3%     R-sq(adj) = 71.4%

Analysis of Variance

SOURCE       DF          SS          MS         F        p
Regression    5     20.1549      4.0310     82.97    0.000
Error       159      7.7246      0.0486
Total       164     27.8795

SOURCE       DF      SEQ SS
M             1      2.2114
log R         1      5.7243
R             1     10.6462
log Sgs       1      0.0167
log T15       1      1.5562

Unusual Observations
Obs.        M   log(Dhc+        Fit  Stdev.Fit   Residual    St.Resid
  1      7.90     0.1790     0.8537     0.0474    -0.6747      -3.13R
  2      7.90     0.1790     0.8578     0.0485    -0.6788      -3.16R
  3      9.20    -0.5086     0.0604     0.1256    -0.5690      -3.14RX
  4      9.20    -0.5086    -0.0932     0.1290    -0.4154      -2.32RX
  5      6.40     0.2279    -0.0574     0.0973     0.2853       1.44 X
  6      6.40    -0.2840    -0.0574     0.0973    -0.2266      -1.15 X
  7      6.40     0.0899    -0.0574     0.0973     0.1473       0.74 X
  8      6.40     0.2279    -0.0574     0.0973     0.2853       1.44 X
  9      6.40     0.2279    -0.0574     0.0973     0.2853       1.44 X
 10      6.60    -2.0000    -0.7829     0.0760    -1.2171      -5.88RX
 11      6.60    -2.0000    -0.6050     0.0565    -1.3950      -6.55R
156      7.50    -1.2218    -1.4717     0.0836     0.2499       1.23 X
157      7.70    -1.2218    -1.4335     0.0883     0.2117       1.05 X
158      7.50    -1.2218    -1.3399     0.0763     0.1181       0.57 X
161      7.80    -1.2218    -1.3097     0.0854     0.0878       0.43 X
162      6.40    -1.2218    -1.0750     0.0762    -0.1468      -0.71 X
164      6.40    -1.2218    -1.0746     0.0801    -0.1473      -0.72 X
165      6.60    -1.2218    -1.5018     0.0862     0.2799       1.38 X

R denotes an obs. with a large st. resid.
X denotes an obs. whose X value gives it large influence.
```